STRUCTURAL INTERPRETATION OF GRAVITY AND AEROMAGNETIC ANOMALIES OVER SOKOTO BASIN, NORTHWESTERN NIGERIA.

BY

MARIUS NNANNA UMEGO

i

A THESIS SUBMITTED TO THE POSTGRADUATE SCHOOL AHMADU BELLO UNIVERSITY, ZARIA, IN PARTIAL FULFILMENT OF THE REQUIREMENTS FOR THE DEGREE OF DOCTOR OF PHILOSOPHY IN GEOPHYSICS.

DEPARTMENT OF PHYSICS
FACULTY OF SCIENCE
AHMADU BELLO UNIVERSITY
ZARIA, NIGERIA.

MARCH, 1990.

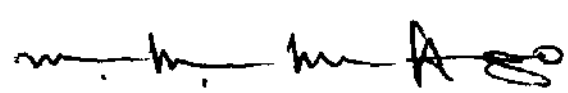
DECLARATION

I hereby declare that:

1. the report presented in this thesis is the result of original research of the author;

2. this thesis has not been submitted to any other institution, organisation or body for any award other than Ahmadu Bello University; and

3. all inclusions from the author's earlier works and those of others have been duely acknowledged.



Marius Nnanna Umego

Date: 30/3/90

CERTIFICATION

This thesis entitled "Structural interpretation of gravity and aeromagnetic anomalies over Sokoto Basin, northwestern Nigeria" by Marius Nnanna Umego meets the regulations governing the award of the degree of Doctor of Philosophy of Ahmadu Bello University, and is approved for its contribution to knowledge and literary presentation.

Professor D.E.Ajakaiye
(Chairperson, Supervisory Committee)
Date: 8/5/90

Dr S. B. Ojo
(Member, Supervisory Committee)
Date: 8/5/90

Professor J. Adetunji
(Head of Department)
Date: 8/5/90

Professor D. I. Saror
(Dean, Postgraduate School)
Date: 12-9-90

DEDICATION

To my wife and children

Carol, Obinna, Ifeanyi, Ijeoma, Nneka and Chima.

Aknowledgements

I acknowledge with thanks the assistance of all individuals who have contributed in different ways towards the successful completion of this project. In particular, I thank my supervisors Professor D. E. Ajakaiye for suggesting that this study be undertaken, and for her encouragement and guidance all through its duration; and Dr S. B. Ojo for his sustained interest, helpful suggestions and provision of some of the computer programs used for the project.

I am greatly indebted to the Director Geological Survey of Nigeria for release of the aeromagnetic maps; the Director Federal Survey Department for providing Benchmark information over the survey area; and the Assistant Deputy Director for Programs, Production and Operations of the Defence Mapping Agency Aerospace Centre of the United States of America for release of the May 1988 edition of mean free-air gravity anomalies and elavations for the survey area.

I am grateful to the Director Internationl Program in the Physical Sciences of the Internationl Science Program, Uppsala University Sweden, for offering me a one year fellowship to accomplish some of the data reduction and interpretation of this project in Sweden. The personal computer which your organization donated to my department was an indispensable tool from the data reduction to the final production of this thesis. I thank Professor L. B.

Pedersen, head department of Solid Earth Physics Uppsala University for use of facilities in my host department, and Dr Dan Dyrelius - my research host, for his assistance with some of the computer programs used and for other useful suggestions. The assistance of Drs T. Rasmussen and Z. Ping of the same department is also acknowledged.

The assistance Dr S. I. Abaa and Messrs M. E. Weakes and A. E. Ikpokonte all the of the Geology Department, Ahmadu Bello University with the identification of rock samples and other helpful criticism and suggestions on the geology of the area is also acknowledged. The many helpful discussions, encouragements and other assistance received from my head of department Prof J. Adetunji, my colleagues in the Geophysics Group and other staff of the Physics Department especially Messrs B. Nwosu, J. Datiri, J. Daveu, B. Yinusa, P. Bamidele and A. Fagbemi are gratefully acknowledged. I am also grateful to the following individuals for their kind assistance with computing facilities at various stages of this project; they include colleagues at the Center for Energy Research and Training, the acting director of the Iya Abubakar Computer Center Mrs S. N. Braide, Dr Femi Peters of the Chemistry department, Dr S. Ebele of the Biological Sciences department, and Dr Asiribo of the Institute of Agricultural Research. Finally I thank the Ahmadu Bello University for providing partial

financial support in the form of a research grant to enable me complete this project.

Special thanks are also due to my brothers for their encouragement, and my late parents both of whom were not opportuned to see me through. My ultimate gratitude is to the Almighty Father for whatever I am and will ever be.

Abstract

The first composite magnetic anomaly map of the Sokoto Basin has been compiled at a scale of 1:3,000,000 from a total of thirty Geological Survey of Nigeria aeromagnetlc maps. The composite map revealed major structures in the Precambrian basement beneath the sediments, and delineated areas for more detailed investigations. A system of large scale NE-SW and NW-SE trending magnetic lineations were also revealed, and these have been interpreted to be part of the continent-wide conjugate strike-slip fault system of probable tectonic origin. The magnetic lineations and intrusive activities are concentrated along three prominent linear belts which probably represent pre-existing zones of crustal weakness in the continental crust. The significance of these zones with regard to mineralization and seismicity have been highlighted. A magnetic depth to basement analysis has revealed that the basement surface is generally shallow, and attain a maximum depth of 1.8 km at the extreme NW corner of the basin. The regional dip is gentle, and measured 0.4 in the northwestern direction.

Also gravity data were collected along all motorable roads in the basin and in parts of the adjoining basement block of northern Nigeria. Three-dimensional interpretation of the gravity data led to the following conclusions: (1) The isolated Older Granite outcrops around Gusau coalesce into one big

pluton just beneath the ground surface and extend to a depth of 4.3 km with steeply dipping contacts which suggest a magmatic origin for these granite bodies. (2) The metasediments of the Anka Schist Belt are generally outward dipping, and attain a general thickness **of** 2.5 km, terminating in a characteristic flat base. This simple structural style suggests that the sequence was probably affected by only one tectonic event which left a N-S trending structural grain on these rock units. (3) A number of depressions in the subsurface basement rocks have been revealed where sedimentary thicknesses range from 0.5 to 1.0 km.

Over the basin, both gravity and magnetic data have revealed an irregular basement floor resulting from gentle folding of the basement rocks along a general N-S axis, at wavelength scales of roughly 100 km and amplitudes of only a few hundred meters. Several sediment-filled troughs and depressions on the basement surface have been revealed which form targets **for** groundwater exploration. The absence of major faulting even at the sediment-basement boundary tend to suggest that this southeastern sector of the Iullemmeden Basin probably originated from gentle epeirogenic warpings in contrast to the western and northeastern parts.

T A B L E OF C O N T E N T S

Chapter		Page
	Title page	i
	Declaration	ii
	Certification	iii
	Dedication	iv
	Acknowledgements	v
	Abstract	viii
	Table of contents	x
	List of tables	xiv
	List of figures	xv
	List of appendices	xviii
	Abbreviations and symbols ...	xix
1	INTRODUCTION	
1.1	General introduction ...	1
1.2	Review of previous geophysical studies in the area ...	2
1.3	The present survey ...	7
1.3.1	Choice of methods ...	7
1.3.2	Scope and objectives ...	9
1.3.3	Limitations ...	11
2	GEOLOGY	
2.1	Introduction ...	14
2.2	General geology of the Iullemmeden Basin ...	14
2.3	Detailed geology of the Sokoto Basin	17
2.3.1	The Basement Complex ...	20
2.3.2	Pre-Maastrichtian deposits ...	22

2.3.3	The Maastrichtian deposits	...	23
2.3.4	The late-Paleocene deposits	...	23
2.3.5	The Eocene-Miocene deposits	...	24
2.3.6	The lateritic and ferruginous deposits		24
2.3.7	Faults and folds	...	25
2.3.8	Economic geology	...	26

3 DATA REDUCTION

A. GRAVITY DATA

3.1	Introduction	...	27
3.2	Conversion of instrument reading to gravity values	...	28
3.3	Latitude correction	...	28
3.4	Free-air reduction	...	30
3.5	Bouguer reduction	...	31
3.6	Other corrections	...	32
3.6.1	Tidal effect	...	32
3.6.2	Drift correction	...	33
3.6.3	Terrain correction	...	34
3.7	Gravity anomalies	...	35
3.8	Accuracy of the Bouguer gravity anomaly	...	36

B. DENSITY DETERMINATION

3.9	Sampling technique	...	40
3.10	Method of density determination and analysis	...	41

C. MAGNETIC DATA

3.11	Data source	...	46
3.12	Compilation	...	47
3.12.1	Digitizing	...	47

3.12.2	Gridding	...	48
3.12.3	Recontouring	...	50
3.12.4	Merging	...	50
3.13	Discussion	...	51
4	GRAVITY INTERPRETATION		
4.1	Introduction	...	55
4.2	The Bouguer anomaly map	...	55
4.3	Regional - residual separation	...	57
4.4	The residual anomaly	...	71
4.5	Quantitative interpretation of the residual anomalies	...	74
4.5.1	Theory of the foward modeling method		80
4.5.2	Model fitting procedure	...	85
4.5.3	Three-dimensional interpretation of the residual anomalies	...	88
	Profile A-A'	...	88
	Profile B-B'	...	90
	Profile C-C'	...	94
	Profile D-D'	...	96
4.6	Discussion	...	98
5.	MAGNETIC INTERPRETATION		
5.1	Introduction	...	103
5.2	Qualitative interpretation	...	104
5.3	Quantitative interpretation	...	111
5.3.1	Introduction	...	111
5.3.2	The computational method	...	113
5.3.3	Basic theory of the Werner deconvolution technique	...	114
5.3.4	The interpretation procedure	...	116

5.3.5	Estimation of the magnetic basement surface ...	118
5.3.6	Preparation of the generalised magnetic basement depth map ...	122
5.3.7	Discussion of the magnetic basement depth map ...	127

6.	SUMMARY AND CONCLUSIONS	
6.1	Introduction ...	133
6.2	Summary of results ...	135
6.2.1	Summary of the gravity results ...	135
6.2.2	Summary of the magnetic results ...	137
6.3	Correlation of gravity and magnetic results ...	139
6.4	Conclusions ...	143
6.5	Recommendations ...	147
	REFERENCES ...	149
	APPENDICES ...	157

LIST OF TABLES

Table	Title	Page
2.1	Geological sequence in the Sokoto Basin.	21
3.1	Densities of rocks sampled in the survey area.	42

LIST OF FIGURES

Figure	Title	Page
1.1	Simplified geological map of Nigeria showing boundary of study area.	3
1.2	Map of the study area showing the distribution of the gravity stations.	10
2.1	Structural map of the Iullemmeden Basin.	15
2.2	Geological map of the Sokoto Basin.	19
3.1	Bouguer anomaly map of the survey area.	37
3.2	Illustration of the extra margin included in the gridding of each map.	49
3.3	Total magnetic field intensity contour map of Sokoto Basin.	52
3.4	Density plot of total magnetic field intensity over Sokoto Basin.	53
4.1	Location map of the 1° cells for the DMAAC data set.	60
4.2(a)	Bouguer anomaly map of the Iullemmeden Basin and surrounding areas.	61
4.2(b)	Bouguer anomaly map of the Iullemmeden Basin area.	62
4.3	Regional gravity field of the survey area from the DMAAC data set.	64
4.4	Residual anomaly map of the survey area derived from the DMAAC regional field.	65
4.5(a)	Bouguer anomaly, assumed DMAAC regional and residual anomaly along profile B-B'.	66
4.5(b)	Bouguer anomaly, assumed DMAAC regional and residual anomaly along profile A-A'.	67
4.6	'Local regional' gravity field over the survey area.	69
4.7	Residual anomaly map of the survey area derived from the 'local regional' field.	70
4.8	Residual anomaly map superimposed on a simplified geological map of the area.	72

List of Figures (contd.)

Figure	Title	Page
4.9	Bouguer anomaly, assumed regional and residual anomaly along profiles A-A', B-B', C-C', and D-D'.	75
4.10	Geometrical elements involved in the computation of the gravity anomaly caused by a three-dimensional body.	82
4.11	Three-dimensional model of bodies used for the six major anomalies.	86
4.12	3-D interpretation of the residual anomaly along profile A-A'.	89
4.13	Third 3-D interpretation of the residual anomaly along profile A-A'.	91
4.14	3-D interpretation of the residual anomalies along profile B-B'.	93
4.15	3-D interpretation of the residual anomalies along profile C-C'.	95
4.16	3-D interpretation of the residual anomalies along profile D-D'.	97
5.1	Some inferred lineament trends superimposed on the total magnetic field intensity contour map of Sokoto Basin.	105
5.2	Some inferred lineament trends superimposed on the density plot of total magnetic field intensity of Sokoto Basin.	107
5.3	Map of Sokoto Basin showing major magnetic lineaments derived from the composite maps.	108
5.4	A typical N-S, Werner profile through longitude 5° 15 E.	119
5.5	A typical N-S, Werner profile through longitude 5° 24 E.	120
5.6	The profile of Fig. 5.4 showing the interpreted basement surface.	123
5.7	The profile of Fig. 5.5 showing the interpreted basement surface.	124
5.8	The depth points used as a basis for the contoured magnetic basement depth map.	125
5.9	Generalised magnetic basement depth map.	126

List of Figures (contd.)

Figure	Title	Page
5.10	Some inferred structural features on the basement surface superimposed on the generalised magnetic basement depth map.	128
5.11	E-W cross-sectional views of the basement surface through latitudes 12.5° and 11.5° N.	130
5.12	Cross-sectional view of the basement surface, (a) through latitude 13° N, (b) idealised section of the Sokoto Basin.	131
B1	Geometry and spatial relationship of the thin dyke.	160
B2	Geometry of the thin dyke in the y'z-plane.	161
B3	The anomalies in the different components of total intensity.	161

LIST OF APPENDICES

Appendix		Page
A	La Porte's method of regularization ...	157
B	Magnetic anomaly of a thin dyke ...	159

LIST OF ABBREVIATIONS AND SYMBOLS

ABBREVIATION/SYMBOL	DESCRIPTION
CI	"Continental Intercalaire"
CT	Continental Terminal
DMAAC	Defence Mapping Agency Aerospace Centre
EAEG	European Association of Exploration Geophysicists
GRS	Geodetic Reference System
GSN	Geological Survey of Nigeria
IGF	International Gravity Formular
IGSN 71	International Gravity Standardization Net 1971
JICA	Japanese International Cooperation Agency
LANDSAT	Land Resources Technology Satellite
USAID	United States Agency for International Development
^{o}C	Degree Celcius
1 mGal (milligal)	10^{-5} m s^{-2}
γ	Normal gravity
ϕ	Station geographic latitude
nT (nanotesla)	1 gamma = 10^{-5} oersted
1 Gal	10^{-2} m s^{-2}
1 μGal	micro Gal = 10^{-8} m s^{-2}

CHAPTER ONE

I N T R O D U C T I O N

1.1 General Introduction

The mapping of the earth's gravity and magnetic fields has had a long and distinguished history as part of the investigations of the structure and petrologic variation within the earth's lithosphere. Understandably in Nigeria, investigations in both fields have hitherto been confined to limited areas with proven mineral resources and geological objectives. In the Niger Delta area (Figure 1.1) for example, extensive gravity, magnetic and even seismic surveys have been carried out in connection with oil explorations by oil companies. Results of these surveys have been restricted to the prospecting firms and are not available to the wider geoscience community. The Chad Basin (Figure 1.1) has attracted similar attention in this decade mainly for oil and groundwater explorations, but again the results are largely confidential. The other areas where large comprehensive geophysical investigations have been carried out in the country are the Benue Trough (Figure 1.1), pioneered by Cratchley and Jones (1965); and the Younger Granite province pioneered by Ajakaiye (1970). Fortunately results of surveys in these two regions are readily available as most of the surveys were carried out by academic and other research institutions. In other areas of the country, geophysical surveys have

largely been conducted on an ad hoc basis aimed at solving particular geologic problems.

Recently there has been a conscious effort on the part of the geoscience community in the country to coordinate efforts and standardize these surveys to produce composite regional potential field maps of the various geological provinces, and thereby to establish regional gravity and magnetic data banks for the provinces and hence for the entire country (Ajakaiye, personal communication) .

1.2 Review of Previous Geophysical Studies in the Area

No other sedimentary basin in the country has suffered as much neglect in terms of ground geophysical surveys as the Sokoto Basin which is situated in the northwestern part of the country (Figure 1.1). The reason for this apparent neglect is not quite obvious but may be related to the following:

i) no proven hydrocarbon accumulation potential in the basin,

ii) no known economic mineral resources in the basin,

iii) adverse climatic conditions for the greater part of the year coupled with relatively poor road network

iv) lack of an academic/governmental institution with the relevant geoscience department in the region.

In contrast, ground geological mapping has been systematic and can be considered adequate. Kogbe (1979, 1981) and Wright et al. (1985) concluded on the

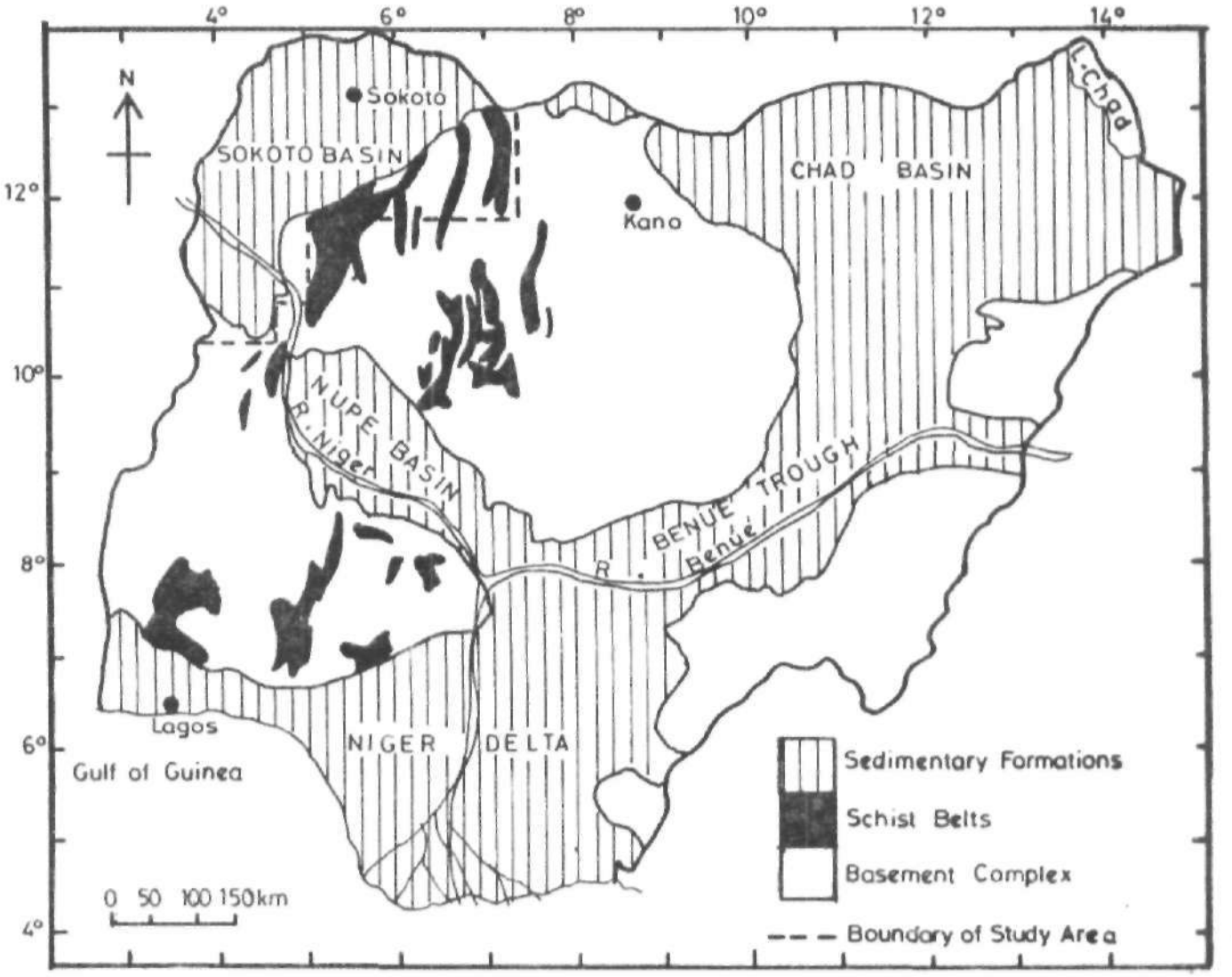


Fig. 1.1 Simplified geological map of Nigeria showing boundary of the study area.

basis of their geological investigations that the basin is interesting from both economic as well as socio-economic points of view. They both recommended an intensive programme of geological and geophysical investigations to be carried out over the basin.

The first comprehensive geophysical investigations in the region was the aeromagnetic mapping which was part of the nation-wide airborne geophysical series carried out for the Geological Survey of Nigeria (GSN). A high sensitivity aeroradiometric survey was also carried out as part of the series over the basin. The results of these surveys have been published as contour maps on a scale of 1:100,000 which are in the custody of GSN.

Ananaba (1983) carried out a reconnaissance remote sensing study over the entire area of the country north of 8° latitude using LANDSAT images. From the mosaic of LANDSAT images he compiled and analysed two major indicator maps namely: drainage map and lineament map. His interpretation of the lineament map was based on the special and directional attributes of their assemblages, and a purely statistical approach was adopted in order to make realistic inferences on the mineralogical implications of the data. Two mean tectonic trends - NE-SW and NW-SE, were established for the country. The lineaments mapped were however not classified as faults, joints, etc. and as such the LANDSAT study would require ground geological and

geophysical follow-up. A lineament density map was also compiled and on comparison with the primary mineral map of Nigeria revealed some remarkable correlation between the areas of high lineament density and areas of known primary mineral occurence (Ananaba and Ajakaiye, 1987).

Uwah (1984), carried out a ground follow-up radiometric survey of some radiometric anomalies delineated from the aeroradiometric survey mentioned above. The field scintillometer and gamma ray spectrometer survey was confined to three locations with a total area of about 1 km in the vicinity of Dange village. These locations were considered to have the highest possibility of uranium mineralization in the Sokoto Basin. These high activity areas were observed to coincide with sedimentary sections with exposed compacted lateritic ironstones. The study concluded that the measured uranium concentrations were lower than the level normally regarded to be of economic importance. Also attention was drawn to a large negative magnetic anomaly centred roughly at latitude 12^{o} 15' N and longitude 5^{o} $23^{'}$ E, within the so-called most probable areas of uranium mineralization and recommended the area for further investigation. It was adduced that uranium carrying fluids could alter the magnetic properties of a subsurface mineral deposit; and thus the magnetic anomaly was linked with uranium mineralization or uranium enrichment in an iron ore deposit.

A few gravity measurements have also been carried out on some major roads in this area between 1981 and 1982 (Ajakaiye, personal communication). In addition there has been two other published accounts of gravimeter measurements in this area prior to the present survey. Verheijen and Ajakaiye (1978) established a gravimeter calibration line in which about three stations are located within this survey area. Two of these stations were reoccupied in this study. Osazuwa (1985) established a primary gravity net for Nigeria of which five base stations are located within the study area, and these were also reoccupied as base stations in the present survey.

Also the Geological Survey of Nigeria had since the 1930s carried out several electrical resistivity, electromagnetic, and seismic refraction surveys in different parts of the basin. Some of these surveys were done in collaboration with foreign governmental agencies such as the United States Agency for International Development (USAID) and recently the Japan International Cooperation Agency (JICA), to mention a few. The surveys were aimed at studying the aquifers of the basin with a view to selecting favourable sites for groundwater boreholes. The results of some of these surveys have been published either as Geological Survey of Nigeria Bulletins or as special publications (Raeburn and Tattam, 1930; Jones, 1948; Ogilbee and Andersen, 1965; Oteze, 1976; and JICA, 1989). The more recent surveys by the GSN have however remained largely

unpublished. Unfortunately none of the numerous boreholes scattered over the basin is known to have reached the basement, and as such depth to basement estimates have been by extrapolations.

From the foregoing, it is obvious that no comprehensive ground geophysical survey of any kind has as yet been carried out in this basin prior to the present survey. Also none of the published Bouguer gravity maps of the country such as those by Ajakaiye and Burke (1973), and Fairhead and Okereke (1987) has included any data from this area.

1.3 The Present Survey

The present survey was in part motivated by the need to remedy the poor state of geophysical knowledge which exists among geoscientists over this great inland basin; and in particular to investigate the subsurface structure of the basin.

1.3.1 Choice of Methods

Historically, gravity and magnetic methods have been the obvious choice for rapid mapping of extensive areas as a means of evaluating or stimulating the exploitation of earth resources. Generally for large, previously unexplored area, the gravity method is an adequate inexpensive method applied for reconnaissance. For example, where little or no geological information is available in a region, the first question that must

be answered is whether a sedimentary basin large enough and thick enough to justify further investigation is present. Also regional gravity surveys may often make it possible to detail major structural features such as faults or lineaments where mineral accumulations are likely to be found. If the geological structure is simple, the gravity method can provide this kind of information rapidly and economically. The basis for the method in this case is that most sedimentary rocks have densities lower than basement rocks; the density contrast thus makes it possible to map the boundaries and determine approximate depth distribution of the sedimentary basin. In the present study, the gravity method is included to throw more light on the subsurface structure of the basin.

Magnetic methods, on the other hand are most important in their assistance to geological reconnaissance and mapping. In particular the aeromagnetic geophysical method is yet unmatched by any other geophysical method in its rapid rate of coverage and low cost per unit area explored. Its usefulness in the acquisition of data over otherwise inaccessible or remote areas is of particular advantage in the present survey. Aeromagnetic method has also been widely used to determine depth to magnetic basement rocks in sedimentary basins. It is also possible to use the method to reveal major basement surface structures and other encouraging exploration areas which can then be surveyed in detail by more costly methods. Thus, when

basement is the object of study and the sedimentary cover gets in the way, aeromagnetics provide a means of seeing through effectively non-magnetic sedimentary rock cover to reveal patterns of magnetization in crystalline basement rocks (Cordell and Grauch, 1985). In the present survey the method is applied to complement the gravity method in an attempt to elucidate the structure of the basement beneath the Cretaceous - Eocene sedimentary cover.

1.3.2 Scope and Objectives

Initially it was intended to carry out only a regional gravity survey over the entire basin with gravity stations at 4 km intervals along all motorable roads within the basin (Figure 1.2), and some parts of the adjoining schist belt (Figure 1.1). Gravity measurements were to start from Gusau and approach the basin northwards through Kaura Namoda to Gaban Birni, westwards through Maru to Talata Mafara and south-westwards through Anka to Gummi (Figure 1.2). It was later discovered that the road network was not adequate over some parts of the basin. Analysis of aeromagnetic data over the basin area was then undertaken to complement the results from the gravity measurements. From computer - aided interpretation of both data sets it was hoped that the survey would achieve the following specific objectives:

1. contribute to the general knowledge of the regional subsurface structure of the basin,

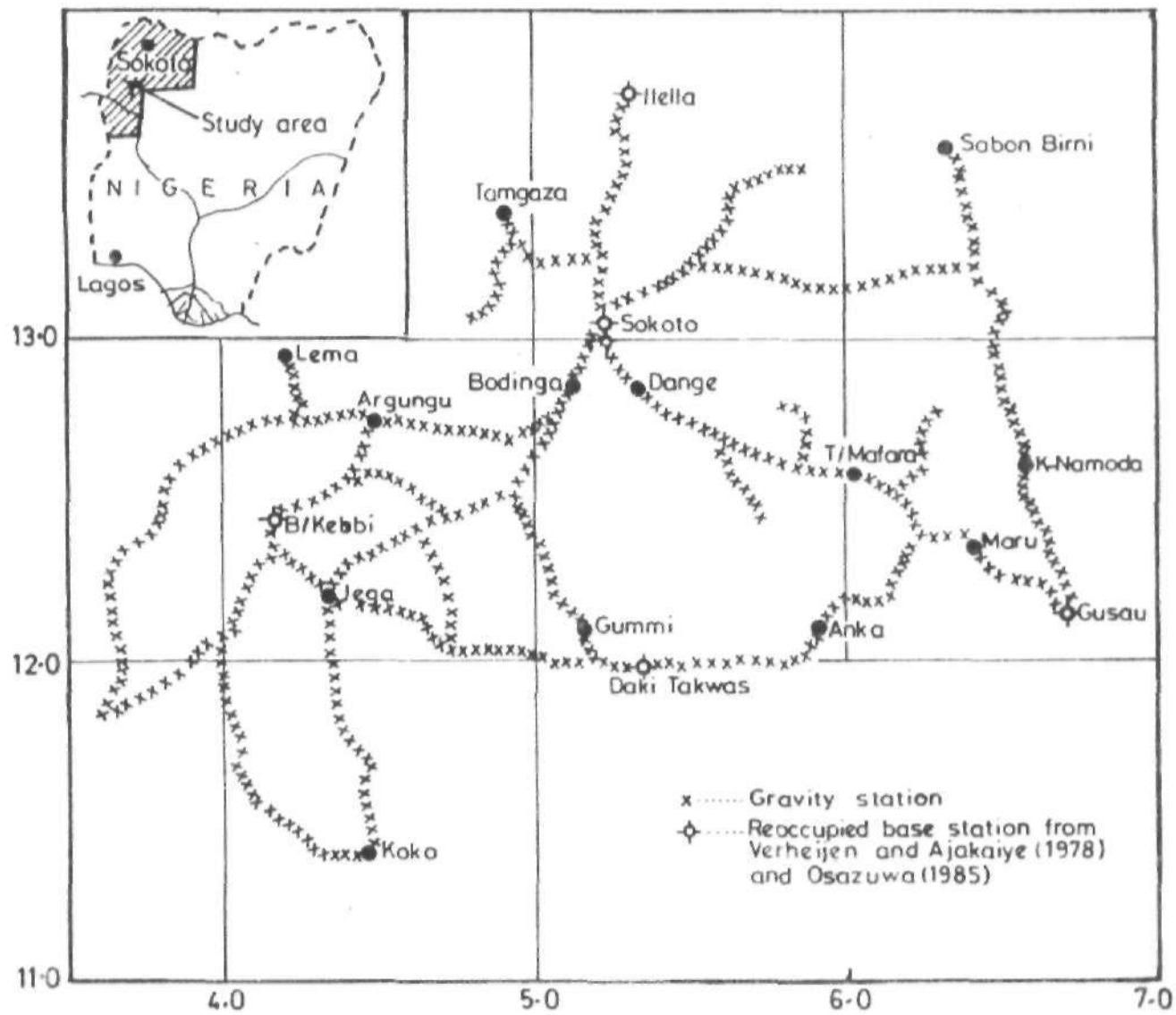


Fig. 1.2 Location map of the study area showing the distribution of the gravity stations.

ii in particular estimate the thickness of the sediments within the basin which has a direct bearing on its hydrocarbon and groundwater accumulation potential,

iii produce a composite magnetic - anomaly map, and a depth to basement map of the basin.

1.3.3 Limitations

Certain problems were encountered during the course of the survey which either slowed down the project or necessitated modifications in the original survey plan. The first of the these problems and infact the most serious of all was associated with the very old base map used for the station location. Part of the road network indicated on the map had long been reconstructed or abandoned altogether and this created difficulty in the location of gravity stations. Some new roads in the area were not on the map, nor in any other published map, and such roads were mapped using major landmarks such as rivers, villages, etc. Coupled with this problem is the fact that the existing road network is not adequate for a uniform distribution of gravity stations in the survey area. For example most of the area north of Argungu and northwest of Sokoto (Figure 1.2) had no motorable roads on any published map. Consequently no gravity stations could be established in such areas.

Similarly most of the benchmarks whose descriptions and heights were obtained from the Federal Survey headquarters in Lagos prior to the field work to facilitate station elavation determination could not be

ABU, ZARIA, NIGERIA.

used during the survey. Some of these benchmarks located on farmlands had been removed by villagers while some others were located along abandened and inaccessible old roads. Also most of the new roads in the area had no benchmarks along them.

The adverse climatic conditions prevailing in this area for the greater part of the year was yet another serious handicap that prolonged the field work. For example, field work can effectively be undertaken only during the dry season (October - May) as most roads are rendered unmotorable during the rainy season (June - September) by floods. The dry season on the other hand is characterised by very strong dust-laden northeast trade winds, and excessive high temperatures. Average daily temperatures between 1100 and 1700 hours (local time) are usually above 30° C. These factors affected the altimeters and the gravity meter adversely to the extent that these instruments tended to drift erratically, and thus limited survey periods to only early morning and late evening hours. The number of days of field work were thus greatly increased and the cost often became prohibitive.

Two major problems were encountered with the rock sampling exercise. The first was in the basement area where it was sometimes difficult to obtain fresh (unweathered) samples of some of the main rock types. For example all the outcrops of phyllites found in the survey area were largely fractured and weathered and no

truely fresh samples of this rock type could be obtained. For the sediments it was difficult to find outcrops of the representative formations as these were largely covered by either the 3-5 m thick lateritic ironstone (Kogbe, 1979) which has developed over most of the Calcareous as well as the Gwandu Formations, or a mantle of drift averaging 2 m in thickness in other places (Jones, 1948). Even at the type localities, some of the samples collected (especially for shales) were unconsolidated, making bulk density determinations almost impossible.

CHAPTER TWO

G E O L O G Y

2.1 Introduction

The Sokoto Basin of Nigeria forms the south-eastern sector of the Iullemmeden Basin, one of the young (Mesozoic - Tertiary) inland cratonic sedimentary basins of West Africa. Thus it is important to discuss briefly the geology of the entire basin for a clearer understanding of the detailed geology of its Nigerian sector.

2.2 General Geology of the Iullemmeden Basin

The large, nearly circular sedimentary basin, generally referred to as the Iullemmeden Basin of West Africa (Figure 2.1), extends from Mali and the western boundary of the Republic of Niger through northern Benin Republic and northwestern Nigeria into eastern Niger (Kogbe, 1981). The basin which covers an area of about 700,000 km^2 , has its centre in the north of Niamey in Niger Republic, and lies entirely within the Pan African Province of West Africa. It is bounded by the Adrar des Iforas, the Hoggar and Air ranges to the north; the Gourma and Liptako mountains and the crystalline rocks at the northern boundary of Benin Republic to the west; and the Nigerian basement rocks to the south and southeast (Figure 2.1).

The basin, like other intra-continental basins of the region and the African continent in general,

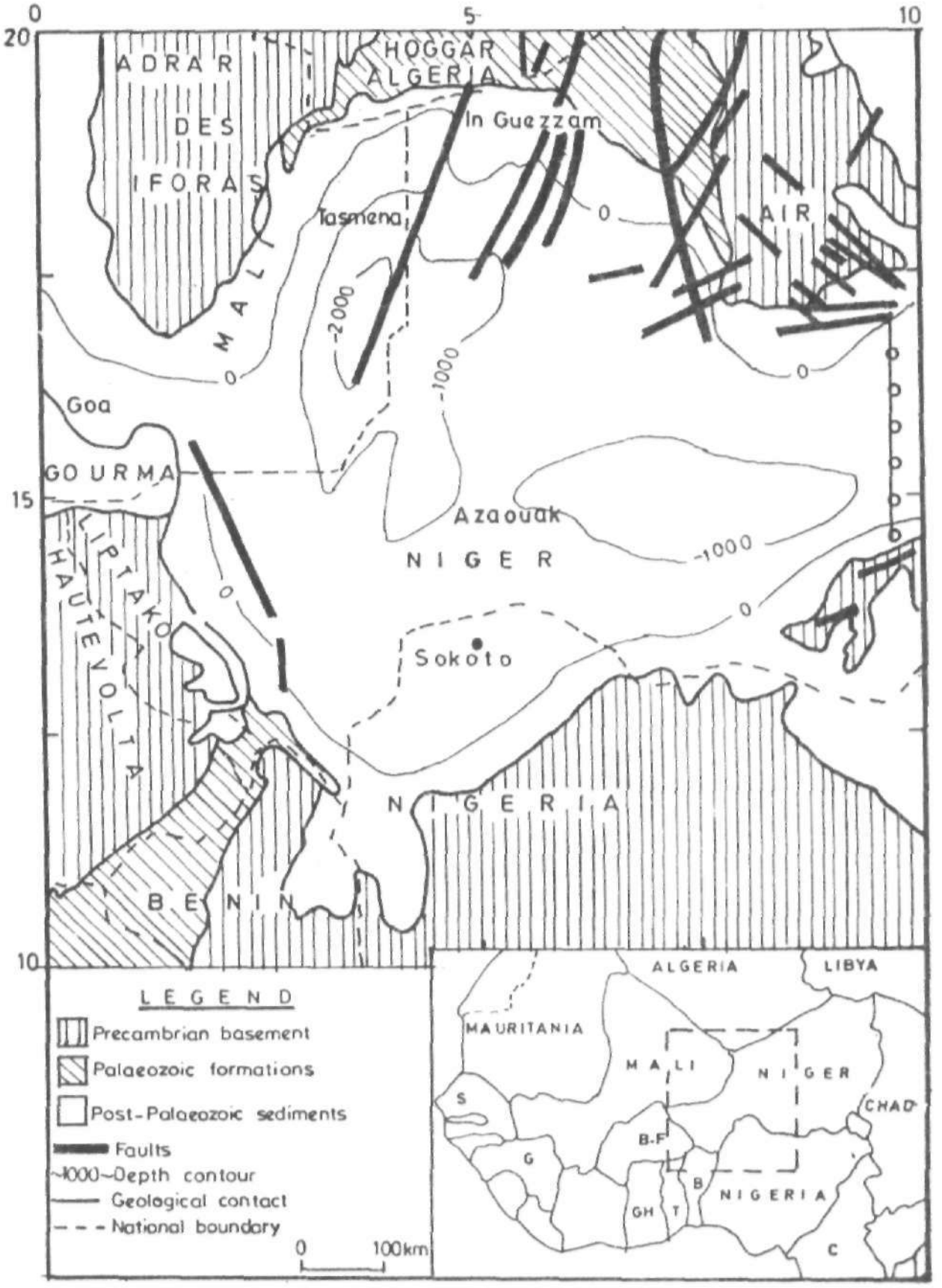


Fig. 2.1 Structural map of the Iullemm eden Basin
(after Kogbe, 1981)

developed by epeirogenic warping or stretching and rifting of tectonically stabilised crust. These movements commenced around the beginning of the Palaeozoic and continued until Upper Cretaceous, and are responsible for the south-westerly progradation of sediments deposited within the basin (Furon, 1963; Kogbe, 1979 and 1981; Wright et al., 1985).

There are three major fault trends in the basin (Kogbe, 1981). These faults are responsible for the existence of several structural depressions within the basin. The most important of these are in a NNE-SSW direction which are responsible for two prominent depressions within the basin. The other two fault directions are WSW-ENE and NW-SE. The NW-SE trending faults mark the western limit of the basin with a down throw of about 500 m (Kogbe, 1979). These faults and associated depressions thus result in local dips in different parts of the basin, which otherwise is generally broad and shallow with gently dipping sediments thickening inwards from the margins.

Fluviate and lacustrine sediments began to be deposited after areas affected by the Pan-African Orogeny had become worn down and peneplained to about the same level as the craton. The phase of continental deposition continued until the Lower Cretaceous. After the breakup of Gondwanaland in the Mid-Cretaceous, marine conditions became established with one of the most extensive transgressions in earth's history

(Kogbe, 1979). These were also relatively short-lived for at the beginning of Tertiary times, the Alpine orogeny commenced and the seas retreated once more. Thereafter sedimentation was largely of fluviatile and lacustrine type.

Economically, the Iullemmeden Basin has not been as important as some other Mesozoic-Tertiary basins of West Africa, because of the absence of any proven petroleum occurence. With the thickest sediments in the range of 2000 m, there is hardly any prospects for oil and gas accumulation (Wright et al., 1985). Chatellier and Slevin (1988) classified the Iullemmeden Basin among the composite and complex multicycle basins in which new field wildcat wells (NFW) were drilled but without any oil and gas discoveries, but noted that most of the basins in this category are under-explored. However other minerals notably uranium, phosphate and a host of other industrial minerals including limestone, kaolinitic clays, gypsum and salt occur widely throughout the basin (Kogbe, 1981; Wright et al., 1985). In addition metalliferous deposits of zinc, lead, are reported to occur in rather small quantities compared to basement terranes.

2.3 Detailed Geology of the Sokoto Basin

The southeastern sector of the Iullemmeden Basin is known locally in Nigeria as the 'Sokoto Basin' or more appropriately the 'Sokoto Embayment' (Abaa, personal communication). The geology of this sector

has been studied in more detail than anywhere else in the Iullemmeden Basin. Notable among these studies in this century are those of Falconer (1911), Raeburn and Tattam (1930), Jones (1948), McCurry (1976), Ajibade (1976), Rahaman (1976), Grant (1978), Kogbe (1979, 1981) and Turner (1983). The general nature of the formations in the basin and their structural relationships presented here is only a summary that is necessary in the interpretation of gravity and magnetic data.

Figure 2.2 is a simplified version of the geological map of the basin. The geological structure so far mapped appears fairly simple - a Precambrian Basement Complex of gneisses, granites, phyllites and quartzites form the foundation of the basin on which lie the Cretaceous and Tertiary sedimentary rocks. The basin consists predominantly of a gently undulating plain occasionally interrupted by low mesa. The regional dip is gentle and is generally northwestwards.

Since the pioneering work of Falconer (1911), there have been three different detailed stratigraphical classifications of the sediments in the area. These are those of Raeburn and Tattam (1930), Jones (1948) and Kogbe (1981). The latter workers have all reviewed and improved on the details of the stratigraphical successions as laid down by the earlier workers. According to Jones (1948), the depositional history of the sediments of the basin can be summarized as follows:

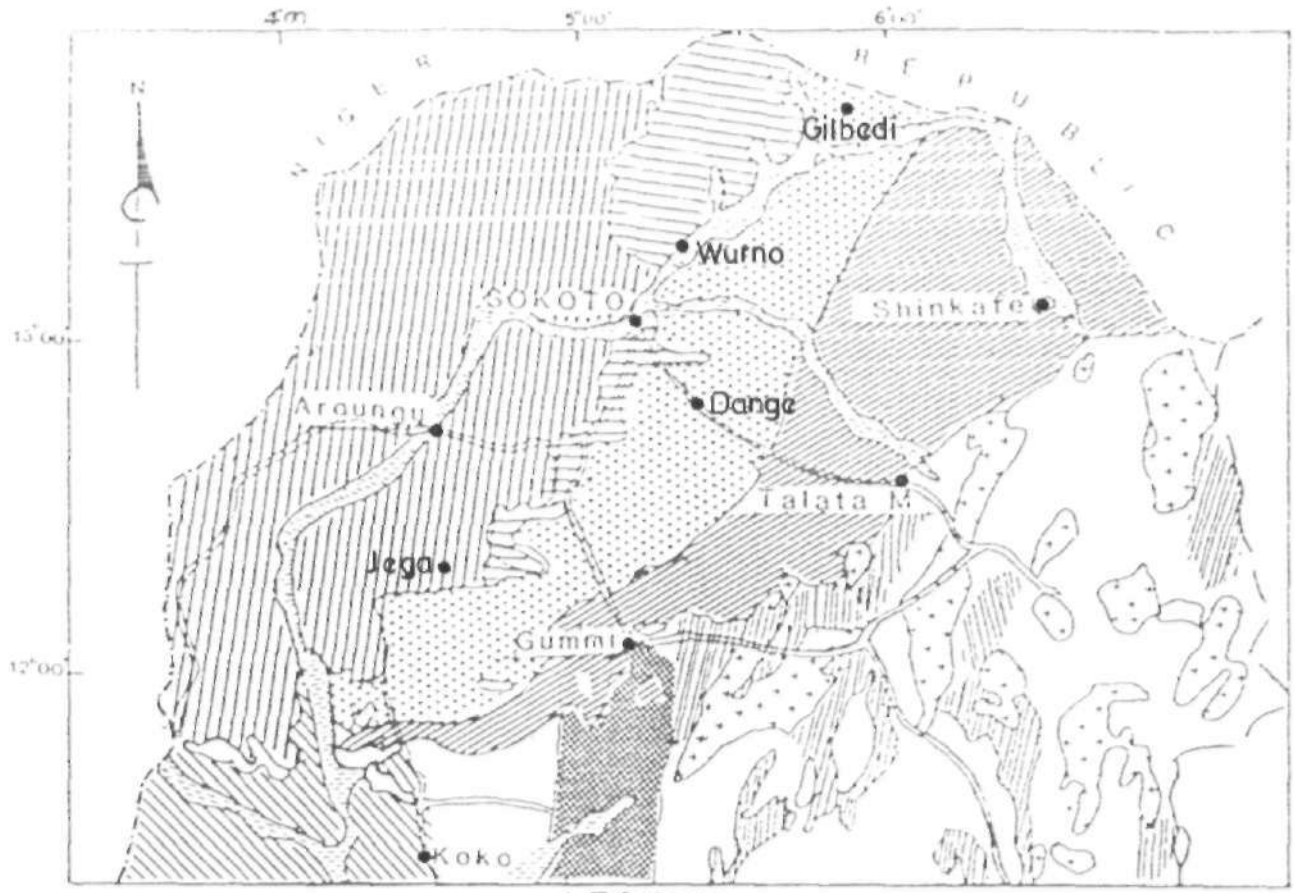


Fig. 2.2Geological map of the Sokoto Basin(after Kogbe,1981)

1. A continental period represented by the Illo and Gundumi Formations. These beds are probably lower Cretaceous and are certainly younger than Cenomanian.

2. A marine period commencing in the Maastrichtian and continuing into the Eocene, during which the Rima Group and the clay-shale and calcareous groups (Eocene) were laid down.

3. A movement of elevation (Alpine Orogeny), probably in late Eocene times leading to the retreat of the sea and accompanied by gentle folding.

4. A continental period represented by the Gwandu Formation which is probably of Upper Tertiary age.

The most comprehensive stratigraphical succession by Kogbe (1981) portrays a geological history which is applicable to a large part of West Africa - a sequence of two continental periods separated by a Cretaceous-Eocene period of marine transgression(s) (Table 2.1).

2.3.1 The Basement Complex

The entire basin is underlain by the Basement Complex which includes all rocks older than the late Proterozoic (McCurry, 1976). The Nigerian Basement Complex lies within the Pan-African Mobile belt of West Africa and is believed to have a polytecto - metamorphic nature (Oyawoye, 1964; McCurry, 1976; Grant, 1978) and consequent metamorphism, migmatization and gneissification have extensively modified the original rocks. Three major rock successions are distinguishable (Odeyemi, 1988) and these are:

Table 2.1 Geological sequence in the Sokoto Basin (after Kogbe, 1981)

Age	Formation	Group	Environment
Quaternary	Sandy drifts, laterites	-----	Continental
Eocene-Miocene	Gwandu Formation	"Continental-Terminal"	Continental
---------- U n c o n f o r m i t y ----------			
Late - Paleocene	Primary Oolitic-ironstone Gamba Formation Kalambaina Formation Dange Formation	Sokoto Group	Marine
---------- U n c o n f o r m i t y ----------			
Maastrichtian	Wurno Formation Dukamaje Formation Taloka Formation	Rima Group	brackish-water with brief marine intercalations
---------- U n c o n f o r m i t y ----------			
Late Jurassic to earliest Cretaceous	Illo and Gundumi Formations	"Continental Intercalaire"	Continental
---------- M a j o r U n c o n f o r m i t y ----------			
Precambrian	B a s e m e n t -- C o m p l e x		

(a) A polycyclic crystalline complex of migmatites and gneisses which are the deminant rocks. The evolution of this complex is believed to have started during the Liberian Orogeny (2,800±200 Ma).

(b) The metasediments and metavolcanics which form the approximately N-S trending schist belts. The period of initiation of the sedimentary process leading to the deposition of these successions had until recently been assigned solely to the Pan-African Orogeny (600 ± 200 Ma). Recent work by Ogezi (1977), Grant (1978), Ajibade and Wright (1988), among others however indicate that part of these sediments may have formed in the Kibaran (1,100 ± 200 Ma) times.

(c) The Older Granite series which belong to a suite of syn- to late tectonic granites and granodiorites that marked the intrusive phase (700 - 500 Ma) of the Pan - African Orogeny in Nigeria. These granitoids intrude both the migmatite - gneiss complex and the schist belts variably and are widespread in other parts of the Nigerian basement and the Pan African Province of West Africa.

2.3.2 Pre-Maastrichtian Deposits

The Ille and Gundumi Groups are lateral equivalents belonging to the upper part of the "Continental Intercalaire" of West Africa (Kogbe, 1981; Wright et al., 1985). They both overlie the Precambrian basement unconformably, and are both of fluviatile and lacustrine origin. Both groups are believed to be the eldest unmetamorphorsed sediments in the basin. The heavy mineral assemblage in them indicates a high grade metamorphic origin, the source being considered to be the Basement Complex (Precambrian) rocks in the adjoining parts of northwestern Nigeria (Kogbe, 1979).

The Ilio Group consists of cross-bedded pebbly grits, sandstones and clays (Jones, 1948; Kogbe,1981). The group includes a band of pisolitic and nodular clays and contains silicified wood but is otherwise unfossiliferous. Laterites and lateritic ironstones form a resistant capping on top of the grits.

The Gundumi Group is also an unfossiliferous set of false-bedded clayey grits and clays, with basal conglomerates. The clays and grity sands represent the various changes in the dynamic conditions prevailing within the depositional environment.

2.3.3 The Maastrichtian deposits

The second phase in the depositional history of the Sokoto Basin sediments started during the Maastrichtian when the marine Rima Group was deposited unconformably on pre-Maastrichtian continental beds. Three formations namely Taleka, Dukamaje and Wurno Formations have been identified to belong to this group (Kogbe, 1981). Principally these formations are composed of fine grained sandstones, mudstones and clays in which is intercalated an important band of shales and limestones.

2.3.4 The Late Palaeocene Deposits

The late Palaeocene sediments called the Sokoto Group was the next in succession, and is made up of the Dange, Kalambaina and Gamba Formations. These formations form an outcrop band about 20 km wide near

the border with Niger Republic, but which narrows rapidly southwards and almost pinches out at Jega (Figure 2.2).

2.3.5 The Eocene - Miocene Deposits

The set of grits and massive white clays with sandstone and mudstone intercalations which overlies the marine Sokoto Group belong to the Gwandu Group (Brynmer, 1948; Kogbe, 1981). These sediments outcrop extensively in Niger Republic and northern Benin, where they are referred to as "Gres du Moyen Niger" and have been correlated with sediments of Miocene - Pliocene age in Central African Republic and in Mauritania, where they are known as the "Continental Terminal". The non-marine origin is certain and the sediments can be attributed to a lacustrine environment (Kogbe, 1979, 1981).

2.3.6 The Lateritic and Ferruginous Deposits

Capping the sediments over extensive areas of the basin are ferruginous deposits which have been subdivided into three major groups namely; ferruginous oolites, crusty - concretionary laterites, and ferruginous sandstones (Kogbe, 1981). These groups of sediments whose occurence is widespread in the Iullemmeden Basin are generally considered to be of primary origin, and attain a thickness of between 3-5 m in the Sokoto Basin area.

2.3.7 Faults and Folds

In the Sokoto Basin the Basement Complex and its supracrustal cover of Younger Metasediments were subjected to two phases of tight isoclinal folding during the Pan African, which are responsible for the N-S trending structures common over much of Nigeria (McCurry, 1976). A series of transcurrent faults have also been observed to affect the basement rocks adjoining the basin. Wright (1968) and Ball (1980) have both identified a system of NE-SW and NW-SE conjugate pair of fractures which exist everywhere within the Pan African Mobile Belt. Wright (1976) suggested that these fracture systems represent important lines of weakness in the continental crust and could be loci of economic mineralization. Ball (1980) attributes this conjugate strike-slip system to brittle deformation during the latter part of the Pan African orogeny. He argues that the geometry is very consistent over large areas and that this may infact be reflecting the stress field operative during the indentation of the Pan African Mobile Belt by a more rigid West African Craton. The sediments in the basin were not subjected to any remarkable degree of faulting as only some WSW - ENE trending faults have been observed in the vicinities of Dange and Gilbedi villages (Kogbe, 1981).

2.3.8 Economic Geology

The most important economic deposits in the Sokoto Basin are clays, ironstones, laterites, limestones, gypsum and gravels. Others include lignite, phosphates and salts, and the presence of radioactive minerals is also probable.

The occurrence of lateritic and ferruginized sandstone is widespread throughout the basin, and these have been utilised mainly for road construction purposes. Limestone deposits from the Palaeocene formations around Sokoto are already being utilised for the manufacture of cement. Also gypsum, which is an essential ingredient in the manufacture of cement occurs scattered within the Dukamaje and Dange shales. The Rima Group of sediments is rich in gravels, lignite and salt deposits. Most of these mineral occurrences are yet to be investigated in detail.

The aquifers within the basin provide the only source of water for the inhabitants during the long (October - May) dry season. A zone of permanent saturation has been established to be continuous throughout the basin and at shallow enough depths to be reached by the local shafts (Jones, 1948). A comprehensive investigation of these aquifers has been embarked upon by a collaborative effort of the GSN and other international government agencies and these efforts are continuing up to the present time (see for example Ogilbee and Andersen, 1965; Oteze, 1976 and JICA, 1989).

CHAPTER THREE

D A T A R E D U C T I O N

A. GRAVITY DATA

3.1 Introduction

The gravity data was obtained during three separate field trips undertaken in February 1986, January 1987 and May 1987 respectively using a LaCoste & Romberg Model G gravity meter #G-446. Station elavations were determined alongside the gravity measurements by means of three Wallace and Tiernan model FA181 aneroid altimeters.

The readings obtained from gravimeter measurements at stations are usually in arbitrary units (scale readings), and represent gravity differences between an arbitrary reference point and the field stations. Also these readings contain the effect of all masses of the earth's body, as well as the effect of the earth's rotation. Before such readings can be put to use, such as for geodetic, geologic, and geophysical investigations they must be converted to gravity values in milligals, brought to a specific standard, and corrected for various large scale influences (on the measured values), such as those due to the earth's rotation and flattening, which would otherwise mask the desired effects resulting from density variations in the upper layers of the earth.

3.2 Conversion of Instrument Readings to Gravity Values

The observed instrument readings were converted to gravity values using the calibration table contained in the Instruction Manual for the LaCoste & Romberg Model G gravity meter #G-446 (1976). The entire calibration table was read in as data into a computer program written by the author which converted all the counter readings to their corresponding gravity values in milligals.

The gravity values are then brought to a specific standard depending on the use to which the results will be put. For regional surveys such as this, it is necessary to make the data/results compatible with other surveys. The values were thus referenced to the International Gravity Standardization Net 1971, (IGSN 71), via a total of five first order gravity base stations of the Primary Gravity Network of Nigeria (Osazuwa, 1985), which were in turn linked with the IGSN 71 Kano base station (Number 955173), having an absolute gravity of 978120.773 mGals (Osazuwa, 1985).

3.3 Latitude Correction

The measured gravity always comprises of a systematically varying part which reflects the figure of the earth and a part relating to density variations of the upper layers of the earth (the object of most gravity surveys). The systematically varying part is a consequence of the increase in gravity from the equator

to the poles caused by the rotation and flattening of the earth.

The gravity at sea level at any latitude is given by the international gravity formula. Changes in the values of certain parameters of the reference ellipsoid in the international formula, such as the equatorial and polar radii, have led to the adoption of slightly different formulae over the years for the computation of the normal gravity. These include:

1930 International Gravity Formula (IGF):

$$\gamma_\Phi = 978.049(1+0.0052\sin^2\Phi - 0.0000059\sin^2 2\Phi) \quad ...3.1(a)$$

1967 Geodetic Reference System (GRS 67) Formula:

$$\gamma_\Phi = 978.031846(1+0.0052788\sin^2\Phi - 0.000023462\sin^4\Phi) \quad 3.1(b)$$

and 1980 Geodetic Reference System (GRS 80) Formula:

$$\gamma_\Phi = 978.03267715(1+0.0053024\sin^2\Phi - 0.0000058\sin^2 2\Phi) \quad 3.1(c)$$

where γ_Φ is the gravity value in Gals at latitude Φ.

To ensure compatibility with other surveys in the country, the 1967 Geodetic Reference System (GRS 67) formula was used to reduce the data for this survey. The calculated value known as the theoretical gravity value or normal gravity is usually subtracted from the observed gravity in order to obtain the gravity anomalies.

3.4 Free-air Reduction

Gravity stations on land are usually at elevations above sea level. The gravity value at such stations are thus lower than the sea-level values because of the decrease of gravity with elevation. In free-air reduction, observed gravity at elevation h is reduced to its sea-level equivalent on the assumption that topographic masses are displaced vertically down to sea level. The reduction is in effect the difference in gravity on the geoid and at elevation h in free air. The reduction is given by the expression

$$\delta_F = 2g_m (h/r)(1-3/2(h/r) + ...) \quad .... \quad 3.2$$

where g_m is a mean value of gravity over the earth; h is the elevation above sea level, and r is the earth's radius. The second term gives approximately 0.3 mGals for an elevation of 2 km, and was thus omitted as elevations were not above 700 m (Dehlinger, 1978).

For greater accuracy, the slight decrease of the vertical gradient of gravity with latitude was not neglected. When this variation is taken into account, the free-air reduction (eqn. 3.2) becomes

$$\delta_F = (0.30877-0.00044\sin\Phi)h-0.073H^2 \quad ... \quad 3.3$$

where Φ is the geographic latitude, h is the elevation in meters, and H is the elevation in kilometers (Heiskanen and Vening-Meinesz, 1958).

3.5 Bouguer Reduction

Gravity is increased by the attraction of the mass between the station elevation and the datum plane (usually the sea level). The vertical component of attraction exerted by this mass is the Bouguer reduction, which is usually subtracted from the observed gravity to reduce the value to sea level.

Attractions produced by masses above sea level can be approximated on three different assumptions namely:

i. the simple Bouguer reduction - in which the mass above sea level is represented by an infinite horizontal slab whose thickness is the height of the station above the datum.

ii. the Bouguer reduction with terrain corrections - in which the top surface of the horizontal slab has the shape of the surrounding terrain.

iii. the expanded Bouguer reduction - in which a slab, whose upper surface represents the actual terrain, has the curvature of the earth.

The simple Bouguer reduction was applied with an assumed average crustal density of 2.67 x 10 kg m for the slab. In cylindrical coordinates the reduction for a slab of constant density (with origin of coordinates at the station) is given by (Dehlinger, 1978)

$$\delta_{BS} = G\rho \int_0^{2\pi} \int_0^{h} \int_0^{\infty} \frac{z r dr dz d\theta}{(r^2 + z^2)^{3/2}} \qquad \ldots 3.4$$

On integration this yields

$$\delta_{BS} = 2\pi G\rho h \qquad \ldots 3.5$$

in which h, the slab thickness, is the station elevation or height above the datum and G is the gravitational constant. However the effect of the horizontal slab of thickness h was replaced by that of a spherical segment of inner radius R, equal to the earth's mean radius, and external radius (R+h), and bounded by a cone of spherical radius $=1^{o}\ 29'\ 58''$ (which corresponds to the external radius of Hayford's O_2-zone), hence the reduction was further modified by the Bullard's term

$$B = 2\pi G\rho h \frac{(R+h)\cos\theta - R}{\sqrt{\{(R^2 + h^2)^2 + R^2 - 2(R+h)R\cos\theta\}}} \quad \ldots 3.6$$

3.6 Other Corrections

Some environmental factors also affect the gravimeter and gravimeter readings to an extent that if these are not corrected for, the accuracy of the gravity measurements will be severely reduced. These include:

3.6.1 Tidal Effect

The attraction of the sun and the moon on the earth makes the force of gravity at a point on the earth to vary with time and latitude. Goguel (1954), showed that the necessary tidal correction can be expressed as

$$c = P + N\cos\phi(\cos\phi + \sin\phi) + S\cos\phi(\cos\phi - \sin\phi) \quad .. 3.7$$

where P is the correction required at the pole and is usually ignored in gravimetric prospecting measurements, and Φ is the latitude. The quantities N and

S are corrections at latitudes 45° N and 45° S respectively. These are given on a daily basis at hourly intervals to an accuracy of 5 mGals in tables published yearly by the European Association of Exploration Geophysicists. Linear interpolations were carried out to obtain intermediate values of N and S between their hourly values. Also the effect of the deviation of the longitude of the gravity stations from the central meridian of the time zone (15° E for Nigeria) was incorporated in the correction. A subroutine written by Osazuwa (1984), was used to compute the tidal correction c, with the aid of Tidal Gravity Corrections tables for 1986 and 1987 (EAEG, 1985, 1986); and the corrections added to the observed gravity values in order to eliminate the variation due to tidal effects.

3.6.2 Drift Correction

All gravity meters are known to have some drift or time variation arising from small mechanical changes in the instruments' springs and associated mountings. These variations called meter drifts, produce measurement errors which can be large compared with the gravity variations of interest. Consequently the gravity measurements were made in such a way that corrections can be made for meter drifts. Measurements along a traverse began at a base station, and this base

station was revisited after a short interval (not exceeding three hours), in order to monitor the drift behaviour of the instrument.

A linear drift was assumed in each interval, and the drift rate, μ, was computed using the formula:

$$\mu = \frac{(g_{A2}-g_{A1}) - (g_{02}-g_{01})}{t_2 - t_1} \quad \ldots 3.8$$

where g_{A2} and g_{A1} are the absolute gravity values at the terminating stations of the loop, and g_{02} and g_{01} are the corresponding observed gravity values at these stations at times t_2 and t_1 respectively. To refer any intermediate observation made at time t_s to the time t_1, the required drift correction is given by:

$$\delta_s = \mu(t_s - t_1) \quad \ldots 3.9$$

An algorithm developed by Osazuwa (1984) which carries out the drift correction was used to correct the meter readings for drift.

3.6.3 Terrain Correction

This correction which allows for surface irregularities in the vicinity of the gravity station requires a good topographic contour map of the survey area for its computation. The terrain correction was not carried out in this survey because there was no contoured topographic map for the area. However using the elevations of the gravity stations, terrain correction was attempted for some of the stations but

it was found that the contribution to the Bouguer anomaly from this factor, out to zone M of the Hammer terrain correction chart, (Hammer, 1939) was zero because of the small elevation differences. Thus the terrain in the vicinity of the gravity stations was considered generally flat, so the simple elevation correction applied is assumed to provide adequate compensation for topographic effects.

3.7 Gravity Anomalies

When the observed gravity has been corrected for the effects of the environmental factors listed above, two basic gravity anomalies are recognized and these are distinguished by the gravity reductions which has been applied to the observed gravity g_{obs}. These are:

i. the Free-air anomaly - obtained when the free-air reduction has been applied to the observed gravity and this is defined as

$$\Delta g_F = (g_{obs} + \delta_F) - \gamma_\phi \qquad \ldots 3.10$$

ii. the (simple) Bouguer anomaly - obtained when Bouguer reduction combined with the free-air reduction and terrain correction, (where applicable) are applied. This is defined as

$$\Delta g_{BS} = \{g_{obs} + \delta_F - (\delta_{BS} + B)\} - \gamma_\phi \qquad \ldots 3.11$$

A third anomaly, isostatic anomaly, is also distinguished mainly in large scale gravity surveys when isostatic correction has been applied to account for large scale density variations within the crust. In this survey, this correction was not applied because of the generally flat topography and the relatively

small area (approximately 60,500 km^2) covered by the survey.

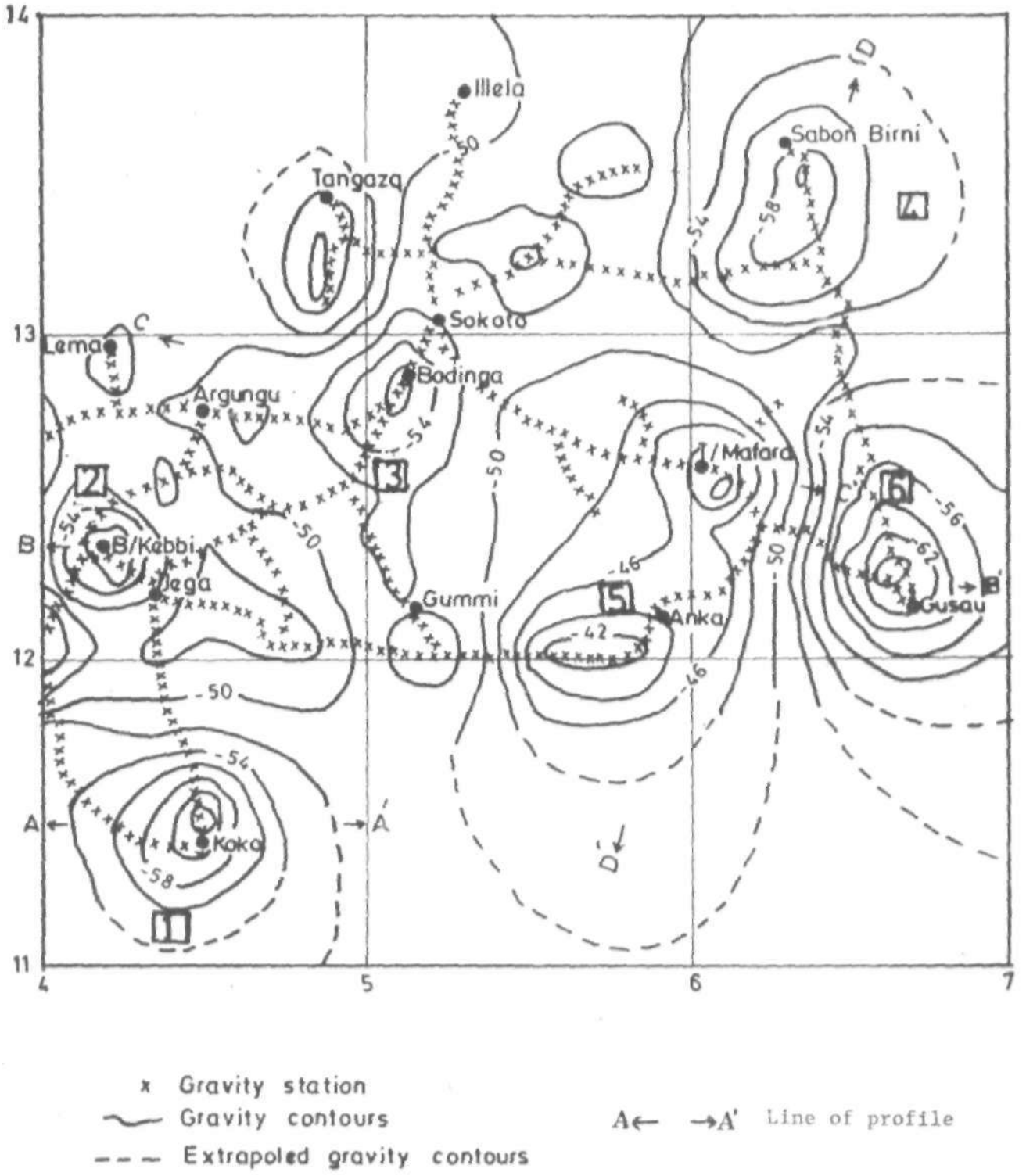
The gravity anomalies, (equations (3.10) and (3.11)), resulting from the data reduction exercise are usually presented as maps of gravity isoanomalies. Manual preparation of such maps can be very subjective and time-consuming especially if the station density is not adequate. On the other hand, graphical processing of geophysical data by means of a computer is often based on a set of values of a function at points on a regular grid. The function which in this case is the gravity field anomaly f(x,y), can as in most regional surveys be distributed irregularly, thus necessitating an operation which has been labelled 'regularization' or 'gridding' (Baranov, 1975; Paterson and Reeves, 1985). A software package from the Golden Software Inc. of the United States of America was utilised for gridding and contouring of the gravity data on the IBM PC/AT to produce the Bouguer anomaly map (Figure 3.1).

3.8 Accuracy of the Bouguer Gravity Anomaly

Several factors which could introduce errors in the computed Bouguer anomalies include the completeness of the formulae used and the correctness of the numerical values of the constants occuring in them. For example there could be

i. error in the calibration factor of the instrument used,

ii. error due to non incorporation of terrain correction, and



x Gravity station

~~ Gravity contours

--- Extrapoled gravity contours

A← →A' Line of profile

Fig. 3.1 Bouguer anomaly map of the survey area. (Contour interval 2 mGals)

iii. error due to wrong assumption of mean crustal density for the Bouguer correction.

The calibration factor of the modern LaCoste & Romberg gravity meters depends only on the quality of the measuring screws and the lever system, both of which are accurately calibrated over their entire range (LaCoste & Romberg, 1976). Thus the calibration factor does not change perceptibly with time, which eliminates the need for frequent checks of calibration (LaCoste & Romberg, 1976). Any errors arising from this factor are thus thought to be negligible. Similarly errors due to non incorporation of terrain correction are considered insignificant because of the reasons adduced in section 3.6.3. With respect to the third factor, an assumed average crustal density of 2.67×10^3 kg m^{-3} was used for the Bouguer correction, while the measured mean density of the basement rocks was 2.70×10^3 kg m^{-3}. There was thus a difference of 0.03×10^3 kg m^{-3} between the assumed and 'actual' values which for the elevation range of 313 m over the area could contribute a maximum error of about 0.39 mGal.

In addition, it is necessary to assess the effect of random errors of the parameters of the formula, the values of which are determined separately for each gravity station. These parameters include the measured gravity value g, the geographic latitude ϕ, and the station elevation h.

From repeated readings of the measured gravity at a number of control stations, it was found that the

gravity value at any station is accurate to within 0.11 mGal. The gravity stations were plotted on a 1:500,000 base map to an accuracy of ±500 m because of the difficulties discussed in section 1.4, and the latitudes of these stations were obtained by superimposing a regular grid on the base map and this could be in error by as much as 250 m. Thus the total positional error of about 750 m at each station would introduce a maximum error of 0.28 mGal in the gravity value if the error occurs in a N-S direction for a station at the most northerly latitude (13.75° N). Inaccurate determination of station elevation is often the major source of error in any gravity survey, especially when station elevations are determined with altimeters. In this survey all necessary precautions were taken to reduce the level of error in station elevation by ensuring ties to survey benchmarks scattered along roads in the survey area. It was thus possible to determine the elevation of most of the gravity stations to an accuracy of ±3 m. The maximum error in the Bouguer anomaly due to this elevation inaccuracy amounts to about 0.6 mGal. Using the same altimeters in a different survey in other parts of northern Nigeria Verheijen and Ajakaiye (1980) reported an inaccuracy of ±5 m in station elevation; which is about the same order of magnitude as for this survey. Taken together, these different sources of error would thus introduce a standard error of about 0.78 mGal in the value of the Bouguer anomaly at each station.

B. DENSITY DETERMINATION

3.9 Sampling Technique

Gravity anomalies of interest in geophysical exploration surveys usually result from variations in density of materials within the uppermost 5 km of the earth's crust (Grant and West, 1965). Thus an accurate determination of the densities of near surface rocks within a survey area forms an essential component of a gravity survey especially when quantitative interpretation of the gravity anomalies is to be attempted. To this end, rock samples were collected both during the gravity measurements and in a separate field trip undertaken after the gravity measurements and devoted solely to rock sample collection for laboratory determination of average formation densities. Samples were usually knocked off from outcrops along gravity traverses and in special cases samples were obtained from quarries and cuttings at the type localities of the sedimentary formations, such as at the quarry of the Cement Factory at Kalambaina near Sokoto, the local gypsum mining pits at the outskirts of Wurno village and water-well diggings at Dange village. A total of 196 rock samples were collected and identified from the whole area; 64 from the basement rocks of the adjoining schist belt region, and 132 from the three main sedimentary sequences that filled the basin in the survey area.

3.10 Method of Density Determination and Analysis

The bulk density ρ of each rock sample was estimated using Archimedes Principle

$$\rho = \frac{w_a}{w_a - w_w} \qquad \ldots 3.12$$

where w_a is the weight of the sample in air and w_w is the weight of the sample when fully immersed in water. Using a Mettler Balance model P515 with an accuracy of 1.0×10^{-3} kg both the dry and wet densities were determined, and the mean of these two was taken as the representative sample density. The mean density and standard deviation were then computed for each of the major rock types as depicted in Table 3.1.

For purposes of quantitative interpretation the observed mean density of 2.70×10^{3} kg m^{-3} was adopted as the 'true' bulk density of the migmatite-gneiss complex which is considered to be the host rock of the basement complex in this region. Other rocks of the basement complex whose outcrops coincide with gravity anomalies of interest are the Older Granites and phyllites. The Older Granites were also assigned the observed mean density of 2.64×10^{3} kg m^{-3}, but for the phyllites the observed mean density of 2.58×10^{3} kg m^{-3}, could not be used because of the highly fractured and weathered nature of the samples which yielded this low mean value. Also Figure 4.5 revealed a positive residual anomaly (no. 5) at the location where this phyllite is outcropping. This suggests that the density of the phyllites at this location is higher

Table 3.1: Densities of rocks sampled in the survey area.

Period	Formation or Group	Lithologic Unit	No.of Samples	Range of Densities (10^3 kg m^{-3})	Mean Density (10^3 kg m^{-3})	Standard Deviation (10^3 kg m^{-3})
Precambrian	Basement Complex	Phyllites	20	2.39-2.78	2.58	0.120
		Gneisses	18	2.59-2.79	2.70	0.050
		Quartzites	4	2.59-2.63	2.62	0.016
		Amphibolite	7	2.76-2.98	2.88	0.040
		Migmatites	8	2.64-2.73	2.70	0.028
		Older-Granites	7	2.62-2.65	2.64	0.005
Cretaceous and Tertiary Sediments	Gundumi Formation	Ferruginized sandstone	44	2.22-2.95	2.65	0.175
	Rima and Sokoto	Ironstone	16	2.53-3.14	2.97	0.225
		Shale	11	1.49-2.19	1.87	0.105
		Limestone	38	2 24 2.65	2.44	0.044
	Gwandu Formation	Silty Sandstone	14	1.94-2.11	2.03	0.047
		Ironstone	9	1.77-2.21	2.05	0.147

than that of the host rock which is the migmatite-gneiss complex whose density was .pa observed to be 2.70×10^{3} kg m^{-3}. Thus a density of 2.78×10^{3} kg m^{-3}, which is the upper limit of the measured range of densities for the phyllite samples (Table 3.1), was considered to be a more realistic density for the phyl'ites and utilised for the quantitative interpretation.

The adopted density values are comparable with these determined for similar rock types in other parts of the schist belt of northern Nigeria, such as Udensi et al. (1985) who obtained a value of 2.63×10^{3} kg m^{-3} for the Older Granites, 2.70×10^{3} kg m^{-3} for gneisses, 2.70×10^{3} kg m^{-3} for migmatites, and 2.78×10^{3} kg m^{-3} for fresh phyllite samples obtained from a quarry blast. Also Gandu et al. (1985) obtained a value of 2.63×10^{3} kg m^{-3} for the Older Granites, 2.78×10^{3} kg m^{-3} for the schists, 2.69×10^{3} kg m^{-3} for the migmatites, and 2.70×10^{3} kg m^{-3} for the gneisses. Similar results have also been reported by Adeniyi (1987) and Oladosu (1987) in other gravity surveys within the basement block of northern Nigeria.

For the sediments, the difficulties posed by the widespread lateritic cover and the unconsolidated nature of some of the samples collected, made it unrealistic to assign separate densities to the various formations mapped in the basin. The Ille Formation, for example did not outcrop in any area covered by the

gravity stations because of this lateritic cover, and as such no samples of this major formation was obtained. Kogbe (1979) reported that all the sediments within the basin were very shallow; the estimated maximum thicknesses ranging from 350 m for the Gundumi Formation to just 84 m for the Gwandu Formation. It was therefore considered more reasonable to adopt a single mean density of 2.34×10^3 kg m^{-3}, which was obtained from all the samples for the quantitative interpretation.

This mean value of 2.34×10^3 kg m^{-3} appears low when compared with a density of 2.51×10^3 kg m^{-3} obtained by Ojo and Ajakaiye (1976) as the mean density for the sediments in the Nupe Basin, and 2.52×10^3 kg m^{-3} obtained by Osazuwa et al. (1981) for the Gombe sandstone in Upper Benue Trough. Also Ajayi and Ajakaiye (1981) published values ranging from 2.42×10^3 kg m^{-3} to 2.56×10^3 kg m^{-3} for the Cretaceous sandstones of the Benue Trough. No estimates of the density of any shale samples were reported in any of the references cited above, but Grant and West (1965), gave a very wide range of between 1.93×10^3 kg m^{-3} and 2.72×10^3 kg m^{-3} for shales generally. The shale samples of the Rima and Sokoto Groups and the silty sandstone and ironstone samples of the Gwandu Formation were in a highly unconsolidated state and their observed densities in Table 3.1 were thought to be low and not truely representative of the densities of these

formations at depth. Thus when the densities of the shale and Gwandu sandstone and ironstone samples were excluded, the mean density of the remaining samples became 2.55×10^{3} kg m^{-3}, which was also utilised in the quantitative interpretation to produce the alternative models.

C. MAGNETIC DATA

3.11 Data Source

The Geological Survey of Nigeria (GSN) commissioned Hunting Geology and Geophysics Ltd of Canada to carry out airborne geophysical surveys of parts of the country, including a low-level aeromagnetic survey for which flying was completed in July 1975. Final contour maps of the total magnetic intensity were produced as part of GSN Airborne Geophysical Series in 1976 on a scale of 1:100,000 in half degree by half degree sheets for the Sokoto Basin area.

Thirty of these maps covering the entire basin lying within the area bound by Latitude 10.5^{o} to 14.0^{o} N and longitude 3.5^{o} to 6.5^{o} E were acquired for this project by kind permission of the Geological Survey of Nigeria. From these maps it was deduced that the nominal flight altitude was 500ft (152.4 m) above terrain, while the nominal flight line and tie line spacings were 2 km and 20 km respectively. Over the Sokoto Basin the flight line direction was mainly $150^{o}/330^{o}$ while the tie line direction was $60^{o}/240^{o}$. Regional correction was based on IGRF (epoch date 1st January, 1974). It is of interest to note that the orientation of the flight lines is approximately perpendicular to the NE-SW strike of the basin, and as such the most accurate and useful picture of the magnetic anomalies over the region would be obtained.

3.12 Compilation

The compilation of the composite magnetic anomaly map of the entire basin was based on the thirty $\frac{1}{2}^{o} \times \frac{1}{2}^{o}$ contour maps of total magnetic intensity mentioned above. The recovery of digital data from the contour maps included the following operations:

1. digitization,
2. gridding/interpolation,
3. recontouring, and
4. merging.

3.12.1 Digitization: The magnetic isoline intercepts along every flight line on each map were digitized using a computer program Aerodig (Dyrelius, 1983). On the click of the morse, the program automatically records the field value at each intercept together with a transformation of the arbitrary coordinates of the digitizing table to geographic coordinates (latitude and longitude). The data thus generated are stored in files by geographic coordinates and total field values, as well as the map sheet-number and flight line number for easy reference. These files constitute the basic units for the magnetic data bank. On the average about 1,500 line kilometers of aeromagnetic data were analysed for each full $\frac{1}{2}^{o} \times \frac{1}{2}^{o}$ sheet.

This method was considered to be the most accurate way of recovering the original total field data since the recorded digital data is not available (Deds et al., 1985). It is an order of magnitude more accurate than the method of super-imposing a regular

grid on contour maps which was used by earlier workers (Tunyi, 1984; Ajakaiye et al., 1985, and Nwogbo, 1987). The latter method usually involved a lot of manual interpolation and is consequently more prone to computational errors and definitely more laborious.

3.12.2. Gridding: The data from each sheet was transformed into a regular grid using a computer program Interpol (Klingele and Dyrelius, 1972), which is based on La Porte's method of regularization (Baranov, 1975). The basis for the method is parabolic interpolation, and a detailed discoussion of the method is given in Appendix A. A search radius of 0.1 latitude degree (11 km) was used, and the grid size was 0.01 latitude degree (1.1 km x 1.1 km) thus creating a 51 row by 51 column grid or approximately 2,600 grid positions for each sheet. A tolerance of ten percent was allowed for grid point values before masking.

In order to ensure that the data at the boundary of adjacent sheets are compatible (a necessary condition for a successful excution of the next stage), it was necessary to include part of the data from all surrounding maps in interpolating near sheet boundaries. An extra margin of 0.15 latitude degree (16.5 km) was included from adjacent sheets at each boundary. As can be seen from the illustration in Figure 3.2 the input to the interpolation program for each map thus comprised data from a total of nine maps. The actual data utilised are these contained within the

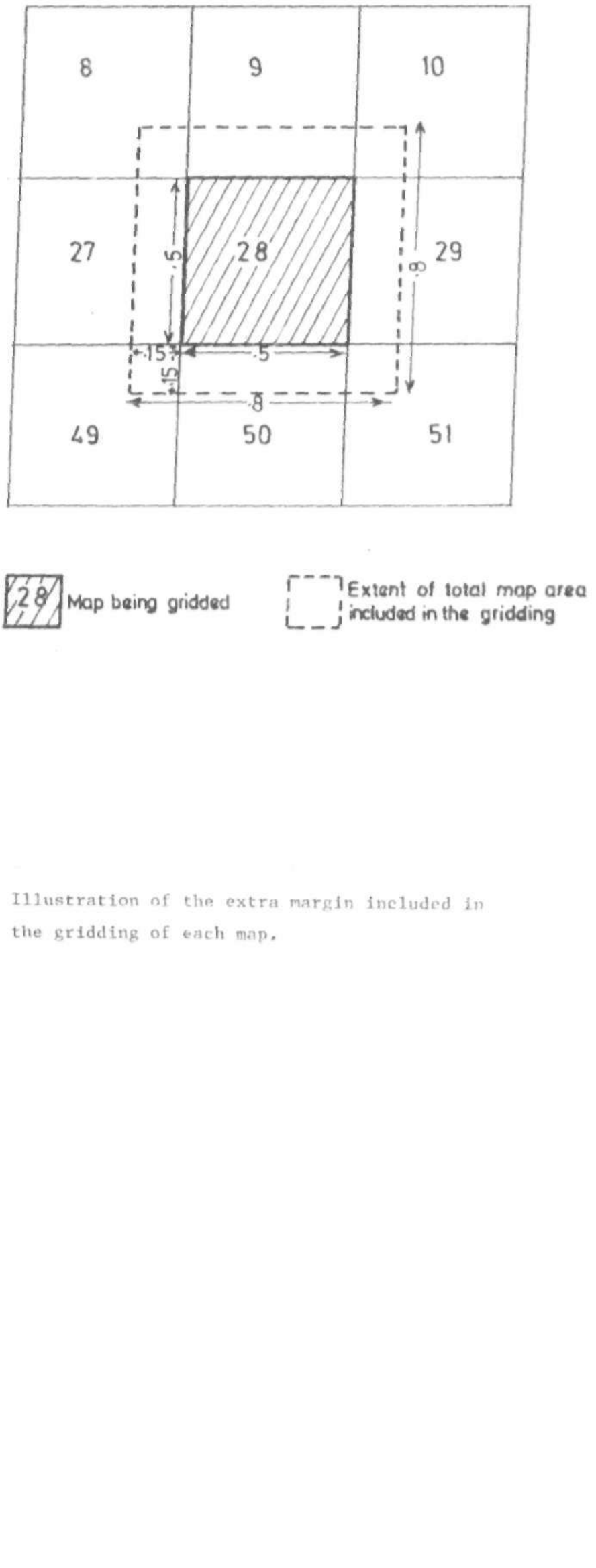


Fig. 3.2 Illustration of the extra margin included in the gridding of each map.

0.8 x 0.8 degree dashed rectangle. In this way it was ensured that the last row/column in a sheet is identical to the first row/column of an adjacent sheet at all boundaries, and vice versa.

3.12.3. Recontouring: The gridded aeromagnetic data generated above was machine contoured using the program Isorev (Klingele and Dyrelius, 1972). The map produced was compared with the original contour map, and any errors/inconsistences resulting from either the digitization or gridding of the data were corrected and the map recontoured. This step was repeated until an accurate map was reproduced. Different grid sizes were tried, and a comparison of the different contour maps showed that the 1.1 km x 1.1 km mesh was most suitable for the purpose of producing the composite map at the desired scale as no further details could be gained by using a smaller grid size.

3.12.4. Merging: The gridded data for the individual sheets were then combined into a master grid for the entire basin using a computer program Combin written by the author. The master grid which represent the total intensity magnetic anomaly field over the basin forms a vital magnetic data bank for this area. It is useful for machine contouring over a wide range of scales and contouring intervals, and also for quantitative analyses, because both the digitizing and gridding operations ensured an accurate recovery of the original total field data. A machine contoured composite

magnetic-anomaly map was then produced from this master grid at a scale of approximately 1:900,000 and contour interval of 20 nT on a Calcomp electro-static plotter (Model 5825) at the Department of Solid Earth Physics, Uppsala University, Sweden. The map was then photographically reduced to the publication scale of 1:3,000,000 (Figure 3.3).

The same data set was utilised on another software package Geopak on a Tektronix 4696 plotter to generate a raster plot (Figure 3.4) at a scale of roughly 1:3,000,000 directly. The raster plot is essentially a variable back- and-white density plot. The format was chosen because density plots are less expensive and faster to produce. With proper choice of contour levels, such plots have immediate visual appeal and do not require close examination that contours do. Also when restricted to black-and-white format relative magnitudes on the plots are more easily discernible.

3.13 Discussion

The advantages of the composite magnetic-anomaly maps (Figures 3.3 and 3.4), and the regional set of digital data produced by the processes discussed above are numerous and obvious. One outstanding advantage is the fact that such a map provides geoscientists with an overall picture of the structure of a large area, even though boundaries may be obscured by overburden. Such maps reveal major magnetic divisions/provinces which may not be recognized in the field if small areas are

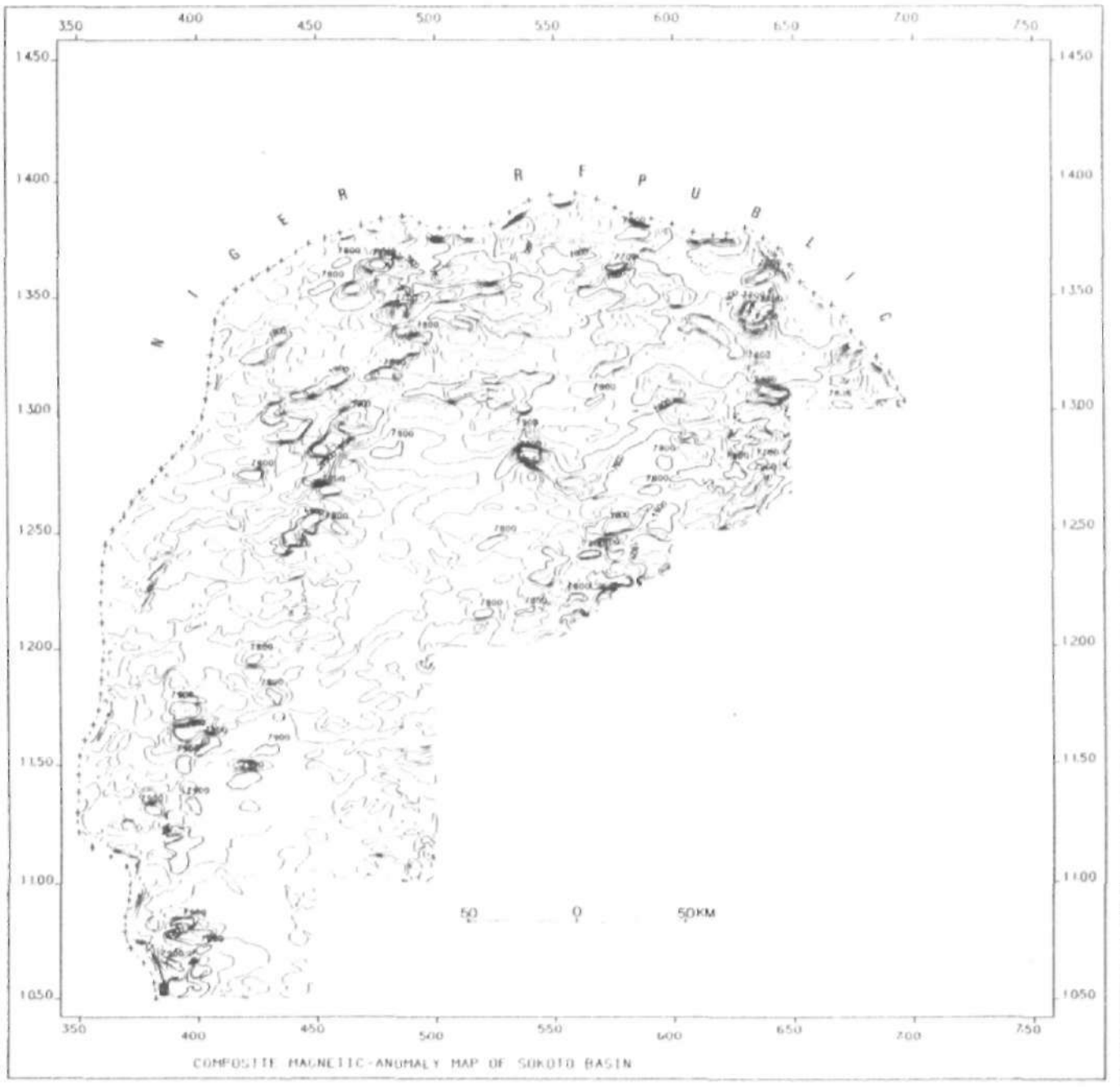


Fig. 3.3 Total magnetic field intensity contour map of Sokoto Basin. Contour interval is 20 nT. Field values are relative to a 25,000 nT base. (Photo - reduction of map compiled at a scale of 1:900,000)

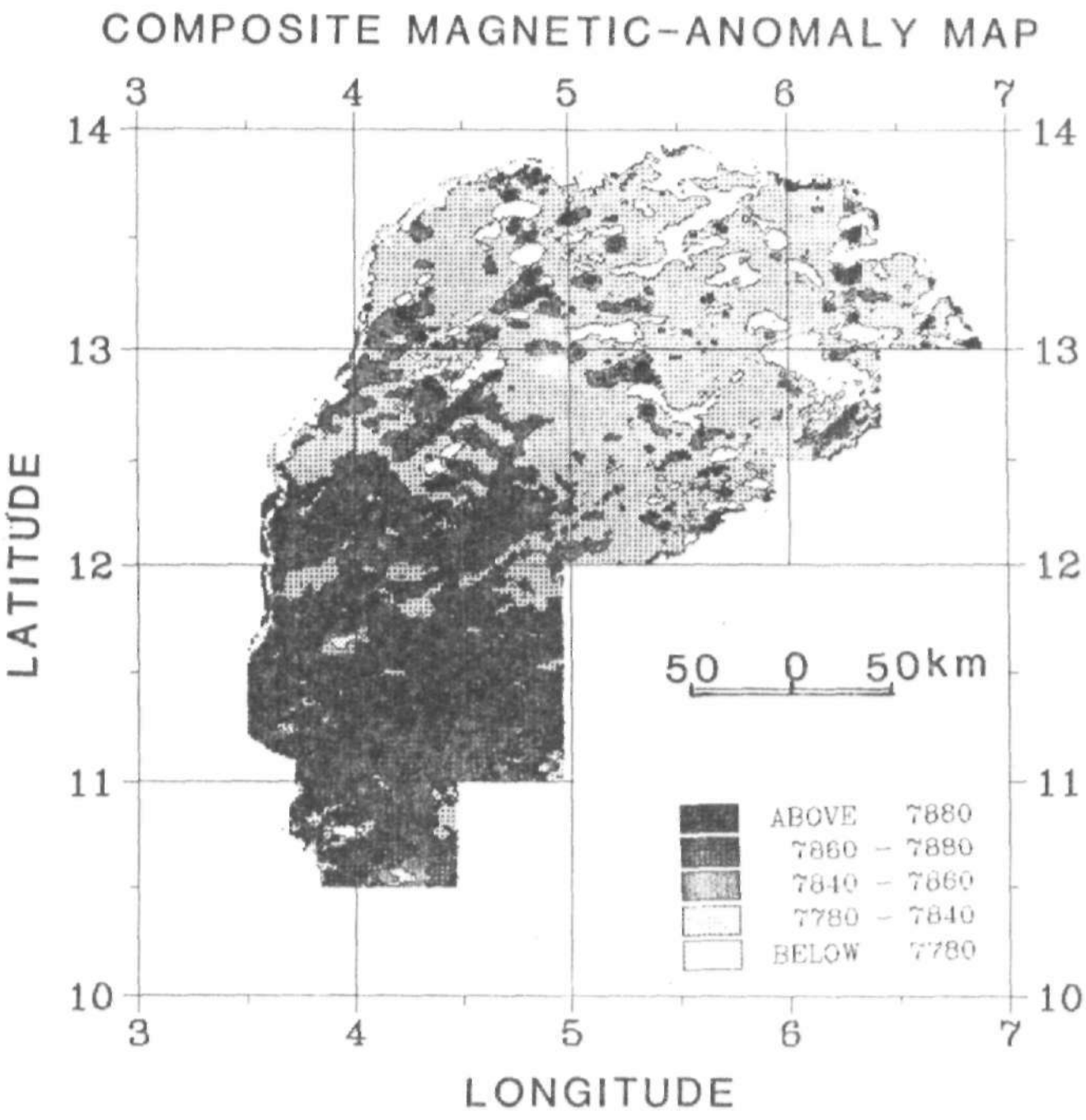


Fig. 3.4 Density plot of total magnetic field intensity over Sokoto Basin.

mapped, and is thus useful in mineral or oil exploration programs. The value of the compiled composite magnetic-anomaly map of the Sokoto Basin is bound to increase as more data on the geology of the basin become available. The task of compilation was greatly facilitated by the fact that the flight operations over the region were uniform, and as such problems associated with adjustment of data to a common datum or elevation did not arise.

CHAPTER FOUR

G R A V I T Y I N T E R P R E T A T I O N.

4.1 Introduction

Two main problems have been identified in gravity interpretation, and these can be summarized as follows:

i. the problem of separating the effects that are associated with geological features of interest from those features which are not of interest, and

ii. the problem of analysing the anomalies of interest once they have been separated from others (Skeels, 1967).

The first problem is commonly termed regional-residual separation and is thus intimately related to the second in that the anomalies of interest should first be isolated before they can be analysed. The second problem is concerned with choosing from a large number of possible geophysical models those which are most compatible with geological and other information at the interpreter's disposal.

ASHIM IBRAHIM LIBRARY
AHMADU BELLO UNIVERSITY
ARIA, NIGERIA.

4.2 The Bouguer Anomaly Map

The Bouguer anomaly map, Figure 3.1, shows that the survey area is characterised by negative Bouguer anomalies in the range of -64 to -42 mGals, with a mean value of -51 mGals. No definite regional trend is immediately apparent on this map, which is probably due to the effect of local shallow structures.

Within the basin area, the map reveals a number of isolated relative gravity lows in the vicinities of

Koko, Birni Kebbi, Bedinga and Saben-Birni villages, and these have been numbered 1, 2, 3, and 4 respectively for easy reference (Figure 3.1). At the eastern boundary of the basin at Talata Mafara, there is a roughly N - S striking relative gravity high which has been numbered 5. A rather steep gradient of about 0.34 mGal km^{-1} separates this anomaly no.5 from another gravity low in the vicinity of Gusau town which has been numbered 6. A similar gradient is noticeable in the northwestern corner of the map between gravity low no.3 and an incompletely defined gravity high to the northwest.

The relative gravity lows within the basin could all be due to increased thickness of low density sedimentary rocks at basement depressions. The gravity high that marks the eastern margin of the basin could be due to a high density rock within the adjoining Anka Schist belt, while the low around Gusau is probably due to the Older Granite intrusives which are widespread in this area. The steep gradient could thus be indicative of a sharp contact between the granites and the surrounding basement rocks. A large portion of the basin, especially north of Argungu and west of Sokoto - Illela road, could not be adequately covered by gravity stations because of inadequate road network.

4.3 Regional - Residual Separation

Observed gravity anomalies usually represent the contributions from all anomalous masses within a given volume, from the grassroots down to the core. It is often desirable to separate attractions caused by regional features from those caused by pertinent local structures. Thus the observed anomaly can be sub-divided into a regional anomaly - representing the effects of broad and deeper regional structures of little or no concern in the analysis; and a residual anomaly - representing the effects of local narrow geological features with shallow origin and which are often the object of gravimetric prospecting surveys. Other definitions of the terms regional and residual anomalies abound in literature as noted by Nettleton (1954), and Skeels (1967) among others. The residual anomaly Δg_{res} is expressed as:

$$\Delta g_{res} = \Delta g_{B} - \overline{\Delta g} \qquad \ldots 4.1$$

where Δg_{B} is the (simple) Bouguer anomaly equation (3.11) and $\overline{\Delta g}$ is the regional effect.

The estimation of the regional effect is of critical importance in gravity interpretation in that it determines what is left for further analysis after its subtraction from the observed Bouguer anomaly. The various schemes which have been used in the past to estimate the regional effect have been categorised into two broad classes namely, the graphical systems and the numerical/mathematical systems, and their operators

commonly referred to as 'smoothers' and 'gridders' respectively. Nettleton (1954) concluded that none of these schemes provides a sound philosophical basis for separating potential field into regional and residual components because of the inherent ambiguity in the sources of potential field. Thus an interpreter often has to decide which of the local anomalies on the Bouguer gravity map are positive and which are negative.

In this work the method of least squares polynomial surface fitting was used to estimate the regional effect. An advantage of this technique is that it makes use of the original data points themselves in estimating the regional, thus eliminating the influence of any contouring errors in the Bouguer gravity map; and is also much faster provided a computer is available. The general equation for the polynomial used to approximate the regional effect is

$$G(x,y) = \sum_{i=0}^{n} \sum_{j=0}^{n-i} c_{ij} x^i y^j \qquad \ldots 4.2$$

where n is the degree of the polynomial and the c_{ij}'s are the coefficients to be determined. A computer program at the Department of Physics, Ahmadu Bello University, Zaria was used to estimate the regional effect by this technique.

In order to get a better estimate of the regional field, various efforts were made to obtain data from areas far beyond the present survey area. A positive

response came only from the United States Defence Mapping Agency Aerospace Center (DMAAC, 1988) which released to me the then latest version (May 1988 edition) of the $1^{\circ} \times 1^{\circ}$ mean free-air anomalies and elevations for the area between latitudes 5 and 20 degrees north, and longitudes 10 degrees west to 10 degrees east (Figure 4.1). The data set covered not only the entire Iullemmeden Basin but also the whole of the Nigerian land mass and other parts of the West African subregion. The $1^{\circ} \times 1^{\circ}$ mean Bouguer anomalies were generated from these two data sets using the equation (Wilcox, 1974):

$$\Delta g_B = \Delta g_F - 0.1119h \qquad .....4.3$$

where Δg_B = $1^{\circ} \times 1^{\circ}$ mean Bouguer anomaly (mGals)
Δg_F = $1^{\circ} \times 1^{\circ}$ mean free-air anomaly (mGals), and
h = $1^{\circ} \times 1^{\circ}$ mean elevation (m).

The Bouguer anomaly was then regridded to a 0.5 x 0.5 degree mesh in order to produce the Bouguer anomaly maps of Figure 4.2(a) and (b). Figure 4.2(a) covers the entire area of the data set from Figure 4.1, while Figure 4.2(b) covers only the Iullemmeden Basin area. The Bouguer anomaly map (Figure 4.2(b)) is characterised by two large negative gravity closures aligned roughly along a N-S axis. One of these marked A is located within the basement block of northern Nigeria, and the cause is neither obvious from surface geology nor has it been earlier investigated geophysically.

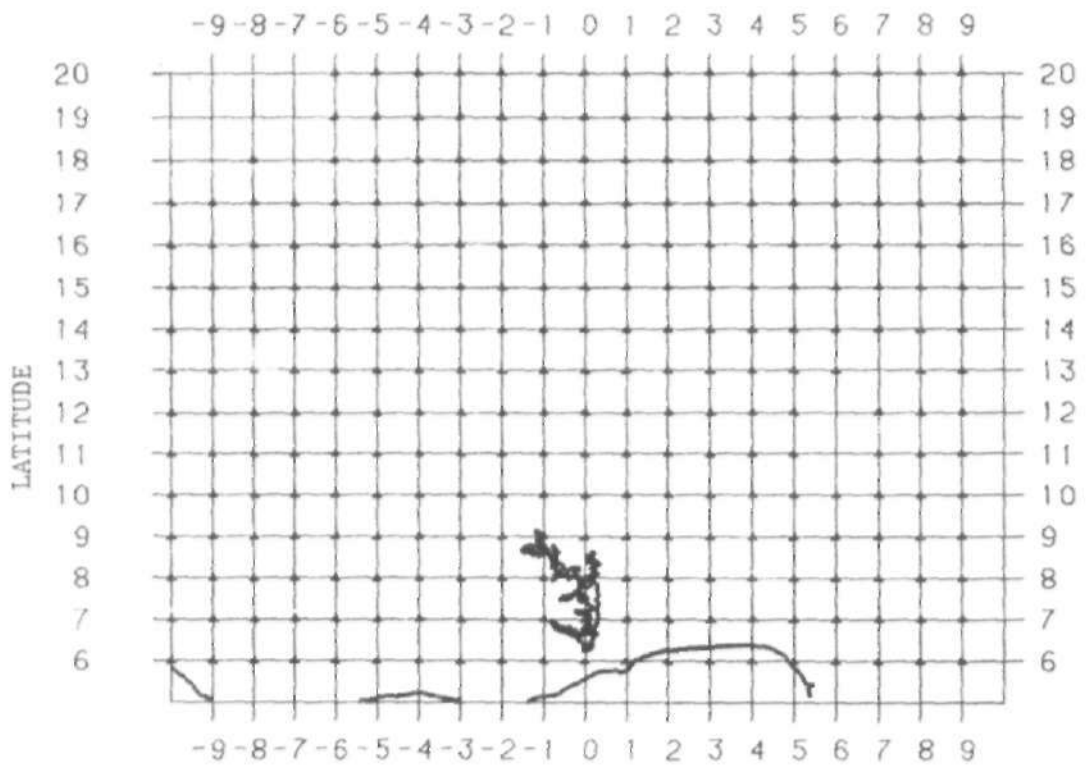
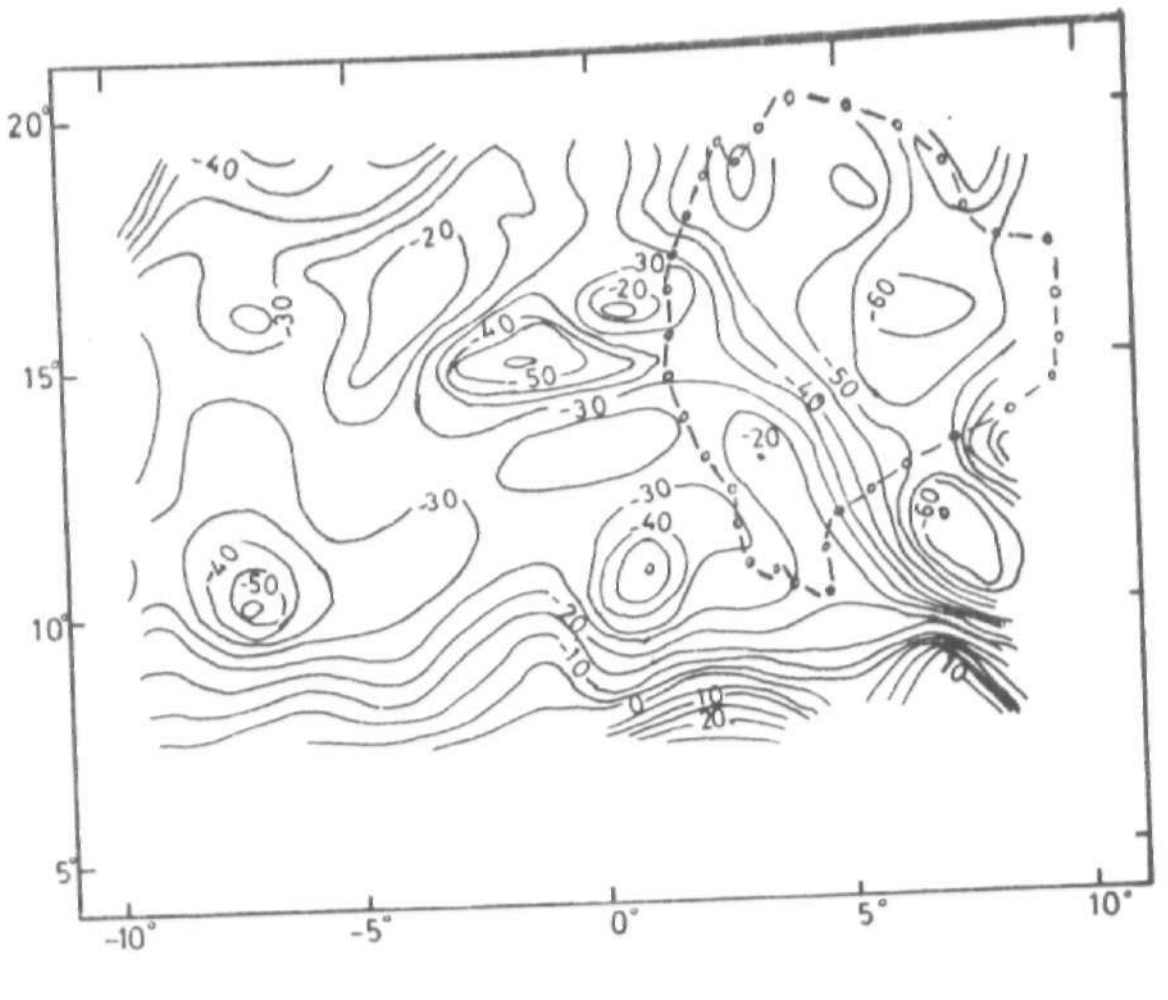


Fig. 4.1 Location map of the 1^{o} cells for the DMAAC data set.



—•—o—o Boundary of Iullemmeden Basin.

Fig. 4.2(a) Bouguer anomaly map of the Iullemmeden Basin and surrounding areas. (Contour interval 5 mGals).

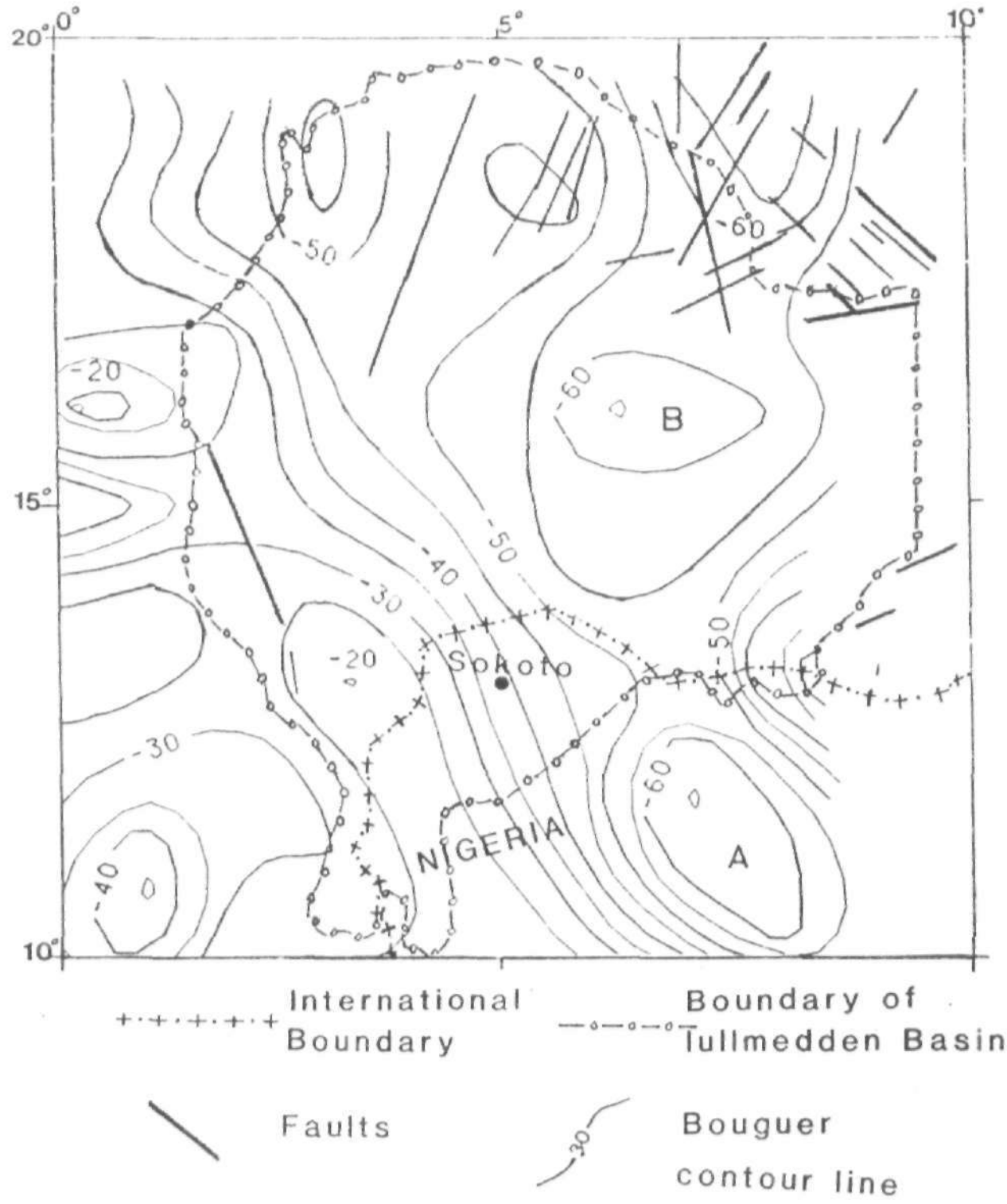


Fig. 4.2(b) Bouguer anomaly map of the Iullemmeden Basin area, superimposed on some tectonic features in Fig. 2.1 (Contour interval 5 mGals).

The anomaly marked B is located near the center of the Iullemmeden Basin inside Niger Republic, coincides with a depression of the basement surface shown in Figure 2.1. Over the Sokoto Basin area, the contours are smoothly varying and trend roughly NW-SE.

The regional gravity field derived by fitting a first degree polynomial to the DMAAC Bouguer anomaly data is shown in Figure (4.3). The map (Figure 4.3) is a plane dipping northeastwards at the rate of 0.01 mGal km^{-1} . Subtracting this regional effect from the observed Bouguer anomaly (Figure 3.1) gave the residual anomaly map shown in Figure 4.4. Some of the anomalies shown on this map (Figure 4.4) cannot be explained by the known surface geology of the survey area. For instance, along profile B-B' which crosses many different rock units having both positive and negative density contrasts relative to the host migmatite-gneiss complex, the residual anomaly is almost entirely negative (see Figure 4.5(a)). Also the residual anomaly along profile A-A' with a magnitude of almost -30 mGals (Figure 4.5(b)) is too large, and its gradient too low to be entirely attributed to near surface, relatively thin sandstones of the Illo Formation. Thus the residual anomalies based on the DMAAC first degree regional field (Figure 4.5) appear to contain a major component which reflects the effect of very deep seated and large structures probably at the lithosphere/asthenosphere boundary, which is superimposed on the relatively smaller gravitational effect of near

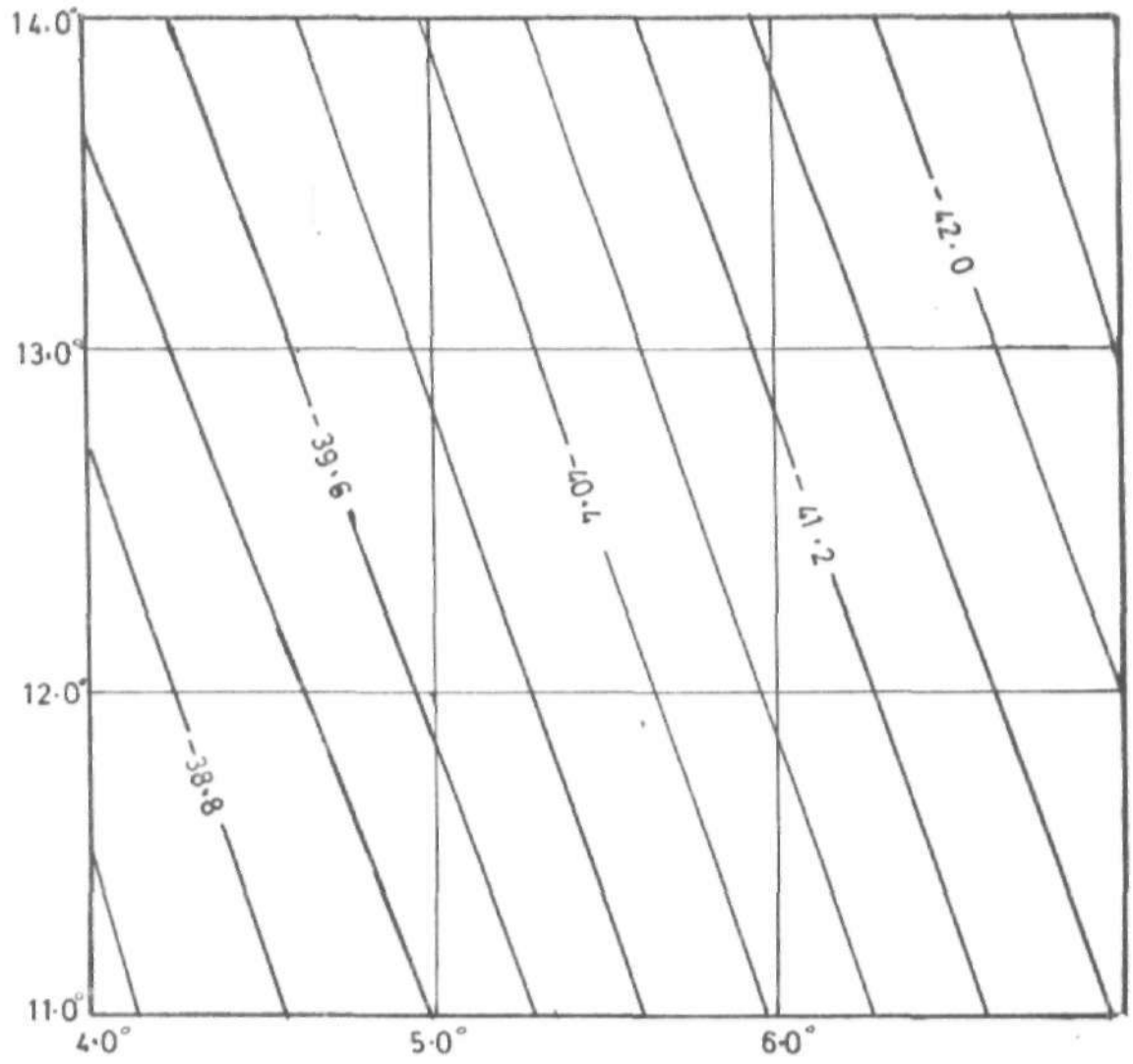


Fig. 4.3 Regional gravity field of the survey area derived from the DMAAC data set.

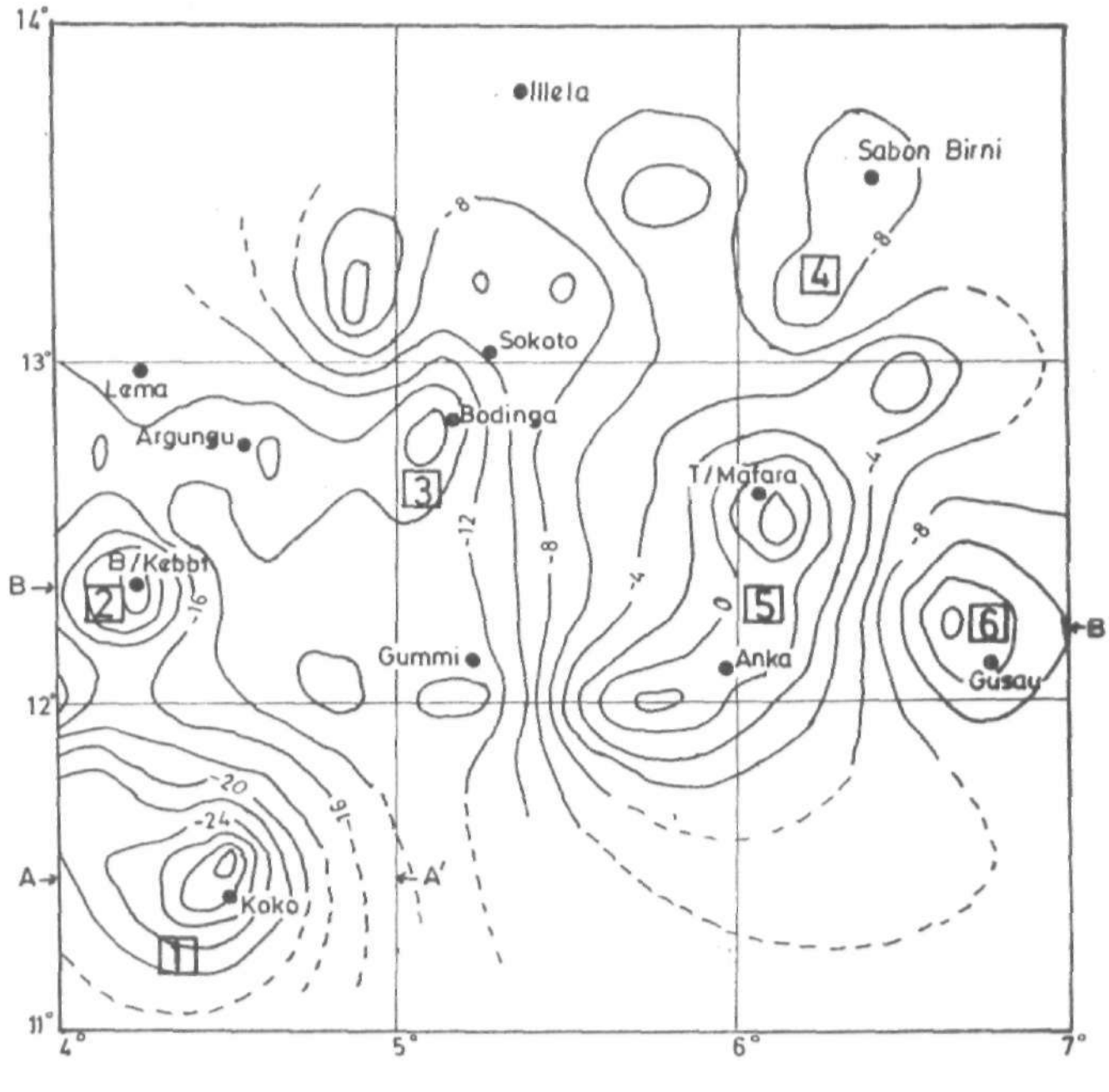


Fig. 4.4 Residual anomaly map of the survey area obtained with the DMAAC regional gravity field.

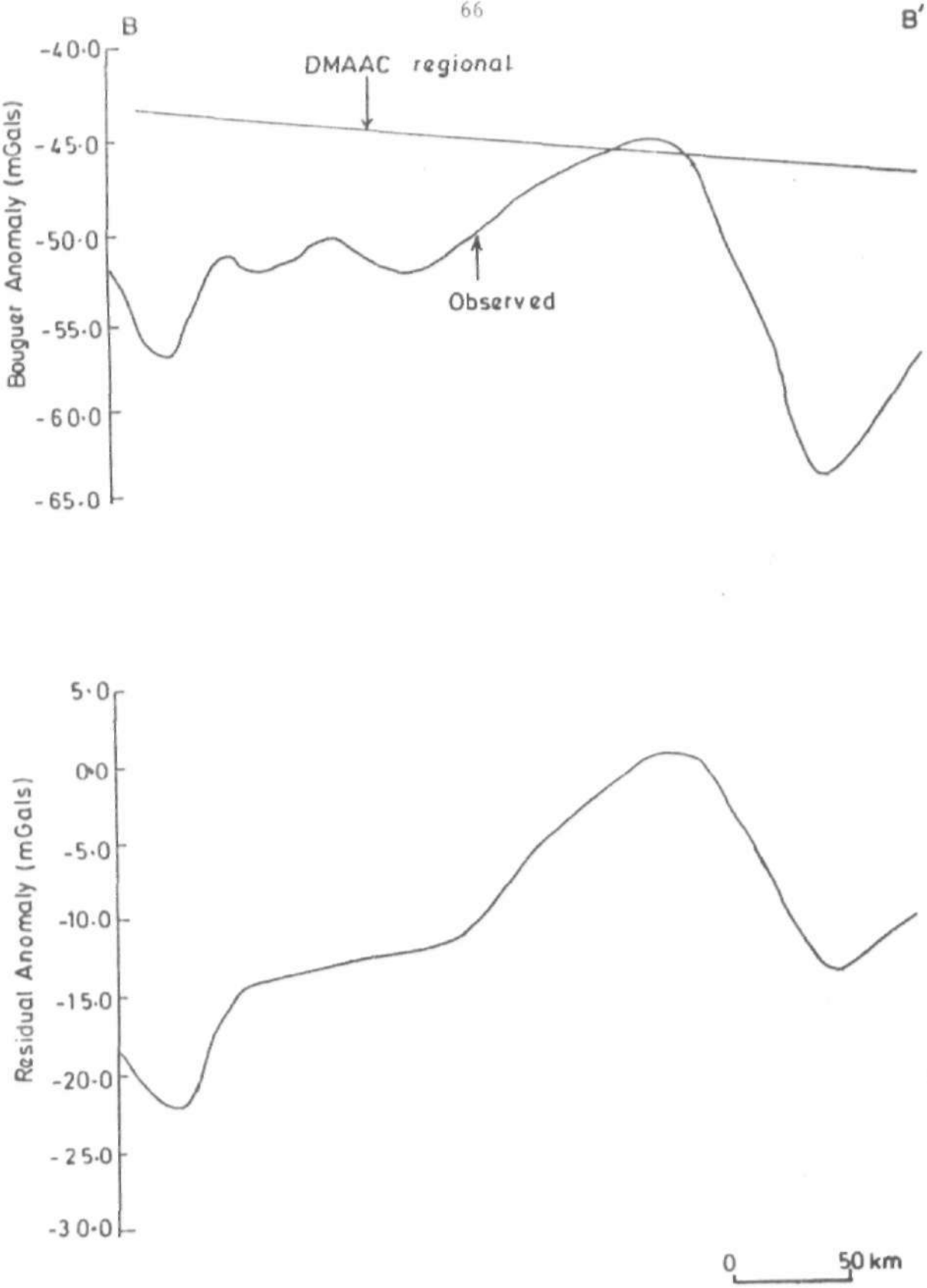


Fig. 4.5(a) Bouguer anomaly, assumed DMAAC regional and residual anomaly along Profile BB'.

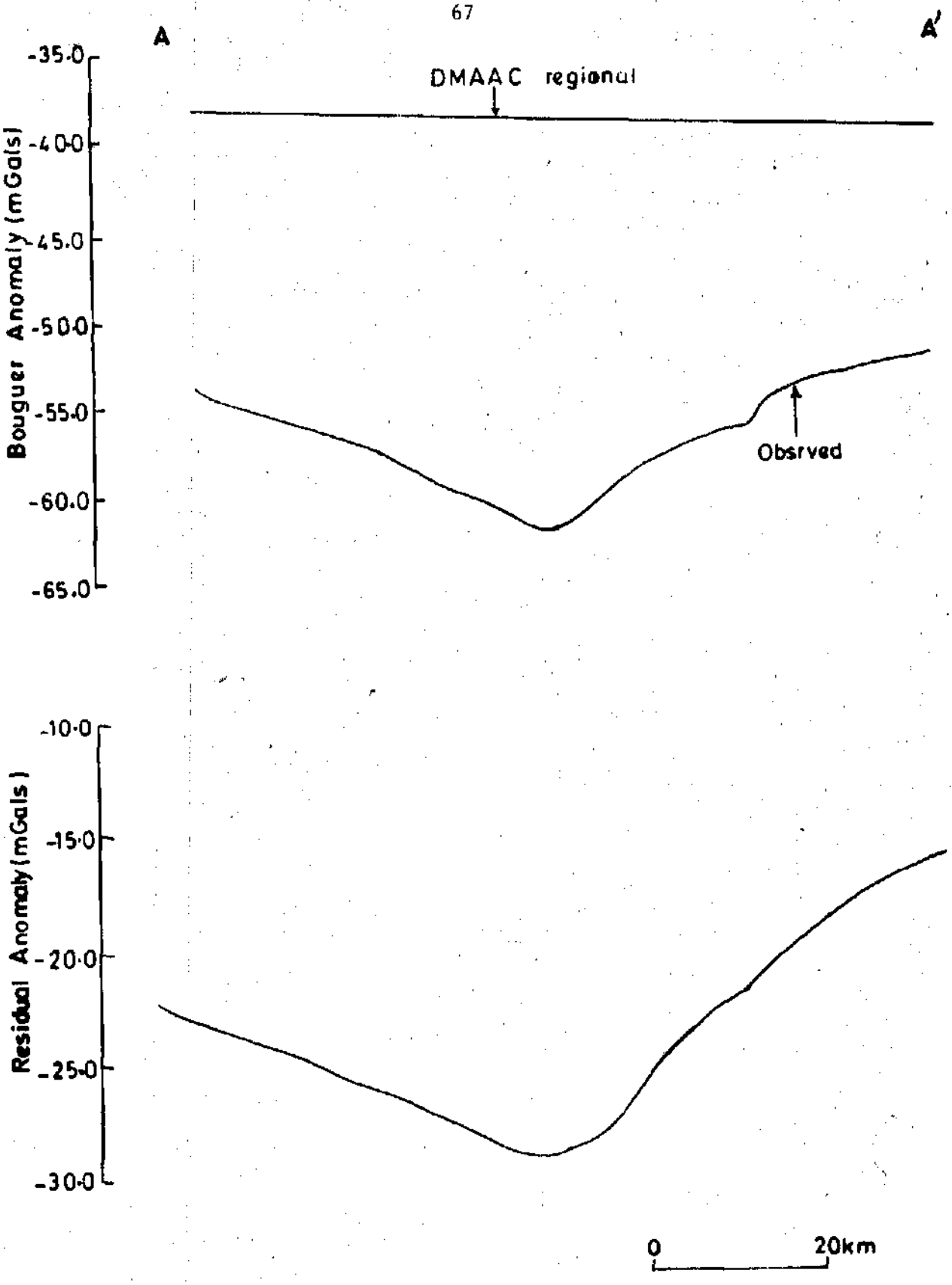


Fig. 4.5(b) Bouguer anomaly, assumed DMAAC regional and residual anomaly along profile AA'.

surface basement features which are the objective of the present study. Because of the limited area of survey and the sparse data coverage caused by the poor road network, it was not considered prudent to attempt the interpretation of these data to very deep levels represented by the lithosphere/asthenosphere boundary. Instead it was decided to fit a low degree polynomial surface to the observed data as an estimate of the regional field. Various degrees of the polynomial were tried, and the first degree surface (Figure 4.6) was eventually selected as best reflecting the regional character of the gravity which correlates better with the known surface geology of the area. The map (Figure 4.6) is also a plane dipping towards the southeastern direction with a gradient of 0.01 mGal km^{-1}. Figure 4.7 is the corresponding residual gravity anomaly map obtained by subtracting this 'local regional' effect from the observed Bouguer anomaly.

A comparison of the two first degree regional gravity maps (Figures 4.3 and 4.6) reveals two different regional trends. While the DMAAC regional map trends NW-SE, the 'local regional' field derived from the observed data shows a NE-SW trend. A possible explanation is that the two regional fields reflect the effects of sources of disproportionate magnitudes at two different horizons. It is suspected that tectonic features in the medium depth range have influenced the 'local regional' field derived from the data over the survey area.

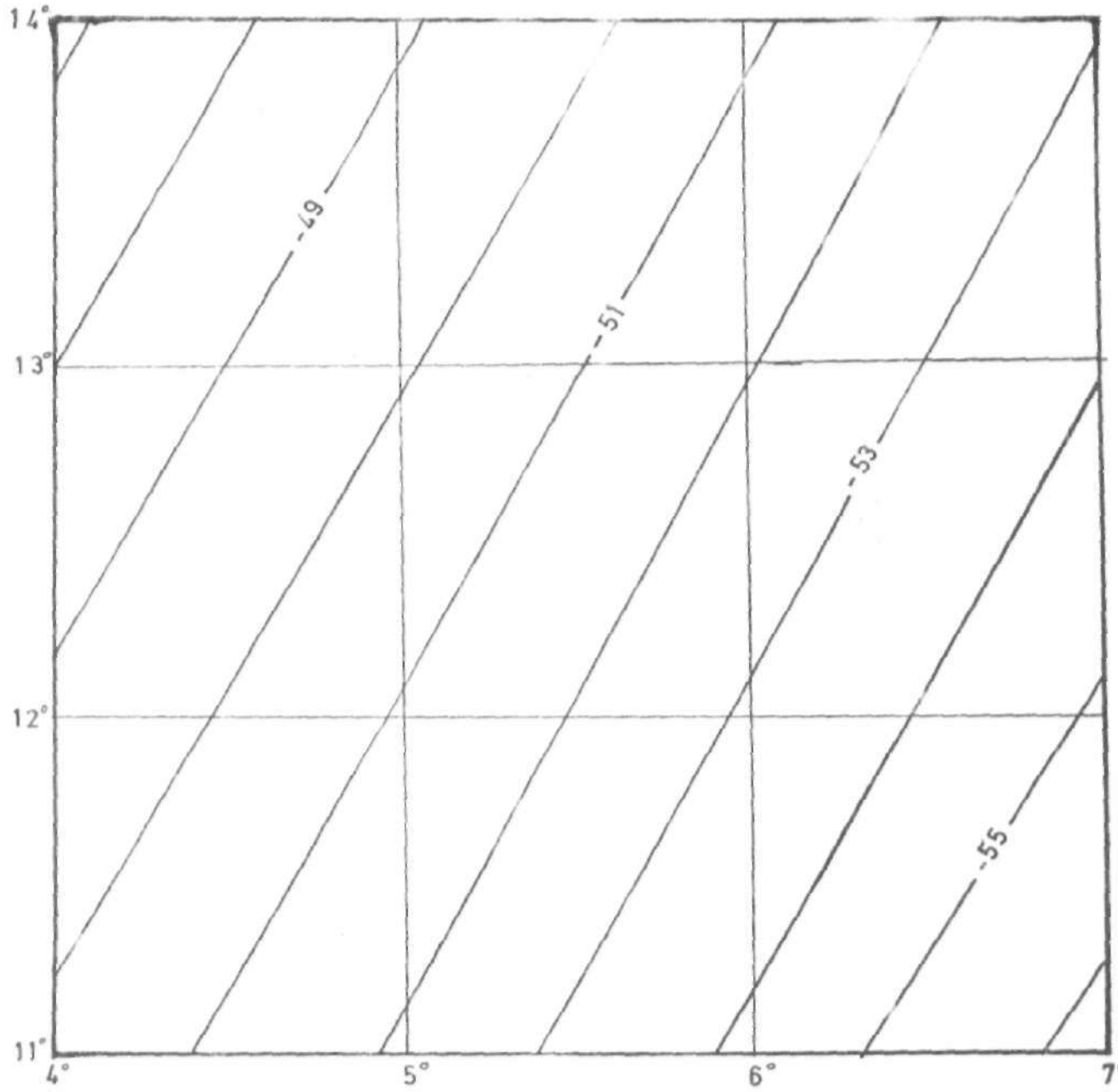
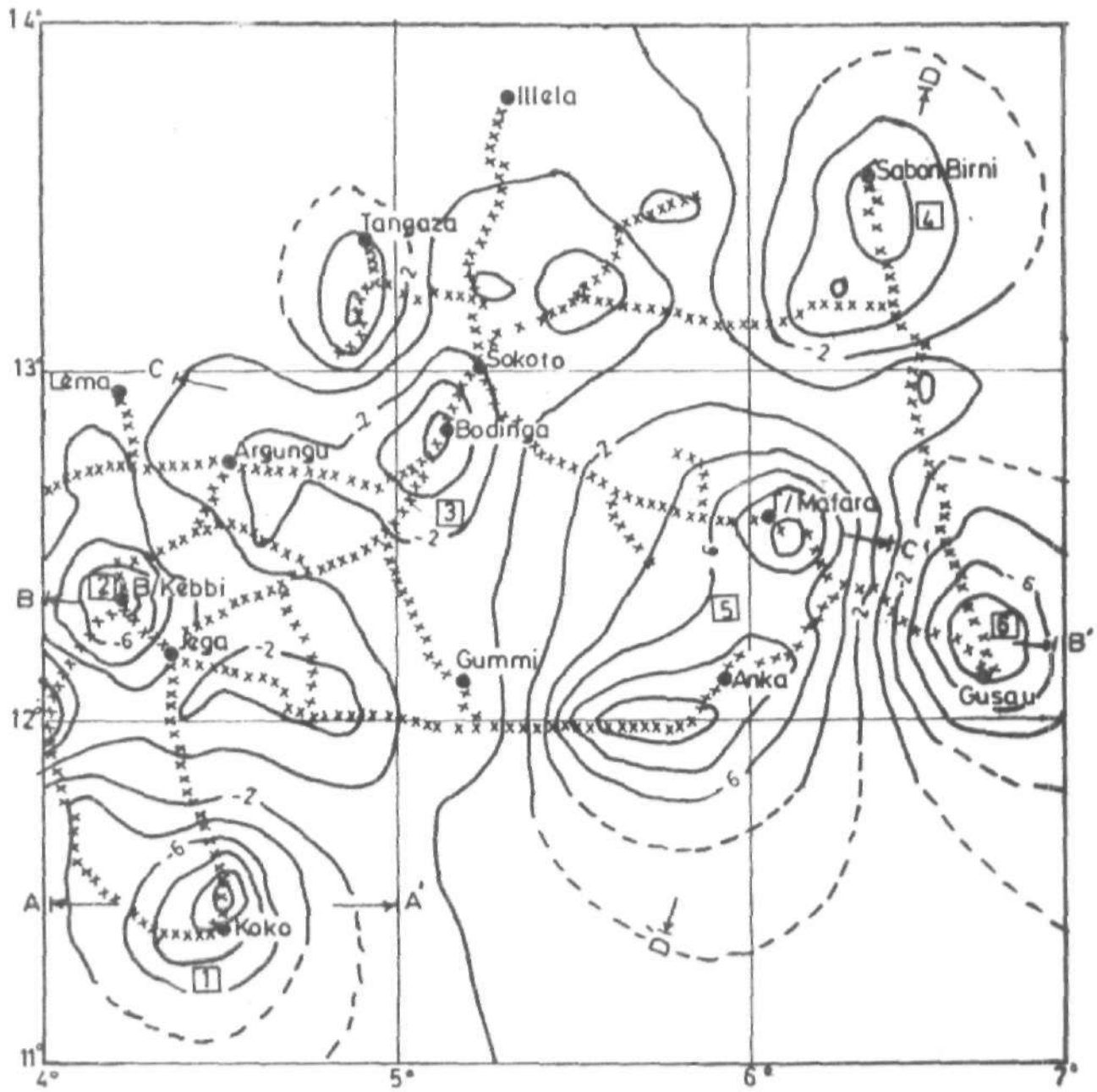


Fig. 4.6 Regional gravity field of the survey area derived from first degree polynomial surface fit to the observed data.



x Gravity station

— — — Extrapolated gravity contours

——— Gravity contours

A← →A' Line of profile

Fig. 4.7 Residual anomaly map of the survey area obtained with the 'local regional' gravity field.

In particular the regional field of Figure 4.6 appear to have been influenced by the 65 mGal negative anomaly A in Figure 4.2(b), towards which it decreases at the rate of 0.01 mGal km^{-1}. The regional effects deduced in earlier surveys in adjacent areas (Oje and Ajakaiye, 1976; and Gandu et al., 1985) appear to have also been influenced by the anomaly A in Figure 4.2(b). A thickening of the crust towards the position of the anomaly A (11.8° N and 7.5° E) could possibly explain the observed regional effect.

4.4 The Residual Anomaly

The residual anomaly map (Figure 4.7) reveals several prominent closures numbered 1-6 as on the Bouguer anomaly map. For easy correlation between geology and geophysics, the residual anomaly map is superimposed on a simplified geological map of the area in Figure 4.8. This map indicates that the 10 mGal positive anomaly no.5 is located at the eastern margin of the basin where the Gundumi Formation is in contact with outcrops of the basement complex. The anomaly extends for a distance of roughly 55 km southwards from Talata Mafara to Anka before extending westwards for a further 50 km. The anomaly coincides with outcrops of undifferentiated metasediments (Kogbe, 1981) which Turner (1983) mapped as phyllite/siltstone in the Anka schist belt. Field observations during this survey confirm that the metasedimentary rock unit that borders the basin at Talata Mafara is infact phyllite (density 2.78 x 10^3 kg m^{-3}) which outcrops extensively at the

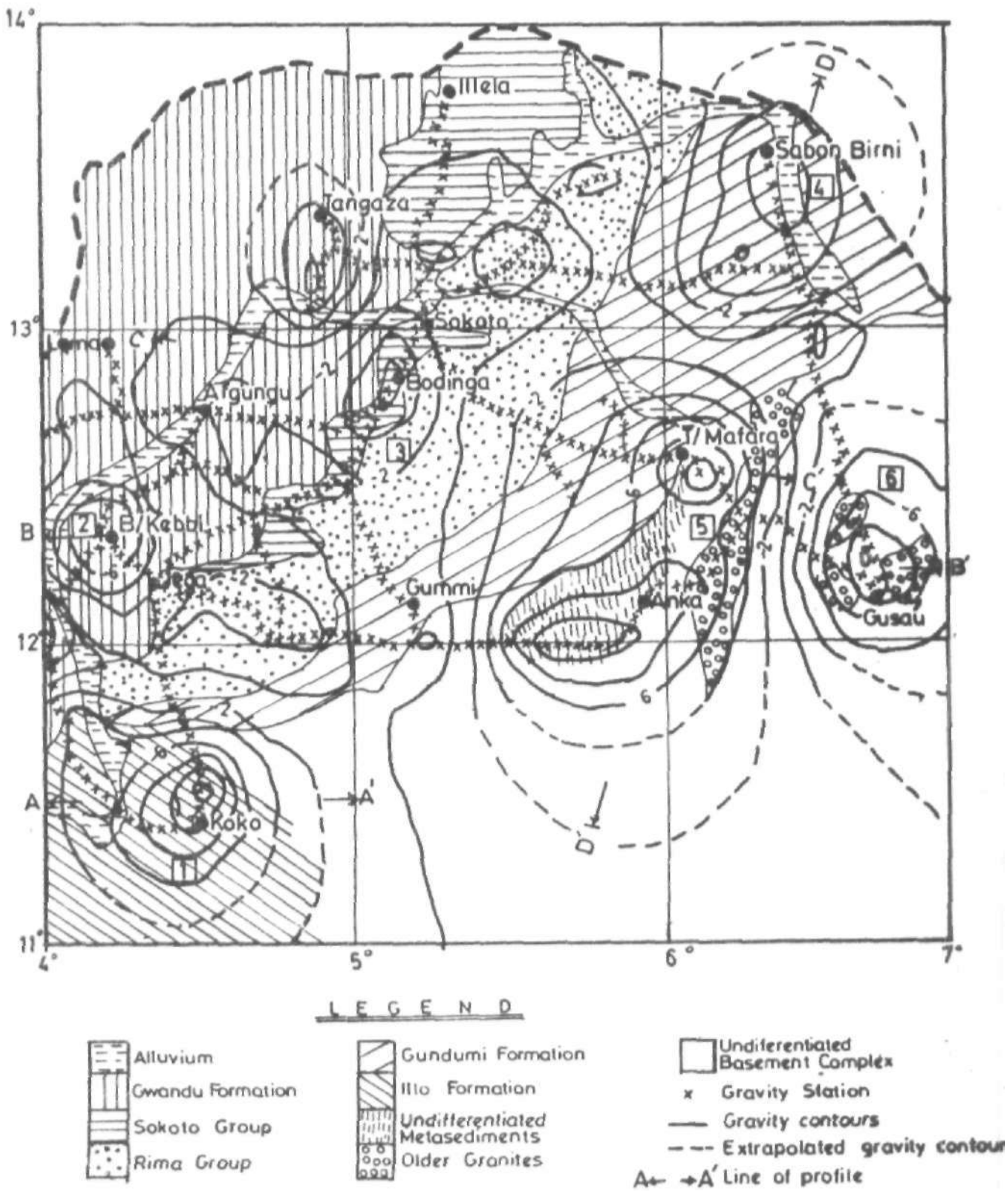


Fig. 4.8 Residual anomaly map of Fig. 4.7 superimposed on a simplified geological map of the survey area.

river bank east of Talata Mafara on Gusau - Sokoto road. The peripheral positive contours on the western side of this body extends into the basin beyond Talata Mafara, and suggests that this phyllite outcrop extends westwards beneath the sediments. Thus the zero contour line in this direction could infact be the 'true' western limit of the Anka schist belt. Furthermore the fact that the gravity method could resolve the meta-sediments in this region suggests that these must be relatively thick.

To the east of this anomaly, and separated by a rather sharp gradient is a 10 mGal positive anomaly no.6. This anomaly correlates well with outcrops of Older Granites (density 2.64×10^3 kg m^{-3}) that have been mapped around Gusau. The shape of this anomaly suggests that the isolated occurences of the Older Granite outcrops mapped on the surface in this area could not be resolved by the gravity data due perhaps to either to the fact that these isolated outcrops coalesce into one big pluton at depth, or that the gravity stations are not close enough.

Anomaly no.1 is located partially in the southern portion of the basin where the basement is overlain by only the Illo Formation. The east-west trending contact between the Illo Group and the younger formations to the north is also marked by east-west trending contours decreasing to the north and to the south indicating a ridge-like structure.

Anomaly no. 2 centered at Birnin Kebbi, is located in the Gwandu Formation, while anomaly no. 3 at Bodinga is located on the narrow strip of the Sokoto Group bound by its contacts with the Rima Group and Gwandu Formation to the east and west respectively. Anomaly no. 4 centered at Sabon Birni is located in the Gundumi Formation. These negative anomalies (nos.2, 3, and 4) could possibly be caused by increased thickness of sediments at basement depressions, low density intrusives in the underlying basement rocks, or even lithologic changes in the basement rocks, or a combination of a number of these factors.

The shape of the major anomalies suggest that the causative bodies are of three-dimensional nature. Four profiles A-A', B-B', C-C' and D-D' which have been chosen across and along the six major anomalies on the residual anomaly map to gain a cross-sectional view of the these three-dimensional bodies are indicated in Figures 4.7 and 4.8. The Bouguer anomalies, assumed regional effects and resulting residual anomalies along these profiles are shown in Figures 4.9(a), (b), (c) and (d).

4.5 Quantitative Interpretation of the Residual Anomalies

In quantitative interpretation of gravity data, attempt is made to determine a source distribution whose gravitational effect matches as closely as possible the measured gravity field on the surface of measurement. Unfortunately this task is made more

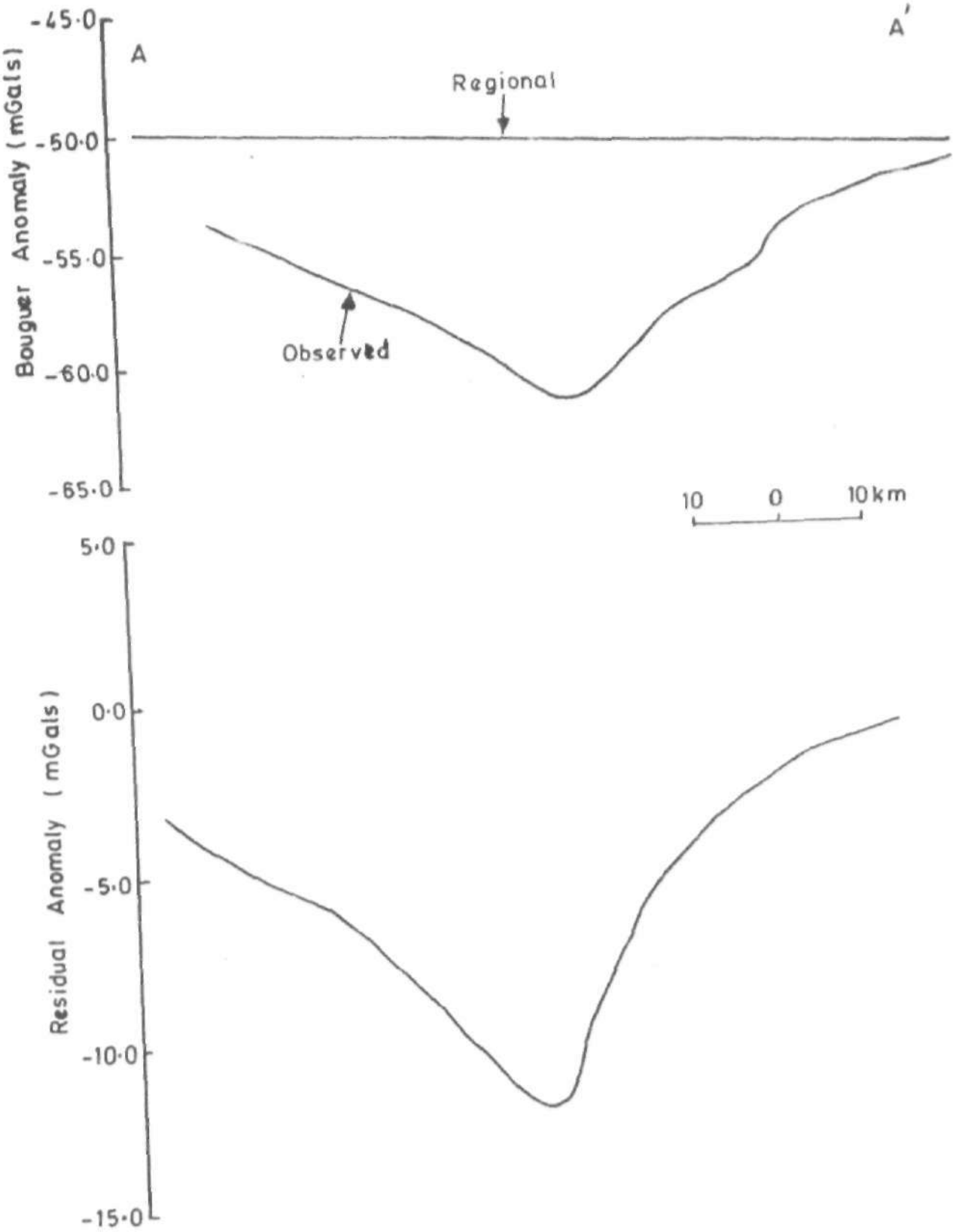


Fig. 4.9 (a) Bouguer anomaly, assumed regional and residual anomaly along profile AA'.

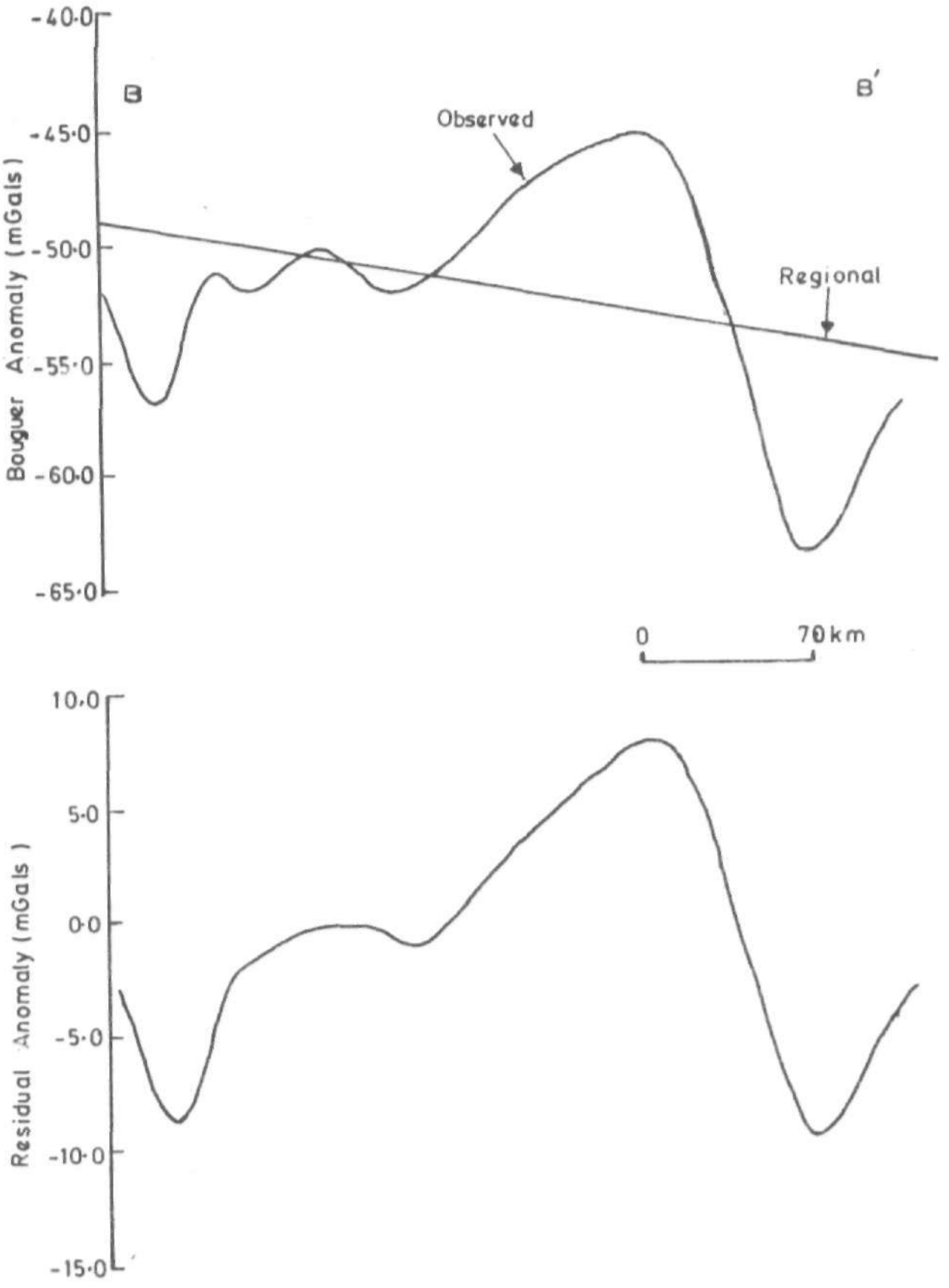


Fig. 4.9(b) Bouguer anomaly, assumed regional and residual anomaly along profile BB′

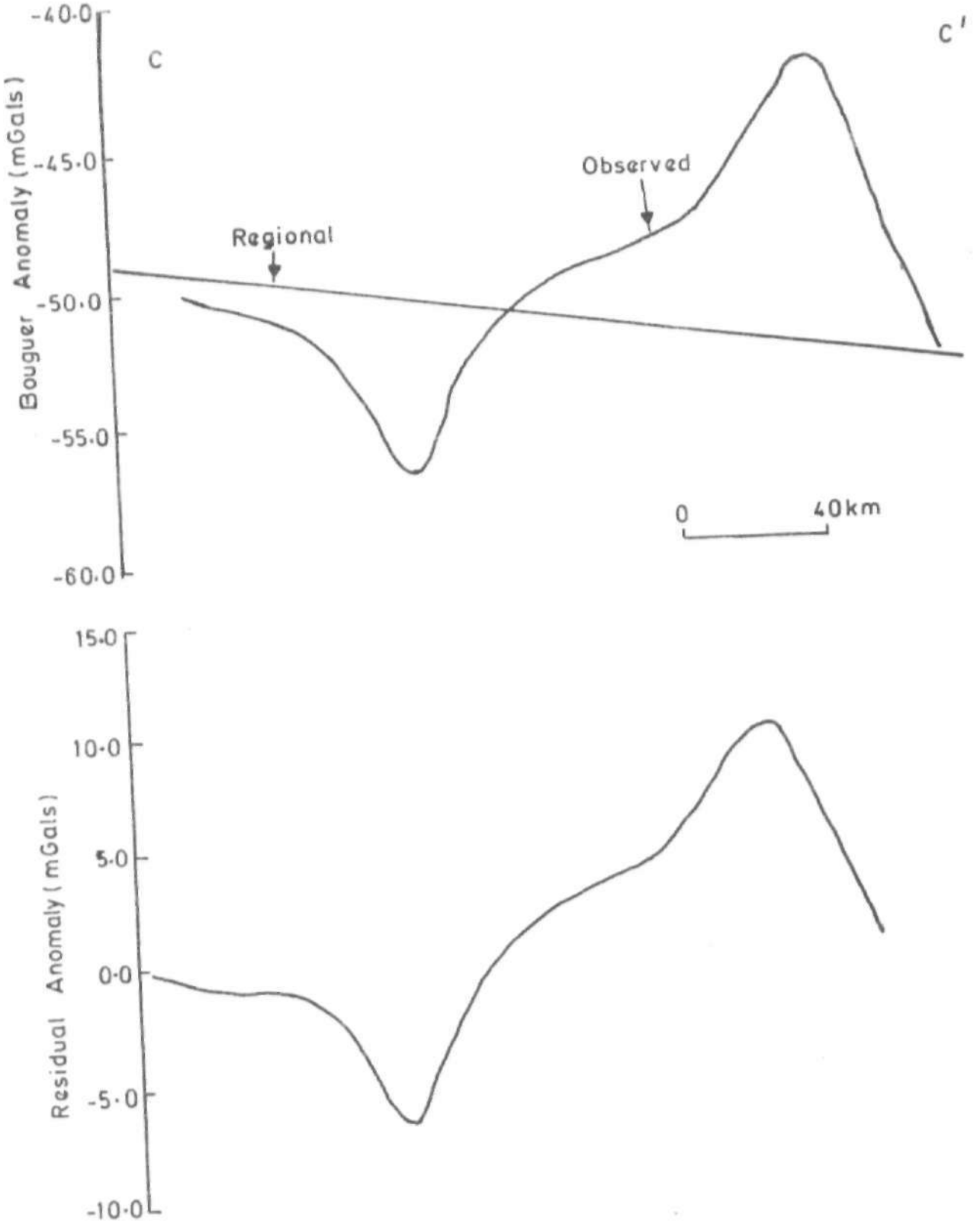


Fig. 4.9(c) Bouguer anomaly, assumed regional and residual anomaly along profile CC'.

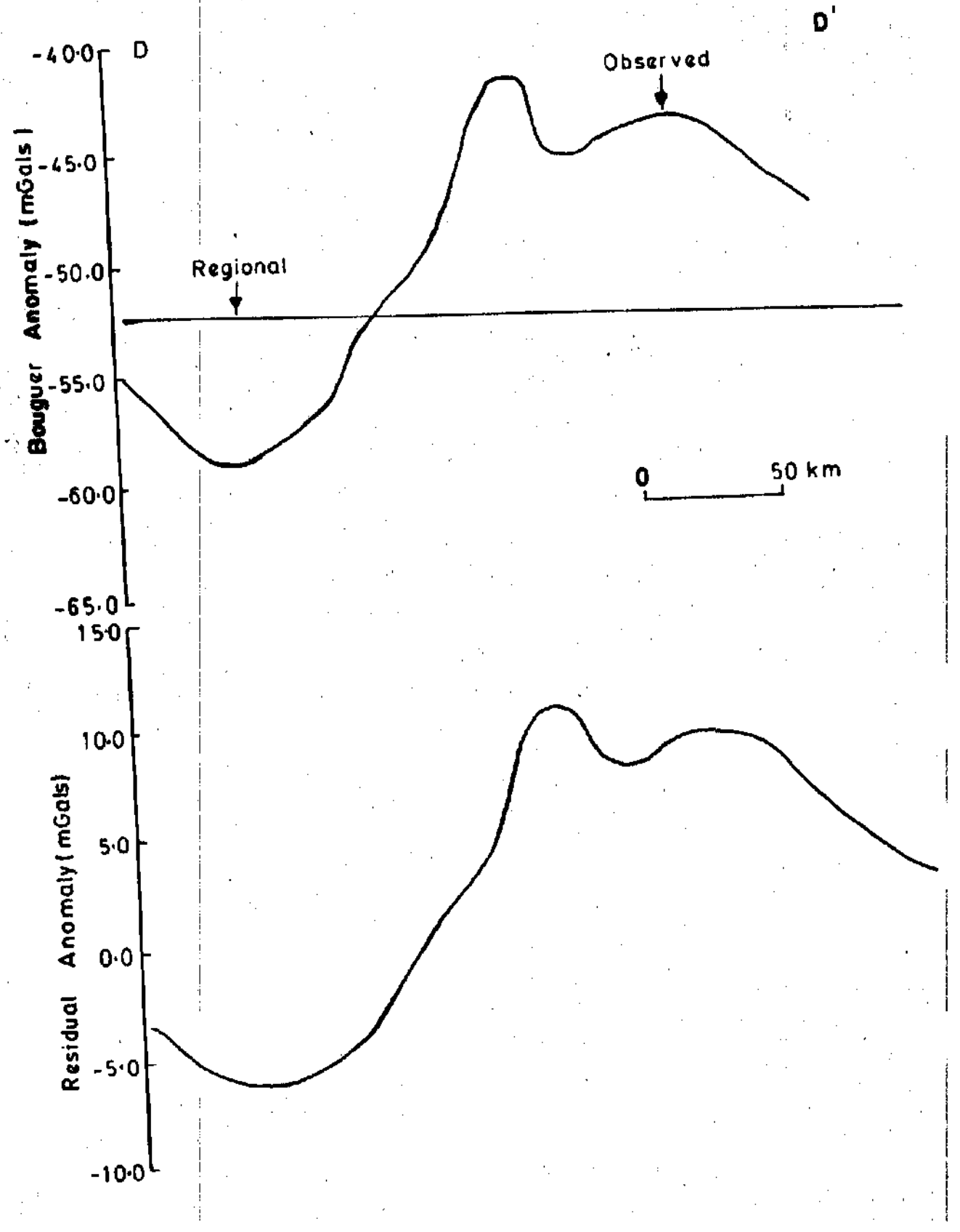


Fig. 4.9(d) Bouguer anomaly, assumed regional and residual anomaly along profile DD'.

difficult by the problem of non-uniqueness in that the same anomalous field on the surface can be caused by different combinations of the spatial distributions of the anomalous subsurface masses and of their densities. This problem is partly overcome by making some assumptions which must be justifiable in the context of what is known or can be reasonably inferred about the geological environment. Thus constraints are introduced in the form of simplification of geometry, limits to size and depth, and range limits on density.

The process by which the source distribution is deter mined follows one of two routes, known as "forward modeling" and "inversion" respectively (Paterson and Reeves, 1985). Here the forward modeling approach is adopted and this comprises the following steps:

i. human estimation of an initial model, compatible with what is known of geology.

ii. computation of the exact theoretical anomaly for this model,

iii. comparison of the observed and computed anomalies,

iv. judicious adjustment of the model by human interaction and within geologically reasonable limits in the hope of improving the fit of the computed data to the observed points,

v. return to stage (ii) and so on, and

vi. stop at stage (iii) once the fit is acceptable.

Besides the apparent time consuming aspect of this trial-and-error process, another disadvantage is that there is usually no guarantee that any improvement will

be obtained at stage (iv). However, the procedure has merit in the ease of programming on microcomputers and the human interaction brought in at every iteration which ensures that the model retains geologic credibility.

Inverse modeling on the other hand, involves determining estimates of model parameters given a set of observational data and a general model for their cause (Paterson and Reeves, 1985). This is an over-determined problem as there are usually far more observations than are needed for a single solution, so that the acceptable solution is that which best fits all the available data. A major advantage of inversion is its ability to operate efficiently in multi-parameter space, and ability to produce solutions within a relatively small number of iterations even with poor starting models. However the technique does not usually allow for user interaction, but when such interaction is necessitated by the need to impose some geologic acceptability on the result, the solution is then no longer necessarily the best possible fit in a mathematical sense.

4.5.1 Theory of the Foward Modeling Method

Most computerised interpretation techniques have identical procedure; namely, complex structures are built up from simple basic units, the numbers and/or sizes of which are adjusted by a continual recycling process until satisfactory agreement is obtained

between the observed and calculated gravity anomalies at field points (Grant, 1972). In this method, first proposed by Talwani and Ewing (1960), polygonal shaped laminae are used as the basic modeling blocks. The three - dimensional body is first represented by depth contours, and each contour is then replaced by a horizontal n-sided polygonal lamina. The gravity effect, (i.e. vertical component of gravitational attraction) caused by each lamina can be determined at any external point (field point), and the gravity anomaly caused by the entire body can then be obtained by numerical integration.

The basic principles of the theory is illustrated in Figure 4.10. Let P, the origin of a left-handed coordinate system, represent the field point at which the gravity anomaly caused by the massive body M is being evaluated. A contour on the body at depth Z is replaced by the polygonal lamina ABCDEF..., of infinitessimal thickness dz. The gravity anomaly Δg caused by ABCDEF... at P is given by

$$\Delta g = V dz \qquad \ldots\ 4.4$$

where V is the anomaly caused by ABCDEF... per unit thickness. V can be expressed by a surface integral, the integration being carried out over the surface of the lamina. This can again be reduced to two line integrals, both along the boundary of ABCDEF...; V is then given by the expression:

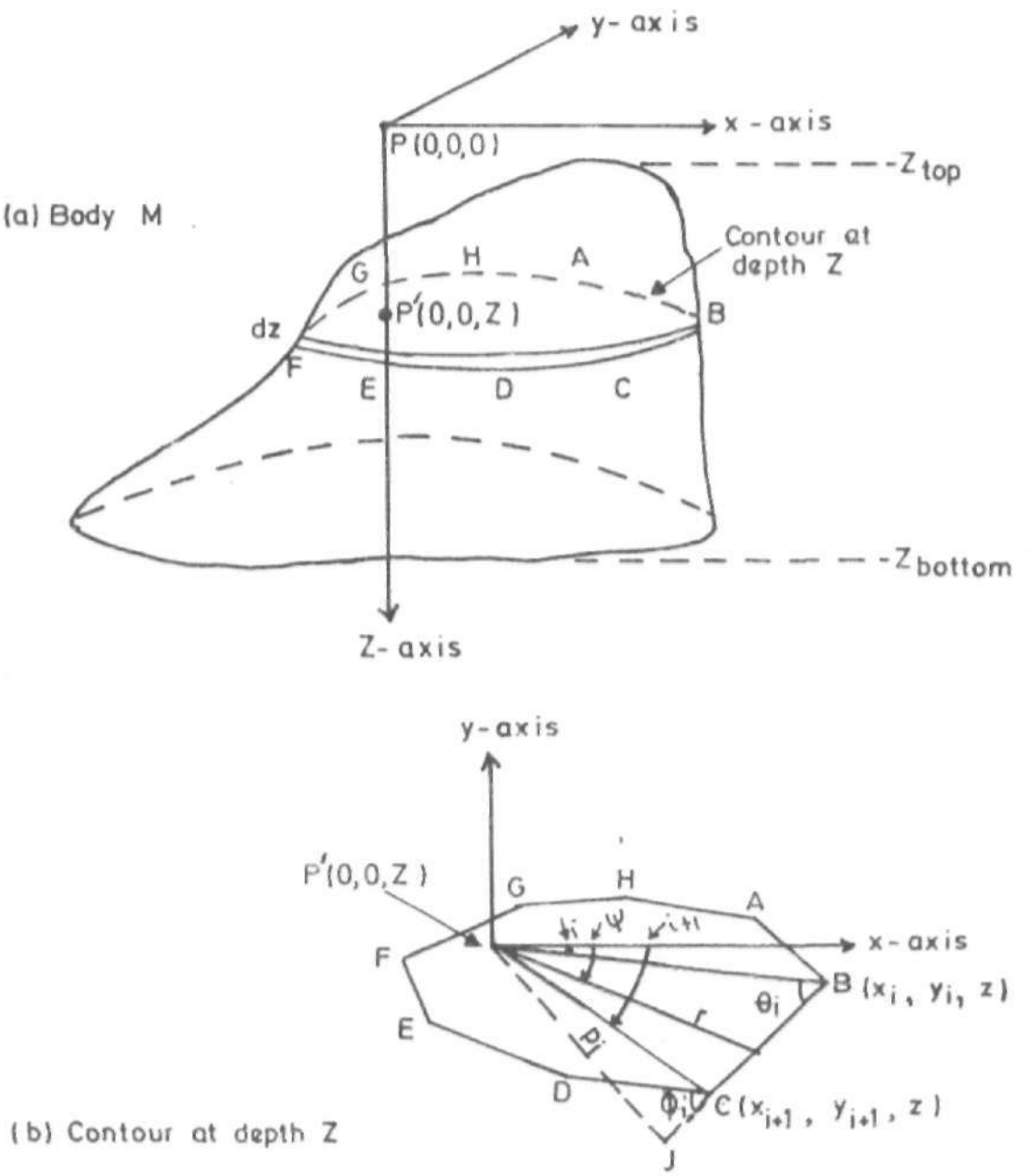


Fig. 4.10 Geometrical elements involved in the compution of the gravity anomaly caused by a three-dimensional body.

$$V = G\rho \left[\oint d\psi - \oint z/(r^2 + z^2)^{\frac{1}{2}}\, d\psi \right] \qquad \ldots. 4.5$$

where G is the universal gravitational constant, ρ is the volume density (density contrast) of the lamina, and z, ψ and r are the cylindrical coordinates used to define the boundary of ABCDEF... (see Talwani and Ewing, 1960).

Let P' be the projection of P on the plane of ABCDEF...; r is the radius vector in the plane of the lamina, and ψ is the angle which this radius vector makes with an arbitrary x-axis in this plane (Figure 4.10(b)). The total contribution to V from BC is

$$G\rho \left[\psi_{i+1} - \psi_i - \arcsin \frac{z\cos\theta_i}{(p_i^2 + z^2)^{\frac{1}{2}}} + \arcsin \frac{z\cos\phi_i}{(p_i^2 + z^2)^{\frac{1}{2}}} \right] \ldots 4.6$$

where p, θ and ϕ are as indicated on Figure 4.10(b). The gravity anomaly caused by the whole polygonal lamina ABCDEF... per unit thickness is obtained by summing up expression (4.5) over the n sides of the polygon to obtain:

$$V = G\rho \left[\sum_{i=1}^{n} \{\psi_{i+1} - \psi_i - \arcsin \frac{z\cos\theta_i}{(p_i^2+z^2)^{\frac{1}{2}}} + \arcsin \frac{z\cos\phi_i}{(p_i^2+z^2)^{\frac{1}{2}}}\} \right] \ldots 4.7$$

The total anomaly g caused by the entire body M can be obtained by integrating (4.3) between Z_{top} and Z_{bottom} i.e.

$$\Delta g_{total} = \int_{z_{bottom}}^{z_{top}} V dz \qquad \ldots. 4.8$$

This integral can be solved either graphically or by numerical integration. The possibility that density

varies with depth may be easily incorporated by assigning a separate density to each contour.

For interpretation by high speed digital computers equation (4.6) is expressed in terms of x_i, y_i, z and x_{i+1}, y_{i+1}, z, the coordinates of two successive vertices of the polygon, for ease of programing thus

$$V = G\rho\left[W \arccos\left\{\left(\frac{x_i}{r_i}\right)\left(\frac{x_{i+1}}{r_{i+1}}\right) + \left(\frac{y_i}{r_i}\right)\left(\frac{y_{i+1}}{r_{i+1}}\right)\right\} - \arcsin\frac{zf_i S}{(p_i^2 + z^2)^{\frac{1}{2}}}\right.$$
$$\left. \arcsin\frac{zf_i S}{(p_i^2 + z^2)^{\frac{1}{2}}}\right] \qquad \ldots\ 4.9$$

where $S = +1$ if P_i is positive, $S = -1$ if P_i is negative

$W = +1$ if m_i is positive, $W = -1$ if m_i is negative

$$P_i = \frac{y_i - y_{i+1}}{r_{i,\,i+1}} x_i - \frac{x_i - x_{i+1}}{r_{i,\,i+1}} y_i,$$

$$q_i = \frac{x_i - x_{i+1}}{r_{i,i+1}} \cdot \frac{x_i}{r_i} + \frac{y_i - t_{i+1}}{r_{i,\,i+1}} \cdot \frac{y_i}{r_i},$$

$$f_i = \frac{x_i - x_{i+1}}{r_{i,\,i+1}} \cdot \frac{x_{i+1}}{r_{i+1}} + \frac{y_i - y_{i+1}}{r_{i,i+1}} \cdot \frac{y_{i+1}}{r_{i+1}},$$

$$m_i = \left(\frac{y_i}{r_i}\right)\left(x_{i+1}/r_{i+1}\right) - \left(y_{i+1}/r_{i+1}\right)\left(x_i/r_i\right),$$

$$r_i = + (x_i^2 + y_i^2)^{\frac{1}{2}},$$

$$r_{i+1} = + (x_{i+1}{}^2 + y_{i+1}{}^2)^{\frac{1}{2}},$$

$$r_{i,i+1} = + [(x_i - x_{i+1})^2 + (y_i - y_{i+1})^2]^{\frac{1}{2}}.$$

Similarly the numerical integration (4.8) is more conveniently performed by fitting parabolas to successive sets of three points (obtained by plotting V against Z) and

then finding the area contained between the parabolas and the Z - axis. Thus if V_o, V_1, and V_2 are the values of V corresponding respectively to contours at heights z_o, z_1, and z_2, then the gravity anomaly caused by the portion of the body lying between horizontal planes at depths z_o and z_2 is given by

$$\int_{z_o}^{z_2} V\,dz = \frac{1}{6}\left[V_o \frac{z_o - z_2}{z_o - z_1}(3z_1 - z_2 - 2z_o) + V_1 \frac{(z_o - z_2)}{(z_1 - z_2)(z_1 - z_o)} + V_2 \frac{z_o - z_2}{z_2 - z_1}(3z_1 - z_o - 2z_2)\right] \quad \ldots\ldots 4.10$$

A single computer program (Talwani, 1965) which handles both computations was adapted for use on the IBM PC/AT and modified to plot the observed and computed gravity anomalies automatically.

4.5.2 Model Fitting Procedure

The causative bodies of the major anomalies (numbered 1 - 6) on the residual anomaly map (Figure 4.7) were determined by the above modeling technique. First, irregularly shaped polygons representing depth contours were fitted to the various anomalies in such a way that the polygons fitted as closely as possible the assumed shape of the causative bodies at different pre-selected depth points (Figure 4.11). In the next step, the coordinates of the vertices of the polygons were determined: the x- and y- coordinates were with respect to latitudes and longitudes as two mutually perpendicular axes in a horizontal plane, the z-axis was vertically downwards. The input to the computerised

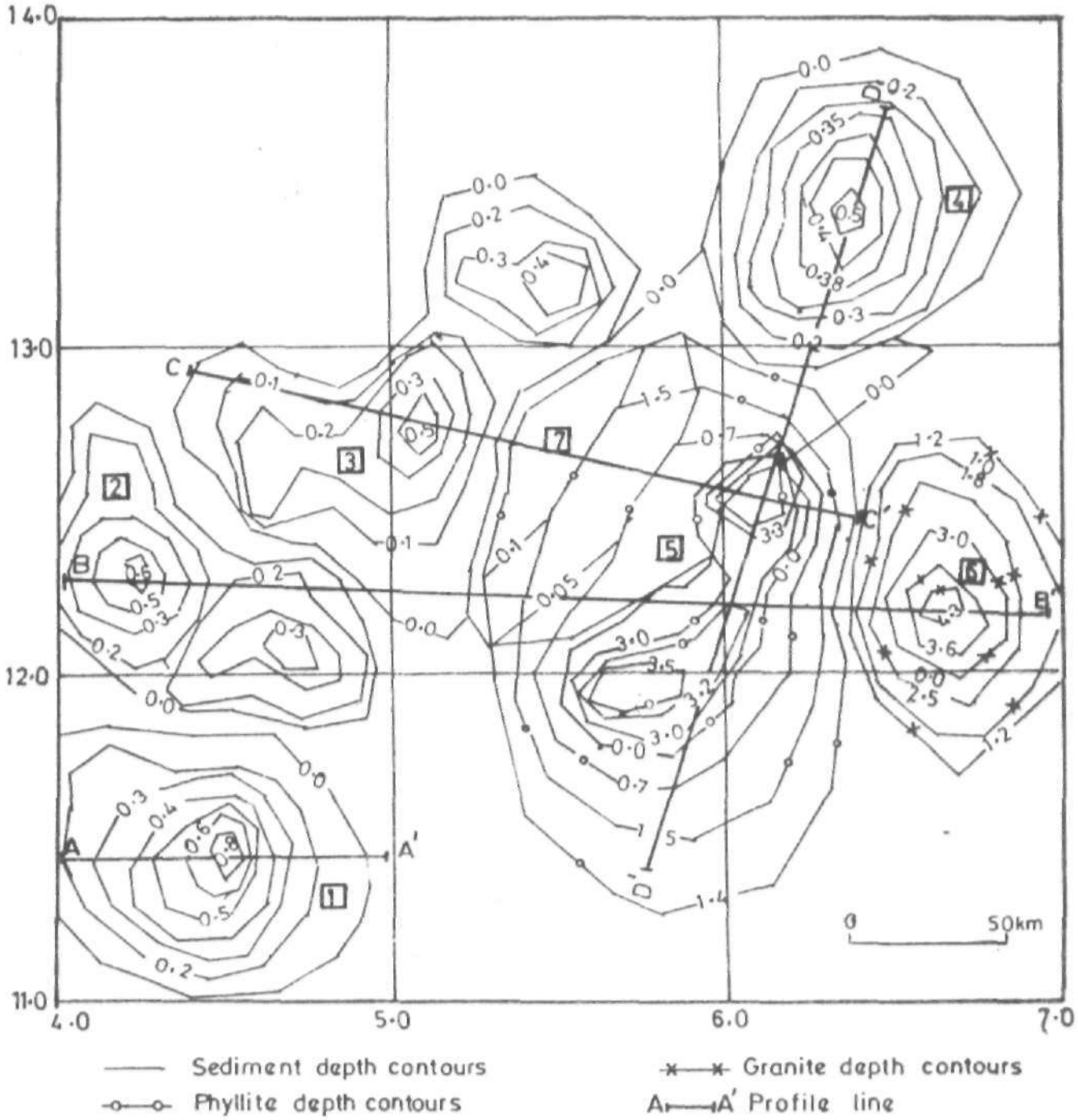


Fig. 4.11 : Three - dimensional model of bodies used for the six major anomalies. Depth contours and depth values (in km) for the first model are shown.

interpretation thus comprises:

i. the coordinates of all the field points as well as the observed residual anomaly at these points along the profile of interest,

ii. the coordinates of the vertices and depths of the polygonal laminae as well as the density contrast for each lamina,

The output comprises:

i. a listing of all the input data which acts as a check (optional),

ii. the contribution of each polygon at each field point

iii. the computed total anomaly (i.e. the result of the numerical integration for each body summed for all bodies) at each field point,

iv. a plot of the observed and computed anomalies at each field point along the chosen profile.

In this survey the field points were chosen at equal intervals along the profiles and computations along different profiles were handled separately. The modification effected on the original program of Talwani (1965) to include automatic plotting of observed and computed anomalies on the graphic screen after each iteration minimised the time consuming trial and error process of the foward modeling technique. In addition the scatter of the points on the plots were used as a rough measure of the goodness of fit.

The accuracy of the method depends on how closely the irregular polygons fit the individual depth contours and how precise the numerical integration was. The fit of the polygons can of course be made as closely as desired by increasing the number of sides.

However as noted by Talwani and Ewing (1960), it was recognized that the close fit of the contours is only important when a portion of the contour boundary lies close to the point at which the computation is being made. Thus by fitting only such portions of the contour very closely, the accuracy of the integration was maintained without increasing the computation time unduely.

As discussed in section (3.10) two different mean densities were utilised for the sediments viz: 2.34 x 10^3 kg m^{-3} representing the mean of all the sedimentary rock samples collected in the basin; and 2.55 x 10^3 kg m^{-3} repre- senting the mean of the remaining samples after excluding the shale samples, and sandstone samples of the Gwandu Formation whose densities were thought to be too low and not truely representative of the shales and sandstones at depth. This led to two alternative models for all structures within the basin, referred to as first and alternative models respectively.

4.5.3. Three-dimensional Interpretation of the Residual Anomalies

Profile A-A': This profile which is centered on anomaly no. 1 with an amplitude of -12 mGals, extends for a distance of about 110 km from west to east across the southwestern corner of the survey area where only the Illo Formation overlies the basement. Figure 4.12 shows the observed and calculated anomalies together

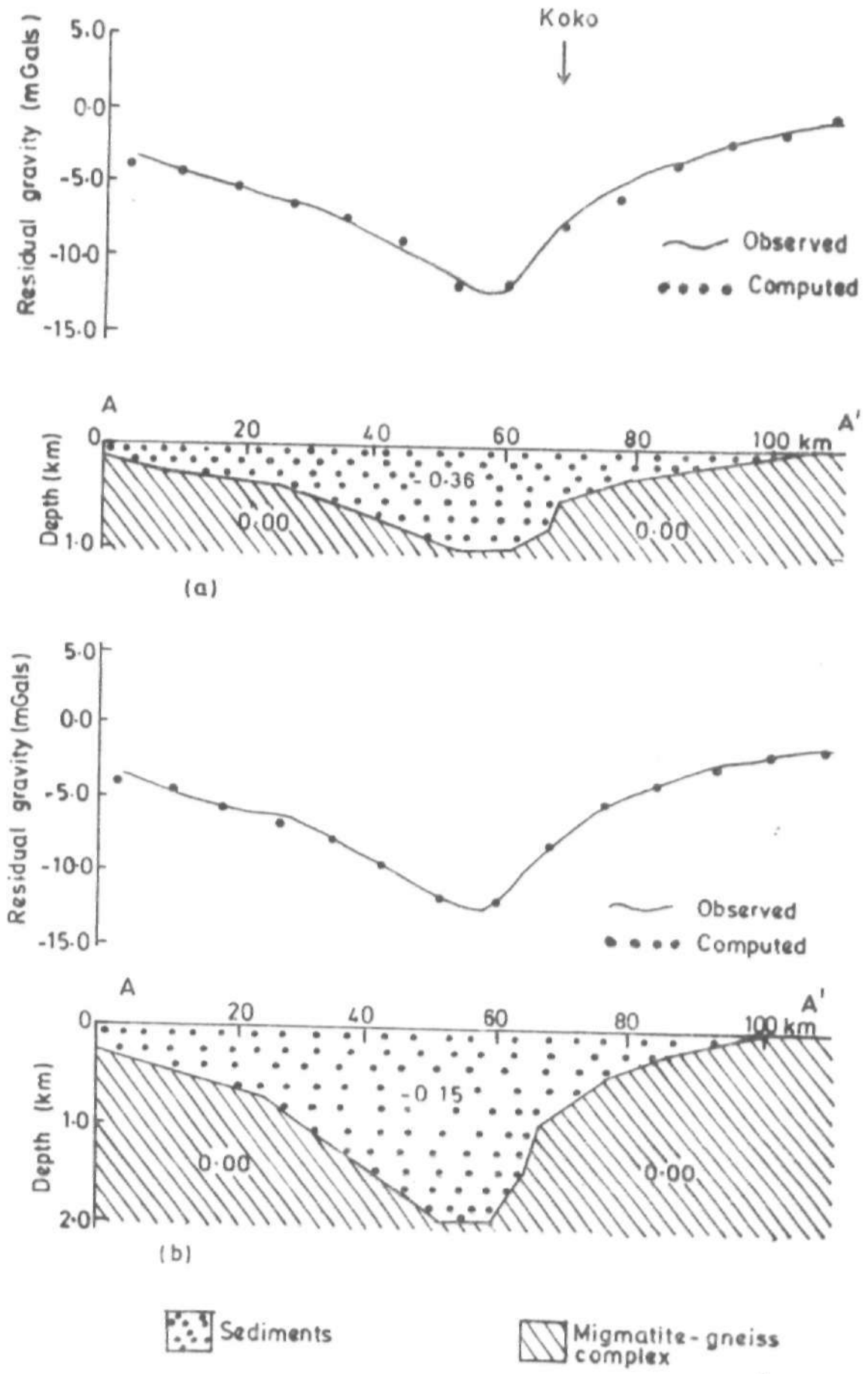


Fig. 4.12. 3-D interpretation of residual gravity along profile A-A', shown as vertical cross section. Density contrast given in g cm^{-3}.

with the vertical cross section for the interpreted models. The models suggest that anomaly no. 1 is caused by a bowl-type depression on the subsurface basement midway along the profile. The sediments in this depression attain a maximum thickness of nearly one kilometer for a sediment density of 2.34 x 10^3 kg m^{-3}, (Figure 4.12 (a)) and a maximum thickness of 2.0 km for a density of 2.55 x 10^3 kg m^{-3} (Figure 4.12 (b)).

Although the computed anomalies fitted the observed anomalies fairly well in both models (Figure 4.12), they were not considered geologically suitable because:

i. it is perhaps unreasonable to infer that the Illo Formation alone could attain a thickness of between 1 and 2 km at the periphery of a basin that is stated to have a maximum thickness of just over 2 km at its deepest portions in Niger Republic (Kogbe, 1981; Wright et al., 1985).

ii. a portion of the anomaly actually extends into the basement area (see Figure 4.8) and this combined with the shape of the residual anomaly is suggestive of an intrusive

Thus various models were tried in which the anomaly was attributed to intrusive bodies buried under thin sedimentary cover. One such model with the best fit shown in Figure 4.13 assumes a granitic intrusive at a depth of 0.40 km beneath the sediments whose root extends to a depth of 5.0 km.

Profile BB': This is the longest of all the profiles extending from Birnin-Kebbi in the West, passing slightly north of Gummi and Anka thence to Gusau in the

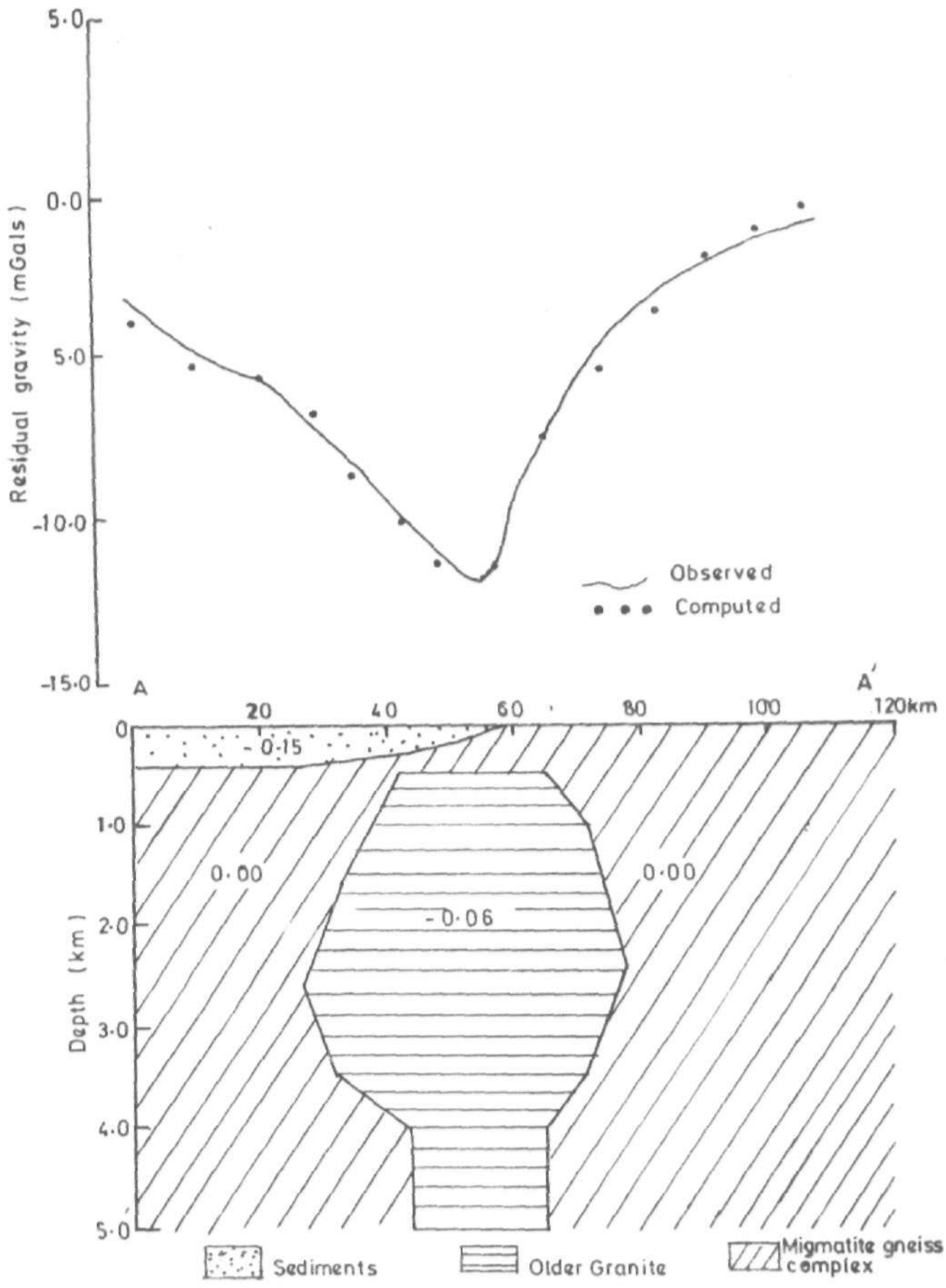


Fig. 4.13 : Third 3-D interpretation of residual gravity along profile AA'

east - a distance of almost 320 km (Figure 4.8). Anomaly no.2 on this profile is centred at Birnin Kebbi and results from a depression of 0.8 km at the basement surface assuming a density of 2.34×10^3 kg m^{-3} for the sediments (Figure 4.14(a)). This depression is nearly 50 km wide in the direction of the profile, and has a strike length of 90 km in a northwesterly direction. From this depression the thickness of the sediments decreases steadily to less than 0.20 km towards Gummi. A slight depression is again evident around Gummi and after this the thickness of the sediments decreases gently until the sediment-basement contact around Anka. The alternative model (Figure 4.14(b)) which assumes a density of 2.55×10^3 kg m^{-3} for the sediments indicates that the sediments attain a maximum thickness of 1.4 km at the deepest point on this profile.

The profile also cuts across the phyllite outcrop of the Anka schist belt which is responsible for the positive anomaly no.5. The width of this outcrop in this Anka area is about 40 km and the general depth is 2.5 km, as deduced from the gravity models assuming a density of 2.78×10^3 kg m^{-3} for the phyllites. The contacts of the phyllites with the host rock is generally outward dipping in both directions - 44° towards the west and 67° towards the east, the phyllite body extending westwards for almost 60 km beneath the area where the Gundumi Formation is mapped on the surface.

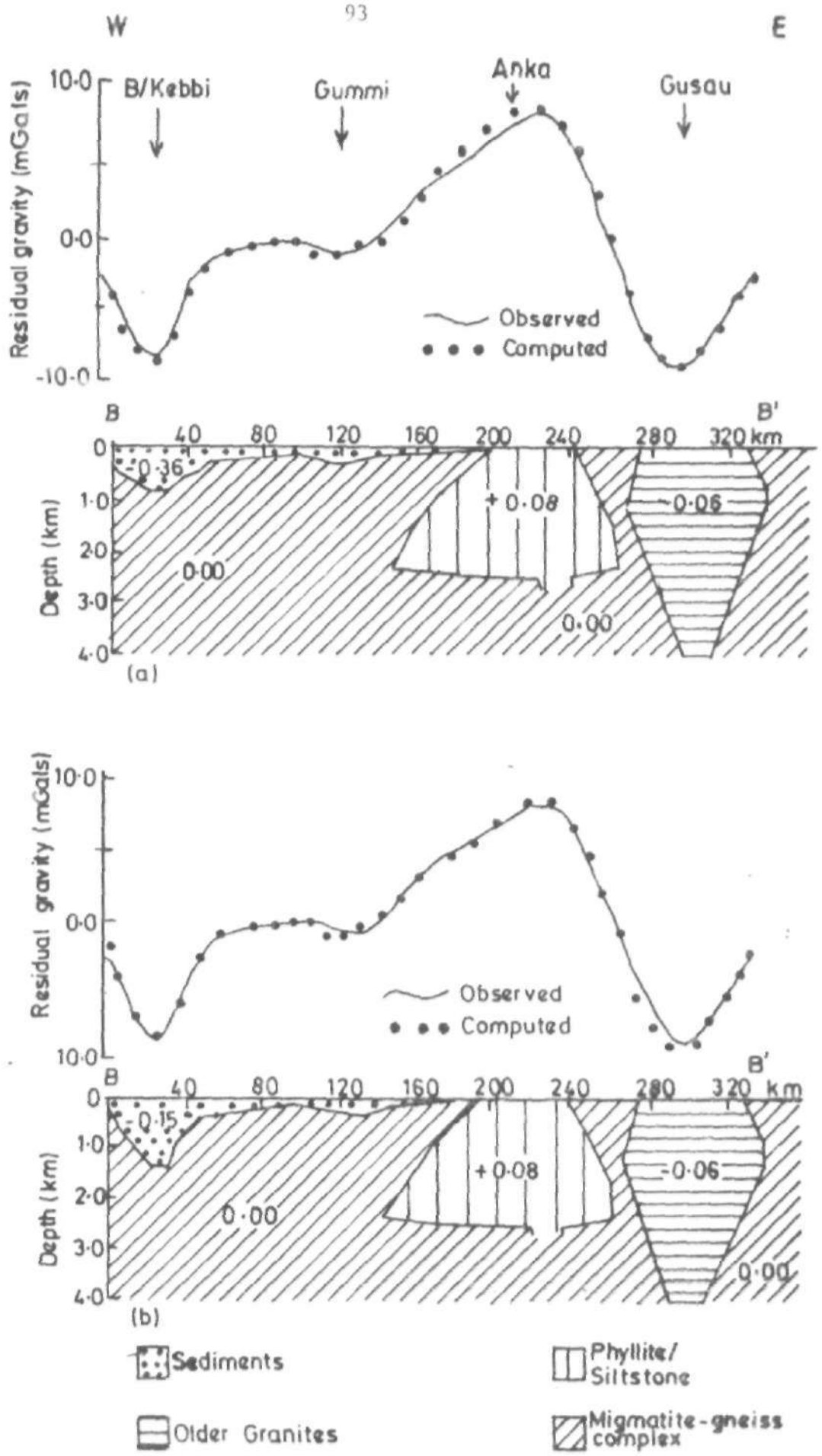


Fig. 4.14. 3-D interpretation of residual gravity along profile B-B', shown as vertical cross-section. Density contrast given in g cm^{-3}.

The negative anomaly no.6 centered at about 40 km to the eastern end of the profile is caused by Older Granite intrusives, three isolated outcrops of which have been mapped around Gusau (Figures 4.8 and 4.14). The modelled granitic body is elliptical in shape and is alligned N-S with a strike length which is approximately 110 km while the width is about 67 km. The model suggests that the granite body dips outwards at angles of 75° and 64° in the western and eastern sides respectively, to a depth of 1.3 km. From this depth the dip is inwards at angles of 72° and 68° in the respective directions until the body terminates in a plug at a depth of 4.3 km.

Profile CC'; This profile was chosen to cross anomaly no.3 and the northern end of anomaly no.5 (Figure 4.8). It extends for a distance of almost 240 km from Lema in the west through Bedinga to a little beyond Talata Mafara in the east. The first model (Figure 4.15(a)) assuming a density of 2.34×10^3 kg m^{-3} for the sediments reveals that the basin is generally shallow along this profile. From Lema the basin dips gently from 0.2 km towards a local depression at Bedinga where the sediments attain a maximum thickness of 0.5 km in a wide depression. The alternative model (Figure 4.15(b)) assumes a density of 2.55×10^3 kg m^{-3} for the sediments and yields a maximum sedimentary thickness of 1.0 km. From there the sedimentary thickness decreases gently until the contact with the basement rocks around Talata Mafara.

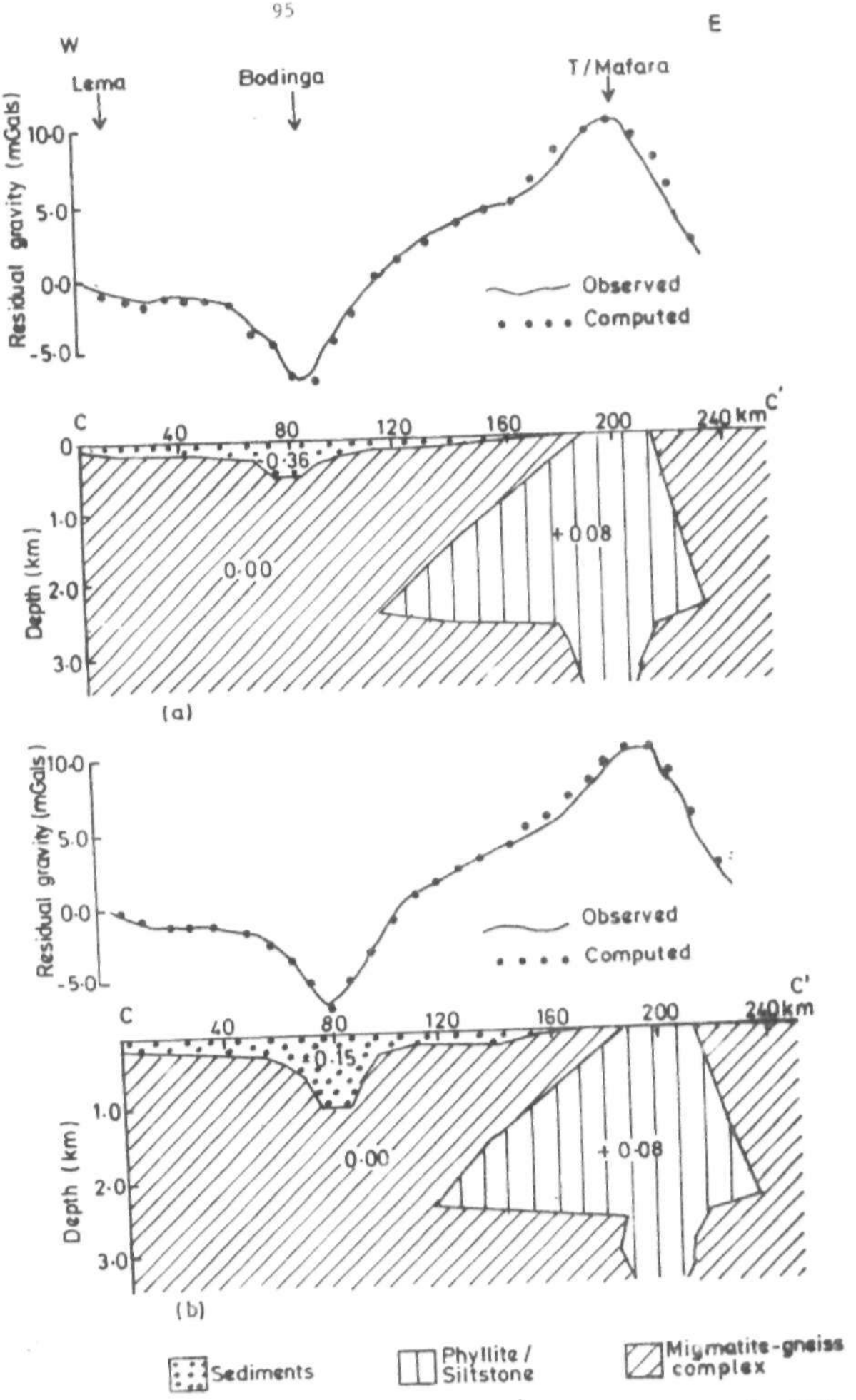


Fig. 4.15. 3-D interpretation of residual gravity along profile C-C', shown as vertical cross section. Density contrast given in g cm^{-3}.

The profile also cuts across anomaly no.5 for a distance of about 20 km. The phyllite body again dips outwards in both directions - 39° towards the west and 71° towards the east attaining a large width of almost 120 km at the base at a depth of 2.5 km. The otherwise flat base extends in a v-shaped form to a depth of 3.5 km over a lateral distance of 40 km.

Profile DD': The first half of this profile lies within the portion of the basin where only the continental Gundumi Formation overlies the basement. It extends in a roughly NNE-SSW direction from Sabon Birni at the northeastern end of the survey area to Talata Mafara and thence to Anka (Figure 4.8). The first model which assumes a density of 2.34×10^3 kg m^{-3} (Figure 4.16(a)) reveals that the Gundumi Formation has a maximum thickness of 0.5 km in this direction, while the alternative model with assumed sediment density of 2.55×10^3 kg m^{-3} (Figure 4.16(b)) yields a maximum thickness of 0.8 km for this formation. The profile gives the strike length of the metasedimentary sequence causing anomaly no.5 as roughly 100 km, and the general thickness as 2.5 km as obtained from profiles B-B' and C-C' respectively. The causative body dips outwards at an angle of 67° towards the NNE direction and 55° towards the SSW direction. The general thickness of 2.5 km is again extended to 3.5 km in a v-shaped root for a lateral distance of about 30 km.

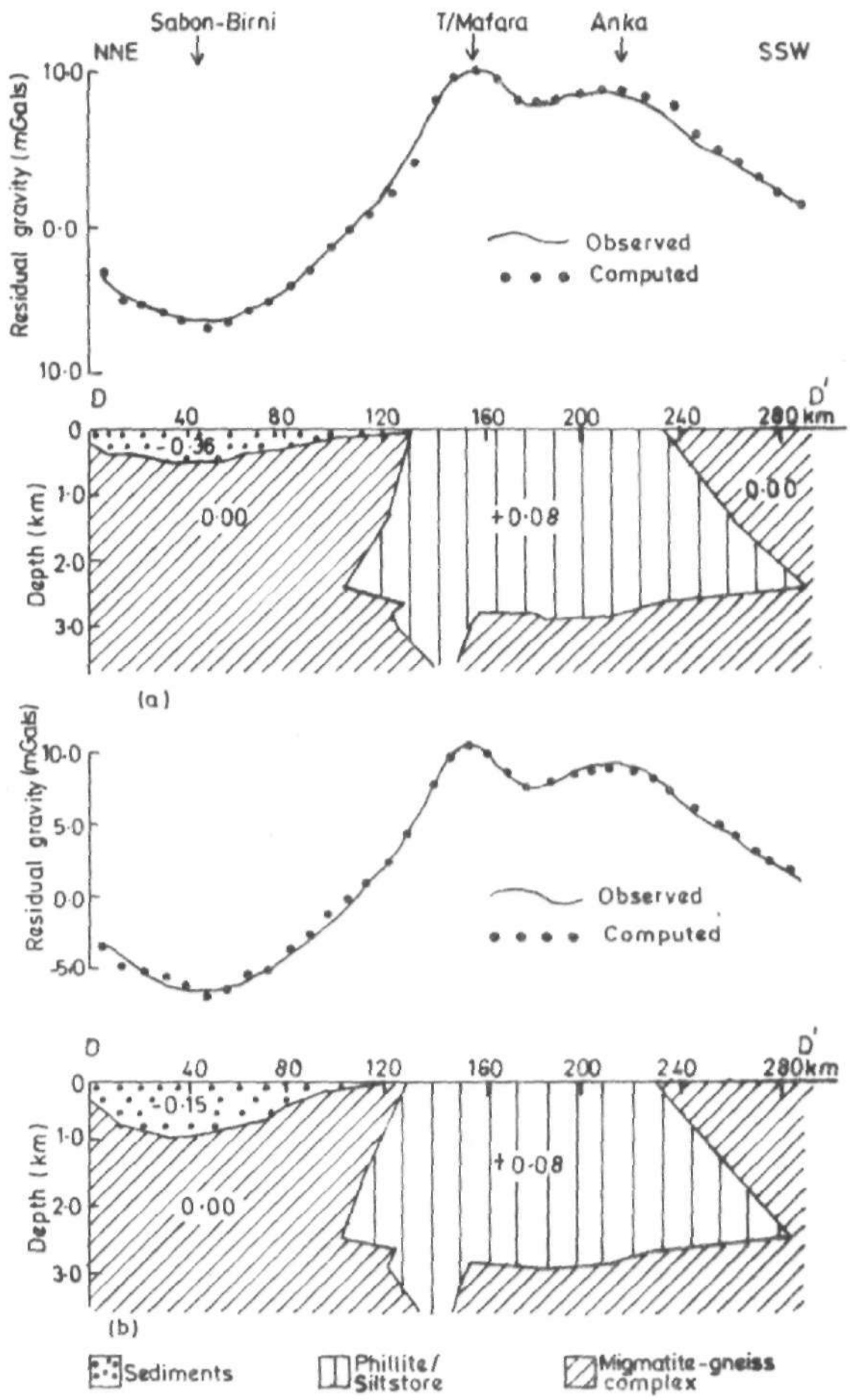


Fig. 4.16. 3-D interpretation of residual gravity along profile D-D', shown as vertical cross section. Density contrast given in g cm^{-3}.

4.6 Discussion

The results of the gravity investigation are generally in agreement with the known/inferred geology of the survey area. In the basement region the prominent negative anomaly no. 6 correlates well with mapped outcrops of Older Granite intrusives with a relatively low density (2.64×10^3 kg m^{-3}) compared with the host rock which in the region are the migmatite-gneiss complex (average density 2.70×10^3 kg m^{-3}) Thus both gravity and density evidence confirm the acidic nature of the Older Granite suites in this part of the basement block of northern Nigeria. The results from three-dimensional interpretation of the single profile that cuts across the Older Granite outcrops have thrown some light on the structure and possible mode of emplacement of these granites. First the sheer size of the granite body at depth is an indication that either the small isolated outcrops around Gusau coalesce at depth as one big pluton (batholith?) still being unroofed at the present time (Fitches *et al.*, 1985); or that the 5 km gravity station spacing in this area is not adequate to resolve the intrusives as distinct small bodies. More detailed gravity investigations will help to resolve this issue as well as determine the extent and fine structure of these bodies. The sharp contact with the host rock and the characteristic ovoid to elongate form concordant to the regional N - S trend support magmatic stoping and/or diapric process as the likely mode of emplacement for

the Older Granites. Thus these granite bodies most probably belong to the widely distributed Pan African magmatic suite.

Also the positive anomaly no. 5 coincides with outcrops of phyllites/siltstone of the Anka Schist Belt (density 2.78 x 10^3 kg m^{-3}) The models show that the metasediments in this area have outward dipping contacts with the host rock. The single phyllite outcrop modelled reveal that this rock unit attained a general thickness of about 2.5 km and the width at this depth extends laterally to a distance of at least twice to four times the exposed width on the surface - giving the sequence a characteristic flat bottom shape. The single root indicated on the models in profiles B-B' and C-C' and D-D' (Figures 4.15 - 4.17) are aligned in a roughly N-S direction and may probably correspond to a fold axis in this general N-S direction. The fairly simple structure revealed for the metasedimentary sequence in this region is an indication that the sequence has probably been affected by only one tectonic episode which has imposed the observed simple fold pattern with axis in a N-S direction. This general N-S structural grain is a Pan African (600 ± 150 Ma) trait. On account of this fairly simple structural style of the metasediments in this region, the gravity results tend to support the view that the Anka Schist Belt belongs to the younger group of metasediments (Turner, 1983; and Fitches et al., 1985). However, Holt et al. (1978) suggested that the belt also has

some Kibaran (1100 ± 100 Ma) trait, which tends to group the Anka belt with the older group of metasediments. More geophysical and geological investigations of this and other schist belts might throw more light on this issue.

From this study, and previous gravity surveys in other parts of the schist belt region of northwestern Nigeria (Udensi et al., 1986; Gandu et al., 1986), there has not been the characteristic paired linear gravity anomalies usually associated with suture zones as reported in Turner (1983). Thus the view that the Nigerian schist belts might possibly represent additional suture zones similar to those found near the active margin between the West African Craton and the Pan African Province (Turner, 1983) is unlikely. The other alternative that the schist belts in Nigeria might represent deformed intracontinental basin(s) (Turner, 1983), developed during the subsidence stage of the Pan - African orogenic cycle (McCurry, 1976, 1978) may be more likely. More extensive gravity investigations of the region are however required to confirm this view.

Over the basin the prominent negative residual anomalies (nos. 2 - 4 on Figure 4.8) have all been attributed to increased thickness of sediments at basement depressions in the absence of any other geological evidence to the contrary. Difficulties associated with a thin crust of lateritic cover over

most of the formations, and the relatively small thickness of some of the formations led to the adoption of a single mean density for the sediments in the interpretation of the gravity data. Maximum sediment thicknesses of 1.0 km and 2.0 km were obtained using mean densities of 2.34×10^3 kg m^{-3} and 2.55×10^3 kg m^{-3} respectively. A choice between the two thicknesses depends on which mean density is considered more representative for the formations in the basin. If available geological evidence on estmates of the maximum sediment thickness in the basin is correct, then the mean density of 2.34×10^3 kg m^{-3} gives results that agree more with the geology. Thus the mean density of 2.34×10^3 kg m^{-3} determined for all the rock samples, and the corresponding maximum sediment thickness of 1.0 km are hence adopted as the representative mean density and maximum thickness of the sediments in the Sokoto Basin. This result is however subject to further verification when more geophysical information become available to constrain the models.

314067

The models reveal a very gentle dip of the general basement surface towards the border with Niger Republic. Superimposed on this gentle regional dip are small undulations that produce basement depressions towards which the basement surface dips locally in varied directions and magnitudes. At least four such depressions were identified in different parts of the

basin in which the sediments attain maximum thicknesses ranging from 0.5 to 1.0 km. A ridge - like feature meanders wildly throughout the basin following almost the zero contour line on the residual anomaly map (Figure 4.7), and this controls the location of the depressions. Two of these depressions on the buried basement surface are aligned roughly along the same N-S axis on profiles B-B' and C-C' (Figures 4.14 and 4.15) which tend to suggest a gentle folding of the underlying basement rocks along a general N-S axis.

CHAPTER FIVE

M A G N E T I C I N T E R P R E T A T I O N

5.1 Introduction

Interpretation of aeromagnetic data took giant foward strides with the introduction of digital data processing, with the result that interpretation is now rapid, objective and anomaly resolution greatly improved (Hartman et al., 1971). Approaches to interpretation have generally been divided into three basic groups:

i. Qualitative method - inspection of maps

ii. Profile method - involving the study of profiles

iii. Map method - involving mathematical processes applied to map data (Reford and Sumner, 1964).

In qualitative interpretation, simple concepts are used to obtain information by detailed inspection of magnetic contour maps. The excellent correlation which often exists between magnetic data and geology is a demonstration of the potential of the qualitative method of interpretation of magnetic anomaly maps.

However, whenever it is important to extract definite parameters from magnetic data, then the more sophisticated quantitative methods of data treatment are invoked. For instance in oil surveys, basement depths are needed, while in mineral surveys susceptibilities and dips are more important. With suitable assumptions on geometry of the magnetic sources, the

problem of determining these parameters often reduces to simple mathematical expressions which can be solved by the profile method. Several other interpretation techniques involving the use of residual maps, derivatives and continuations can be grouped as the map method and is capable of yielding information on depths to the causative bodies as well as emphasize special attributes of the total field map.

5.2 Qualitative Interpretation

The total magnetic intensity composite maps were shown in Figures 3.3 and 3.4 as contour and density plots respectively. The dynamic range of the total intensity magnetic field is 700 nT, the contour levels ranging from 7385 nT to 8085 nT; with an average value of 7820 nT. At first glance the contour map (Figure 3.3) appears clustered with mainly short wavelength anomalies from near surface geology, which are superimposed on a subtle northeast trending grain consistent with the strike of the basin. A close examination however reveals some definite patterns and similarities in the shape and alignment of the short wavelength anomalies.

Most of the short wavelength anomalies are circularly or elliptically shaped, and their alignment clearly define three prominent linear belts marked A-A, B-B, and C-C which trend NNE-SSW, NW-SE, and N-S respectively (Figure 5.1). The shape of these short

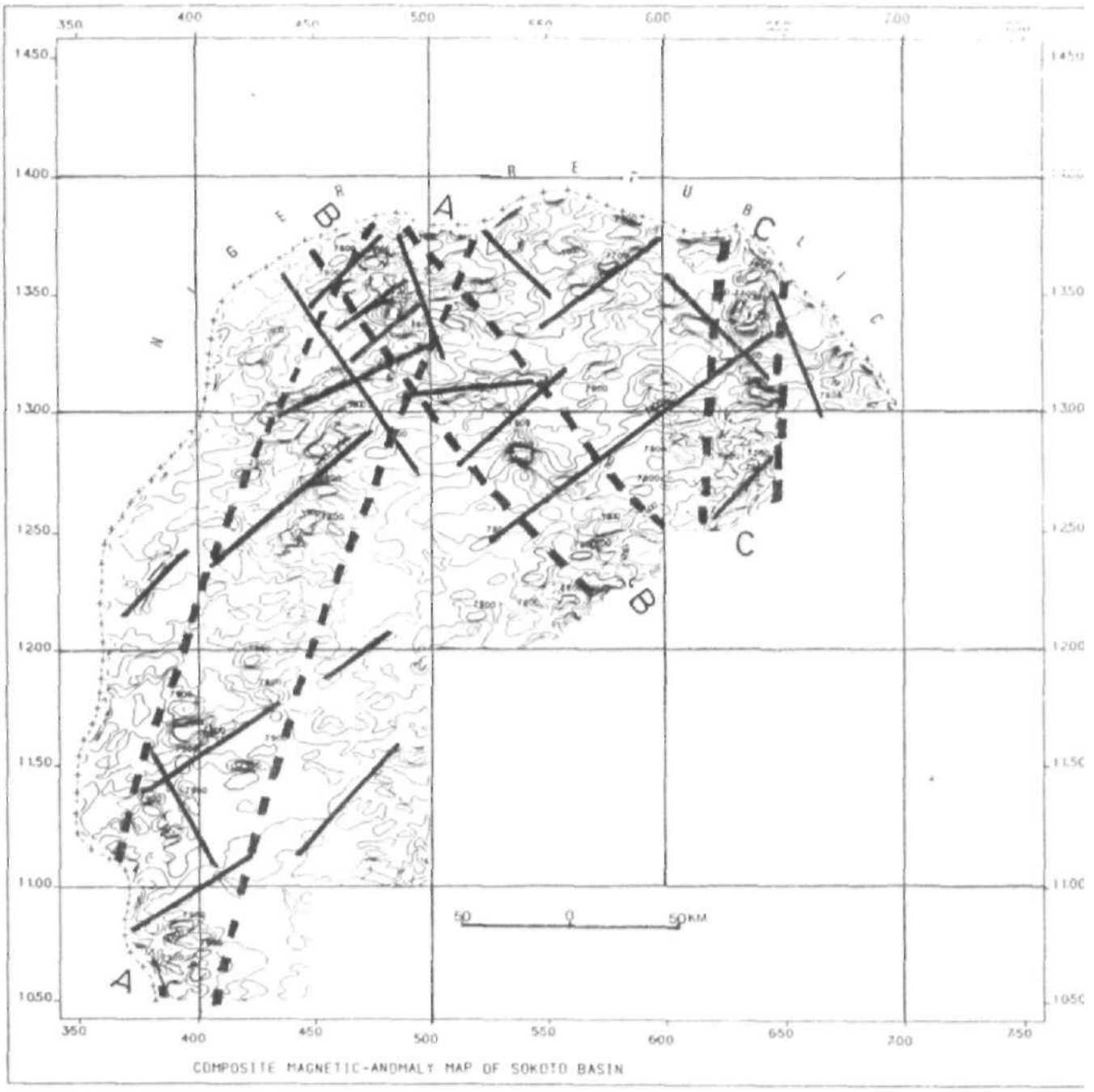


Fig. 5.1 Some inferred lineament trends superimposed on the total magnetic field intensity contour map of Sokoto Basin.

wavelength anomalies is suggestive of shallow intrusives, either within the sediments or on the underlying basement surface.

Another important feature that is evident on both composite maps (Figures 5.1 and 5.2) is the set of large scale magnetic lineations deminant in both the northeast and northwest directions. These magnetic lineations are indicated as thick lines in both Figures 5.1 and 5.2, and then compiled separately as Figure 5.3. A quick look at Figures 5.1 to 5.3 reveals a remarkable consistency in the arrangement and concentration of the magnetic lineations and the short wavelength anomalies along the three linear belts mentioned above, and which has been superposed on the features shown in Figure 5.3. The characterization of these magnetic lineations either as faults, fractures, etc. is of vital importance in the understanding of the tectonic history of this region.

Wright (1968) had earlier identified a conjugate pair of NE-SW and NW-SE fractures in other parts of the African continent such as the Benue Treugh region in Nigeria, the Cameroun rift valley, the Middle Niger lineament, and the Chad and Congo Basins. He attributed these features to the sequence of events at possible sites of partial release of distorting stresses which accumulated from the wedging apart of Africa and South America throughout most of the Cretaceous, and the subsequent readjustment of the shape of Africa due to

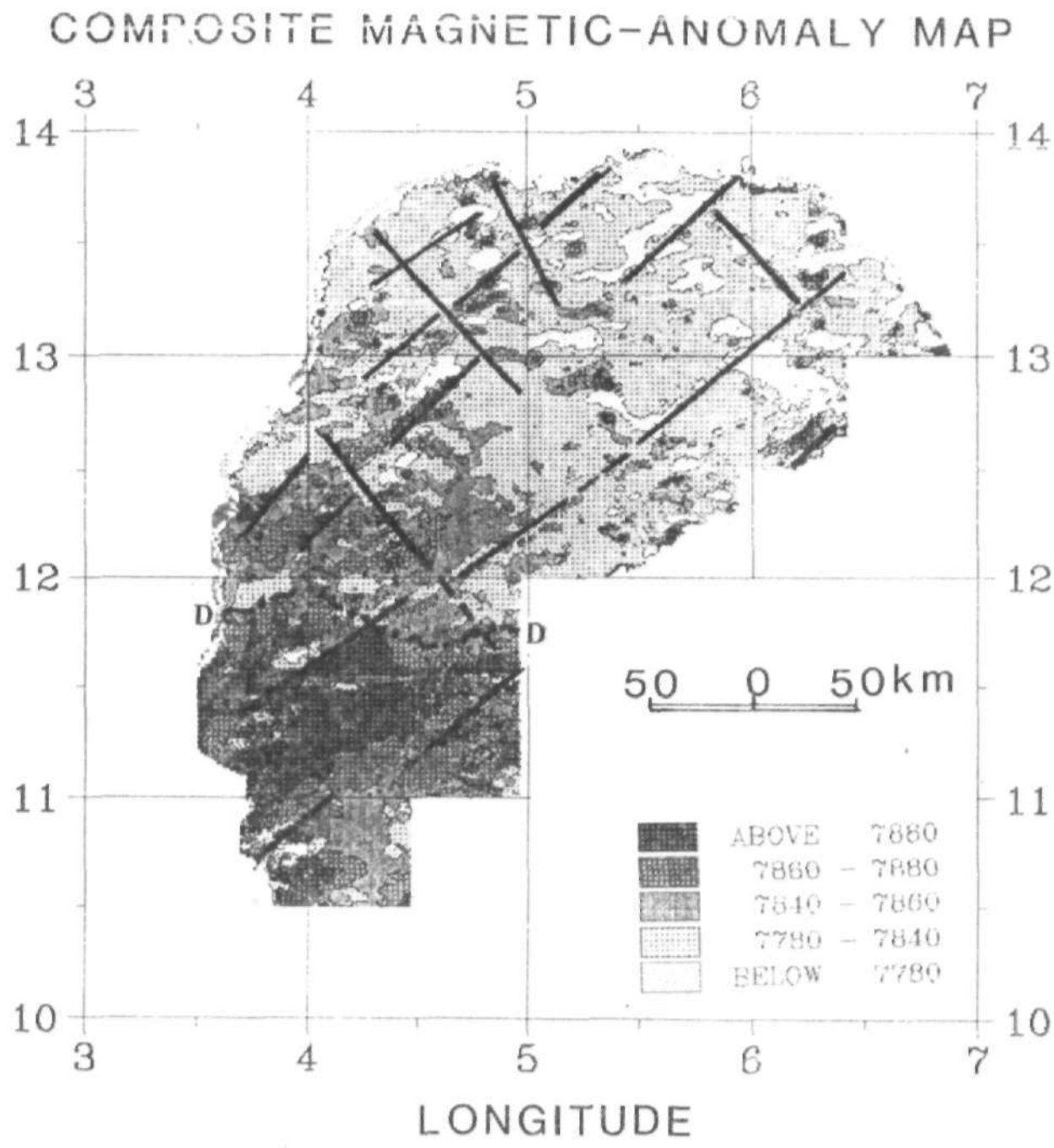


Fig. 5.2 Some inferred lineament trends superimposed on the density plot of total magnetic field intensity of Sokoto Basin.

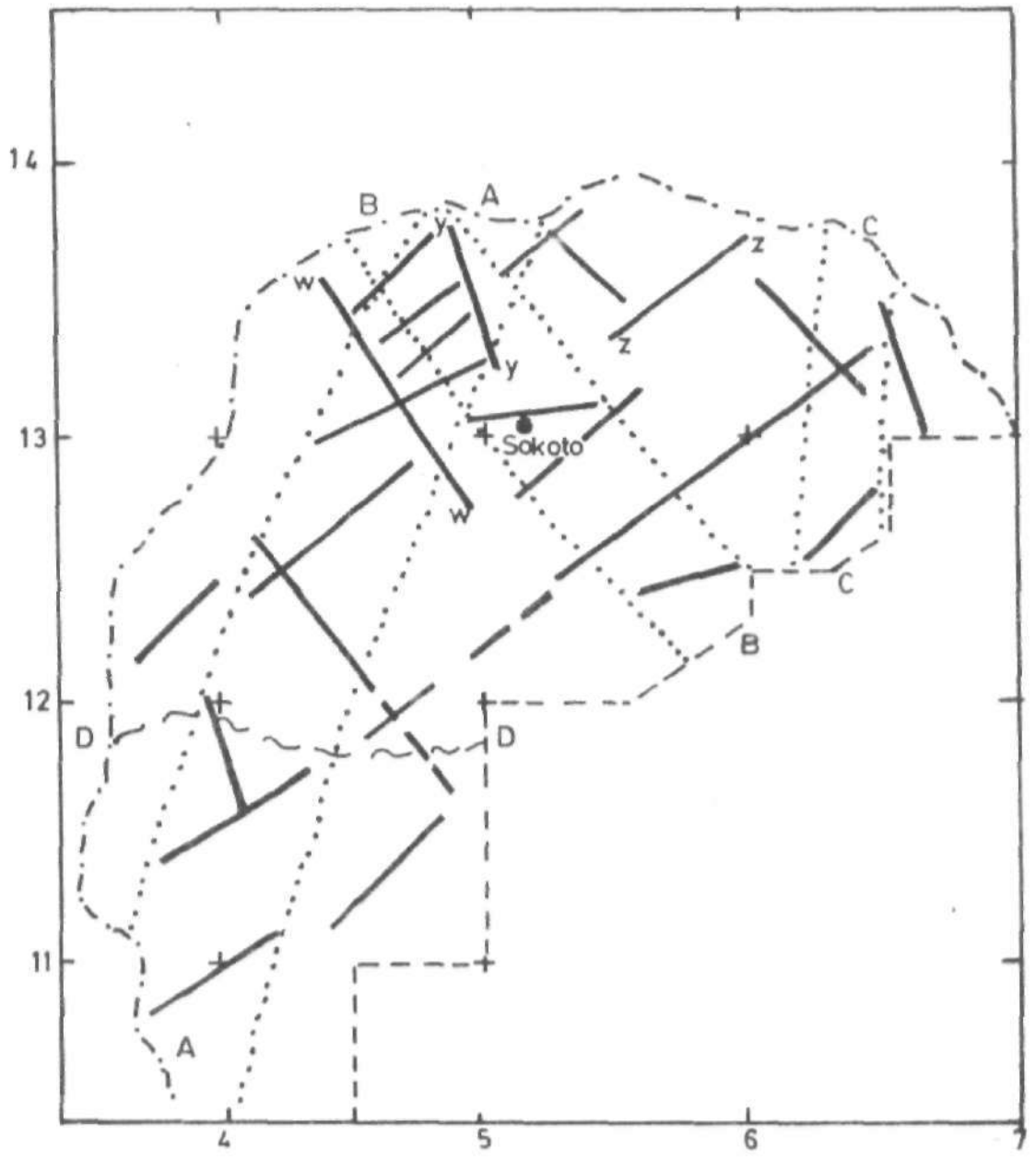


Fig. 5.3 Map of the Sokoto Basin showing major magnetic lineaments derived from the composite maps.

the separation of South America. Ajakaiye et al. (1986) reported the existence of NE-SW trending narrow magnetic lineations upon which were concentrated the Alkaline Ring Complexes. Ananaba and Ajakaiye (1987) had on the basis of lineament analysis of LANDSAT images identified predominant tectonic trends in the NE-SW, NW-SE, and N-S directions over the present survey area in particular and other parts of the country north of 8° N latitude in general. They proposed global tectonics as a possible origin of these lineaments. Similar studies by Ball (1980), Neev et al. (1982), Ananaba (1983), and Oluyide (1988) have also identified a set of NE-SW and NW-SE conjugate strike-slip fracture system interpreted to be of tectonic origin.

Thus the alignment of the three linear belts identified in the present study, and that of the magnetic lineations within them is in agreement with the reported general tectonic trend over this region. The three prominent linear belts probably represent pre-existing lines of weakness in the continental crust which became rejuvenated during the tectonic phase of the Pan African Orogeny. Thus the concentration of intrusives responsible for the short wavelength anomalies along these linear belts is explained. The short wavelength anomalies might be the magnetic expression of shallow granitic intrusives belonging probably to the Pan African (600 $\pm$ 150 Ma) event. In view of the close association of mineralization with

regional tectonics (Ananaba and Ajakaiye, 1987), it is recommended that more detailed ground follow-up studies be concentrated along these linear belts as they could be loci of economic mineralization.

There is almost a one-to-one correspondence between some of the magnetic lineations identified in this study and some faults reported in previous studies (Kogbe, 1979 and GSN, 1988). For example two of three prominent fractures mapped by GSN (1988) NW of Sokoto coincide with two NW-SE trending magnetic lineations (marked w-w, and y-y in Figure 5.3) mapped in this study. Similarly Kogbe (1981) reported a WSW-ENE trending fault in the vicinity of Gilbedi village; and from this study a prominent NE-SW trending magnetic lineation marked z-z in Figure 5.3 is identified in the vicinity of this village. It is thus possible that some of the other magnetic lineations mapped in this study might represent faults or fractures hitherto unmapped in the basement complex, while others could possibly be contacts of rocks of different lithologies.

Other regions on the composite maps outside the linear belts are characterised by rather smooth contours with low gradients which is suggestive of either a deeper source horizon or uniform magnetic properties of the underlying basement rocks. Some other features of the composite maps are better highlighted on the density plot (Figure 5.2). One example is the sudden change in magnetic intensity across the

boundary marked D-D in Figure 5.2 leading to two distinct magnetic zones. The region to the south of this boundary is characterised by magnetic intensity generally above the regional average of 7820 nT; whereas the region to the north of the boundary is marked by near average or below average values. This observation cannot be readily explained on the basis of known geology of the region, but one possible explanation is the presence of contrasting rock types in the underlying basement - more mafic to the south and more felsic rocks to the north. However this conclusion needs further verification.

The composite maps have thus helped to establish a regional framework for the interpretation of magnetic studies of limited areas within the Sokoto Basin, and in selecting areas for detailed investigation. It is hoped that this compilation and a similar one by Ajakaiye et al. (1985), can be utilised in assembling a more comprehensive magnetic data bank and in compiling a composite magnetic anomaly map of the entire country, which would aid regional geologic mapping.

5.3 Quantitative Interpretation

5.3.1 Introduction

As pointed out earlier, quantitative interpretation of potential field data can be done either in map form or on profiles, each with its advantages and limitations. The maps have the advantage of presenting

the total picture available without any assumptions regarding strike and lateral extent of the source (Jain, 1976). These maps however, are often produced from computed gridded data which may not represent the original data in true form. Gridding intervals invariably impose limitations on the resolution achievable, which in turn introduces errors on the contours.

On the other hand profile interpretation methods allow interpretation of data as recorded, or at least eliminates contouring related errors. But the technique often assumes the profiles are normal to the strike direction, and that the bodies extend to great distances on either side of the profile. In practice, this latter limitation is often satisfied, while the effect of the former can be minimised by comparison of results from adjacent profiles.

Another disturbing problem relates to the degree of geological interpretation that should be attempted. While some explorationists feel that magnetic interpretation should be mostly qualitative and never go beyond generalised basement depth maps; others engage in more rigorous mathematical analysis to produce more detailed geological interpretation including detection of local relief on basement surface (Jacobsen, 1961). Each group is right to some extent, depending on the quality of data being analysed, and the amount of other geological and geophysical information at the disposal

of the interpreter. However geophysicists generally agree with the following conclusions (Jacobsen, 1961).

i. Careful analysis of intrabasement-type magnetic anomalies may yield a reliable and useful generalised basement depth map.

ii. Local basement relief based on a study of the usually smaller, suprabasement magnetic anomalies can not be reliably interpreted from magnetometer work alone.

In the present study, the digital data was recovered from contoured maps, albeit by the best possible technique, and the data gridded to produce profiles for quantitative interpretation. Therefore in recognition of the foregoing limitations and mindful of the danger of attempting to obtain more from the data than is warranted, the profile interpretation method was adopted with the primary objectives of

i. analysing the relatively large anomalies to obtain the depth estimates of the causative bodies,

ii. using the result from (i) to prepare the generalised magnetic basement depth map of the basin, and

iii. making any reasonable deductions on the structure of the basin based on the map.

5.3.2 The Computational Method

Various methods have been applied for automatic interpretation of digitised magnetic profile data (Koulomzine et al., 1970; Hartman et al., 1971; Nabighian, 1972; Jain, 1976). The Werner deconvolution technique first described by Werner (1953) was used in this study to calculate the physical parameters, i.e.

depths, horizontal locations, dips and susceptibilities, associated with the magnetic sources when these sources are assumed to be thin dykes. Hartman et al. (1971) expanded the usefulness of the method by considering the thin dyke body as an approximation in resolving other kinds of anomalies. They showed that the magnetic anomaly for a thin sheet is precisely the same as the derivative of the magnetic anomaly for a similarly positioned interface. Thus by performing Werner-based deconvolution on both the total field and the calculated horizontal derivative of the total field, it is possible to identify thin sheets and individual interfaces as well as wide sheets. Using various simulated situations, Jain (1976) established the limits of resolution and possible accuracy of the Werner deconvolution technique.

5.3.3 Basic Theory of the Werner Deconvolution Technique

Using the concept of magnetic 'charge' or pole strength, the expression for the total magnetic field due to a thin dyke with infinite strike length and depth was derived in Appendix B in the form quoted by Hartman et al. (1971) as :

$$F(x) = \frac{A(x-x_o) + Bz}{(x-x_o)^2 + z^2} \qquad \ldots\ldots 5.1$$

where, F = the total magnetic field intensity at x,

x = horizontal distance along the profile,

x_o = horizontal distance along the profile to the centre point above the dyke,

z = the depth to the top of the dyke, and

A and B are functions of field strength, susceptibility and source geometry.

When observation is made on a level plane over level-bounded bodies whose length and depth are infinite and whose strike is perpendicular to the direction of the profile, equation (5.1) can be cast into the following interpretation equation

$$x^2 F = a_o + a_1 x + b_o F + b_1 xF \qquad \ldots. 5.2$$

where x and F are as described in equation (5.1), whence

$$a_o = -Ax_o + Bz, \quad a_1 = A$$
$$b_o = x_o^2 - z^2, \text{ and } b_1 = 2x_o \qquad \ldots. 5.3$$

It follows from equation (5.3) that the depth and horizontal position of the dyke are

$$z = \pm \tfrac{1}{2}\sqrt{(-4b_o - b_1^2)} \qquad \ldots. 5.4$$
$$x_o = \tfrac{1}{2} b_1$$

If allowance is made for the possibility of interference and assuming that the interference can be represented by a polynomial, then on adding the interference term, equation (5.1) becomes

$$F(x) = \frac{A(x-x_o) + Bz}{(x-x_o)^2 + z^2} + c_o + c_1 x + \ldots.. c_n x^n \quad .. 5.5$$

where n is the degree of the polynomial, and the c's are the coefficients. Thus instead of 4 unknowns in equation (5.2), there are now (n + 5) unknowns in equation (5.5). Therefore (n+5) equations are required

to solve for the unknowns. In practice, a first or second degree polynomial is generally sufficient, so that 6 or 7 data points are required for the solution.

Generally the field resulting from a geologic distribution of sources in space can be viewed as the two-dimensional convolution of the spatial impulse response with the source distribution function (Hartman et al., 1971). The problem of determining the source parameters from the recorded field is therefore reduced to a deconvolution. Thus, by deconvolving both the total field and the calculated horizontal gradient of the total field, it is possible to identify thin sheets (dykes, sills, etc.), and individual interfaces (faults, dipping contacts, edges of intrusive bodies etc.), irrespective of their strike, dip or remanent magnetization and at any magnetic latitude with the initial assumption that the bodies strike perpendicular to the profiles.

5.3.4 The Interpretation Procedure

In this interpretation, a total of 350 N-S profiles spaced 1.1 km apart have been analysed using a computer program Magdpeth (Ojo, 1985) which is similar to that described by Jain (1976). Along each profile the data points are at equal linear intervals of 0.55 km but there was also a provision for interpolation in the computer program so that the actual data points utilised were approximately at 0.28 km intervals. A first degree polynomial was considered

adequate for the interference component, so that six points were required for the solution of equation (5.2). The program examines six successive data points and solves the resulting set of linear equations for the physical parameters of interest. The whole sequence is advanced by one point and the examination repeated. If a succession of such examinations consistently indicates a source for an anomaly, and if these indications are themselves consistent, the apparent depth and horizontal location along the profile of the source is recorded. Susceptibility and dip values are computed from A and B, and the local inclination and declination of the main field on the assumption that magnetization is induced. The location and depth estimates for any source was further examined, and solutions that lie within predetermined limits are counted. The number of such counts was used as a weighting factor. Only estimates with weights of three and above were accepted.

The "depth - penetration" of the process depends on the distance between the data points operated upon, that is the operator length. The broader a given anomaly, the longer must be the operator length required to recognize it. For this reason the computation sequence described above is repeated a number of times with the operator length successively increased. Before each pass, the data was smoothed with a low pass filter to remove high frequency ('shallow') anomalies

which have already been recognized, and which would otherwise mask deeper anomalies (Hartman et al., 1971; and Friedberg, 1975).

The accepted depth points along each profile are plotted as a function of the horizontal position of the source along the profile; to produce the so-called 'Werner profiles'. The above is as far as the automation and objectivity of the technique goes. Further interpretation of the 'Werner profile' to define say the basement surface calls for all the professional experience and available geological information at the interpreter's disposal.

5.3.5 Estimation of the magnetic basement surface

Figures 5.4 and 5.5 are examples of typical Werner deconvolution profiles processed to define magnetic basement beneath the principal anomalies. The depth points represent solutions obtained from a suite of 15 six-point operators with lengths ranging from 1.4 km to 20.6 km. The first operator length (1.4 km) did not yield any consistent solution on any profile, while hardly any consistent solutions were obtained beyond the 20.6 km operator length. Wherever necessary, the geometric cosine correction was applied to the computed depths which occur on anomalies on the total field map that cross the profile direction at oblique angles. The nominal flight altitude of 152.4 m was subtracted from all the computed source depths before these depths were plotted.

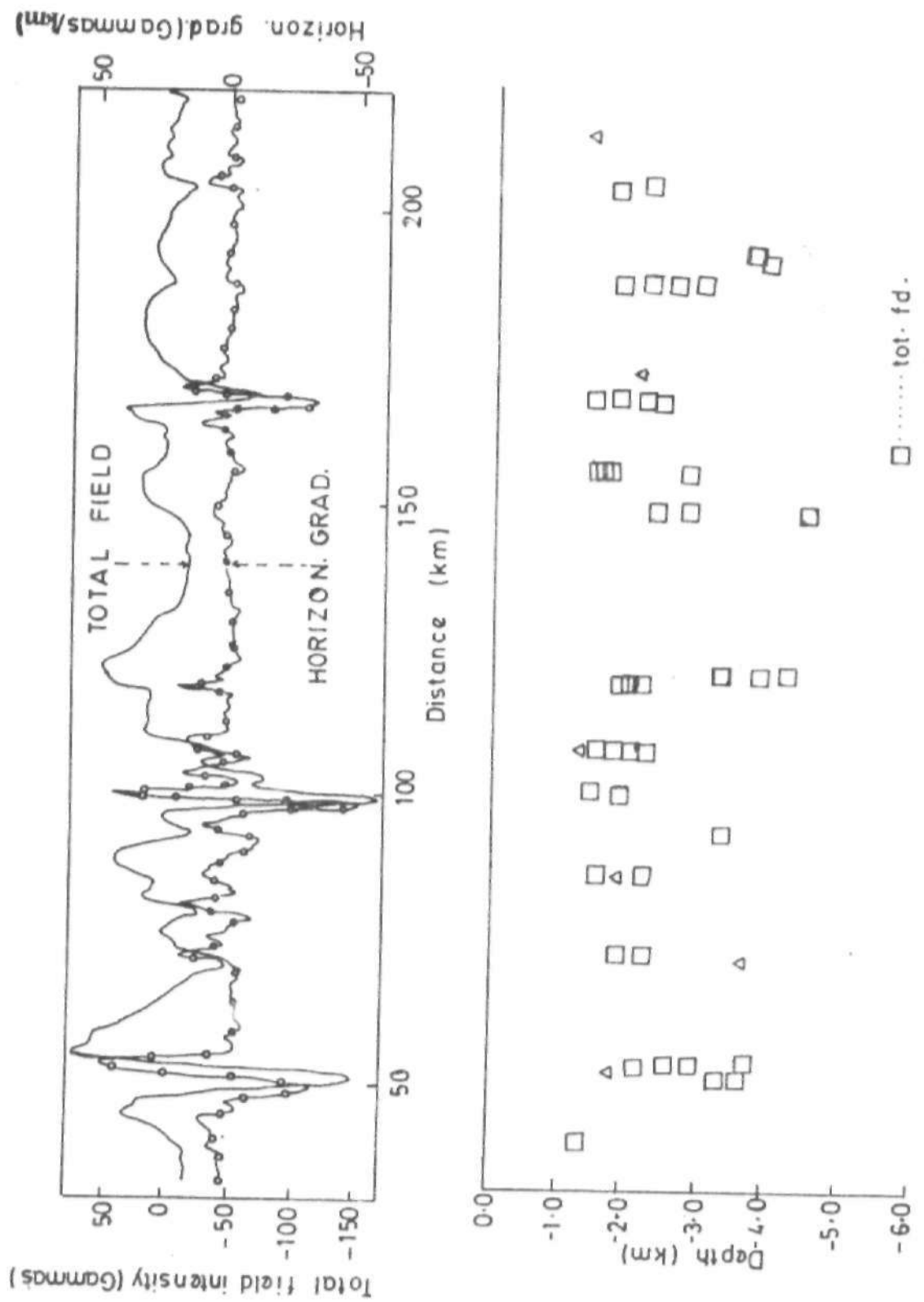


Fig. 5.4 A typical Werner profile processed to define the magnetic basement beneath the major anomalies. (N-S profile through longitude 5° 15' E)

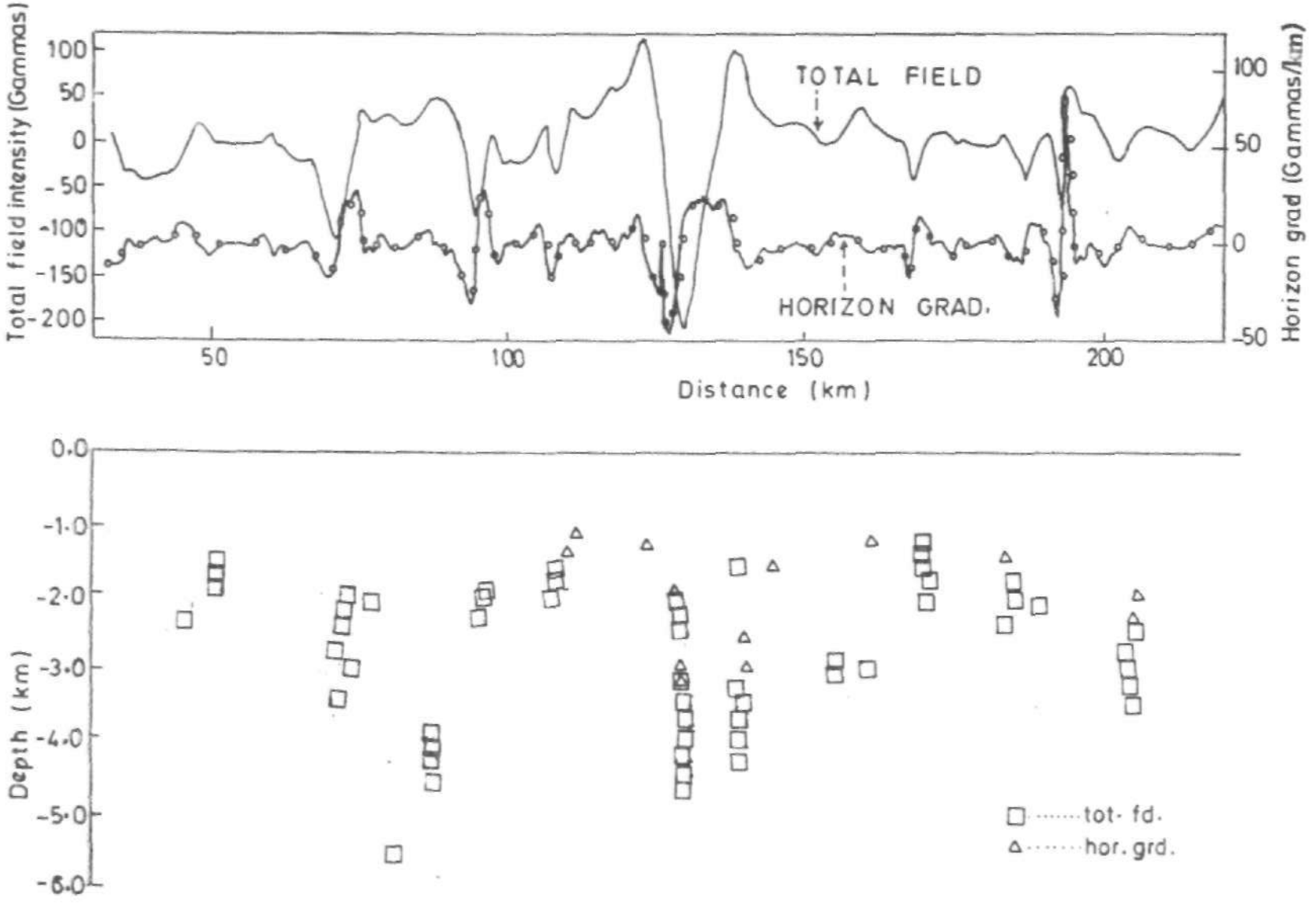


Fig. 5.5 A typical Werner profile processed to define the magnetic basement beneath the major anomalies. (N-S profile through longitude 5° 24' E)

As the profiles were sufficiently closely spaced, it was thought that the inspection of the interpreted depths on adjacent profiles would help to select valid depth estimates from appropriate anomalies to construct a reliable picture of the subsurface geology. However as can be seen from the typical profiles (Figures 5.4 and 5.5) there was a considerable scatter of the plotted depth points, rendering the definition of the magnetic basement surface a difficult task, involving a discriminatory evaluation of the computed depth points in the light of available geologic information. Some of the factors that contributed to the large vertical scatter of the computed depth points include

i. a particular feature can be recognised on more than one pass of the operator, and

ii. most sources often yielded both total field depths (deeper) and horizontal gradient depths (shallower) (Friedberg, 1975).

Ability to identify the nature of the source helped to improve the accuracy of the interpretation. The correct depth points appear very close to the top of the group of points (Hartman et al., 1971). In this study it was possible to choose reliable depth points to within a 14 percent error margin. Hartman et al. (1971) quoted an accuracy of 10 percent from an application of the technique to digitally recorded data. Thus the larger error margin in the present study is due in part to the low quality of the digital data set which was recovered from magnetic contour maps as compared to digitally recorded data.

Figures 5.6 and 5.7 show the Werner profiles of Figures 5.4 and 5.5 respectively after interpretation. The dashed envelopes represent the interpreted magnetic basement surface beneath each of the profiles. As Hartman et al. (1971) noted, a fundamental advantage of the whole technique is that since the depths were objectively determined, another interpreter with a different point of view or additional knowledge of geology can always go back to any feature and reinterpret the local structure far more successfully than he could if he were presented only with a set of depth contours.

5.3.6 Preparation of the Generalised Magnetic Basement Depth Map

The depth points lying on the envelopes in Figures 5.6 and 5.7 represent the magnetic basement surface at their respective locations. The exact depths and locations of these points were then transcribed from the computer listng of the Werner deconvolution profile solution, to avoid errors in reading the plotted depth scales. The X- and Y-coordinates of such points on the basemap were computed and these were recorded along with the depths in a master file. A total of 1,744 such depth points were obtained from all the profiles analysed. Figure 5.8 illustrates a miniature plot of the locations of the depth points used as a basis for the final contour map. The data set was then gridded and machine-contoured to produce the generalised magnetic basement depth map shown as Figure 5.9.

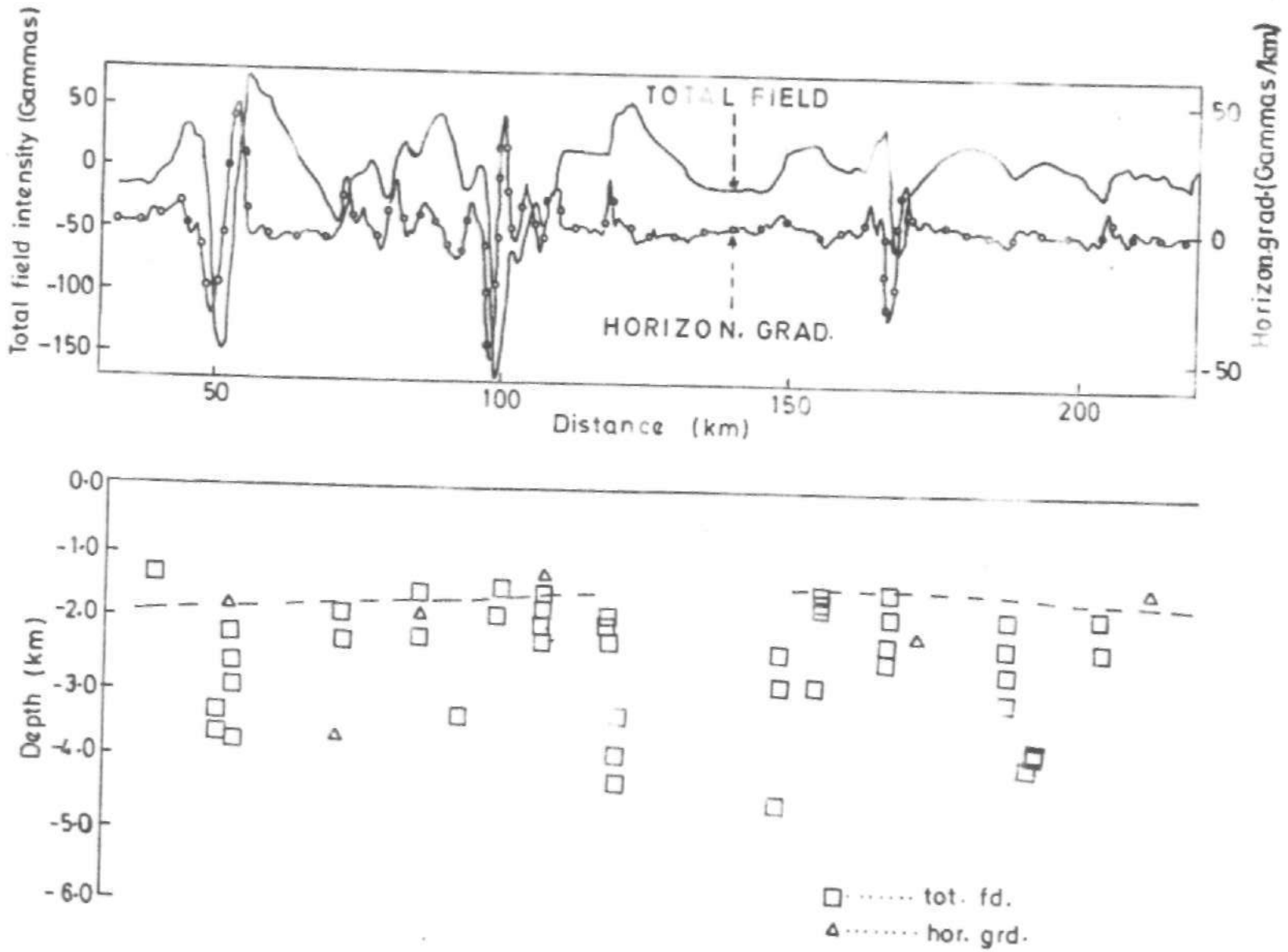


Fig. 5.6 The Werner profile of Fig. 5.4 showing the interpreted basement surface (as dashed lines).

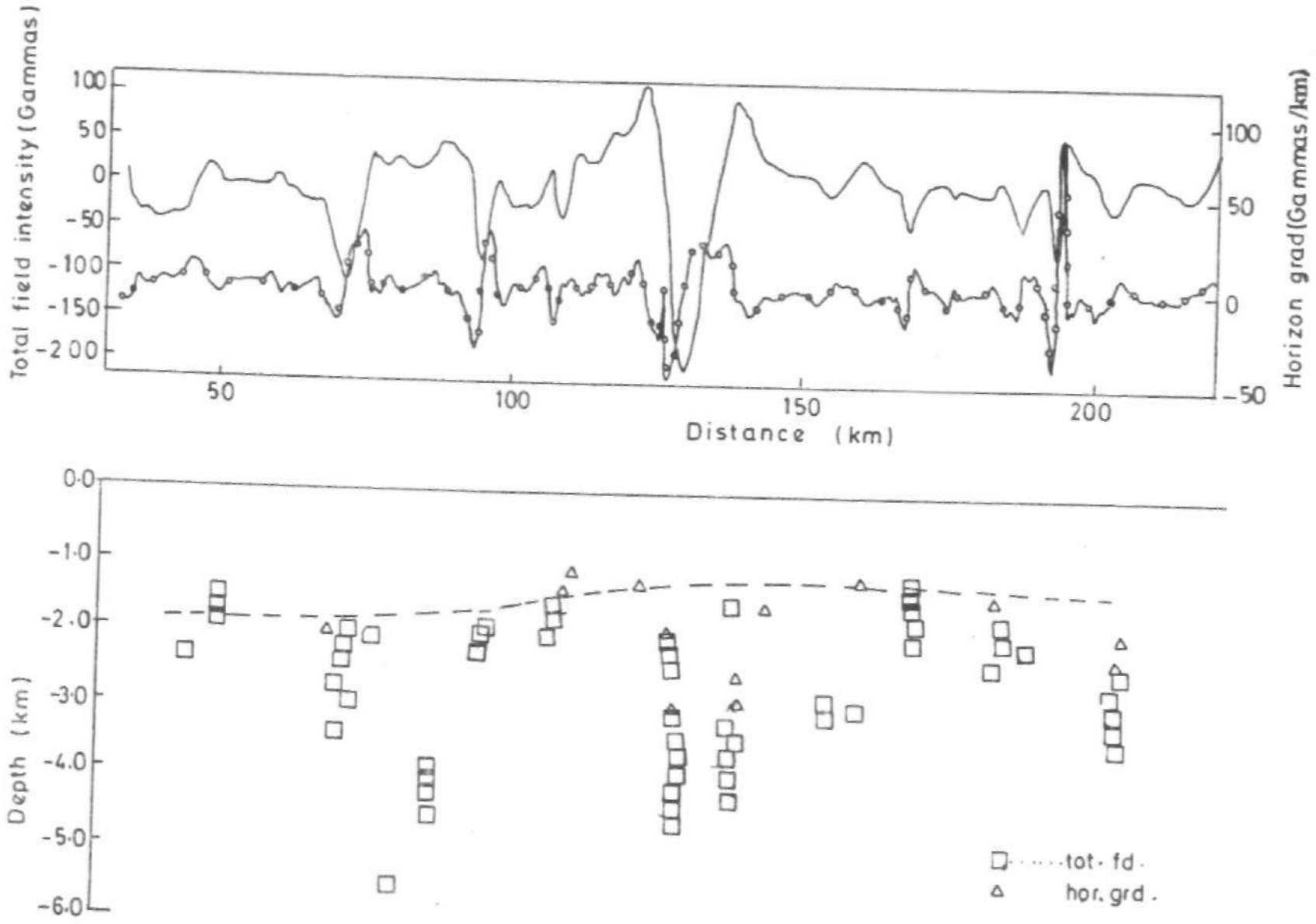


Fig. 5.7 The Werner profile of Fig. 5.5 showing the interpreted basement surface (as dashed lines).

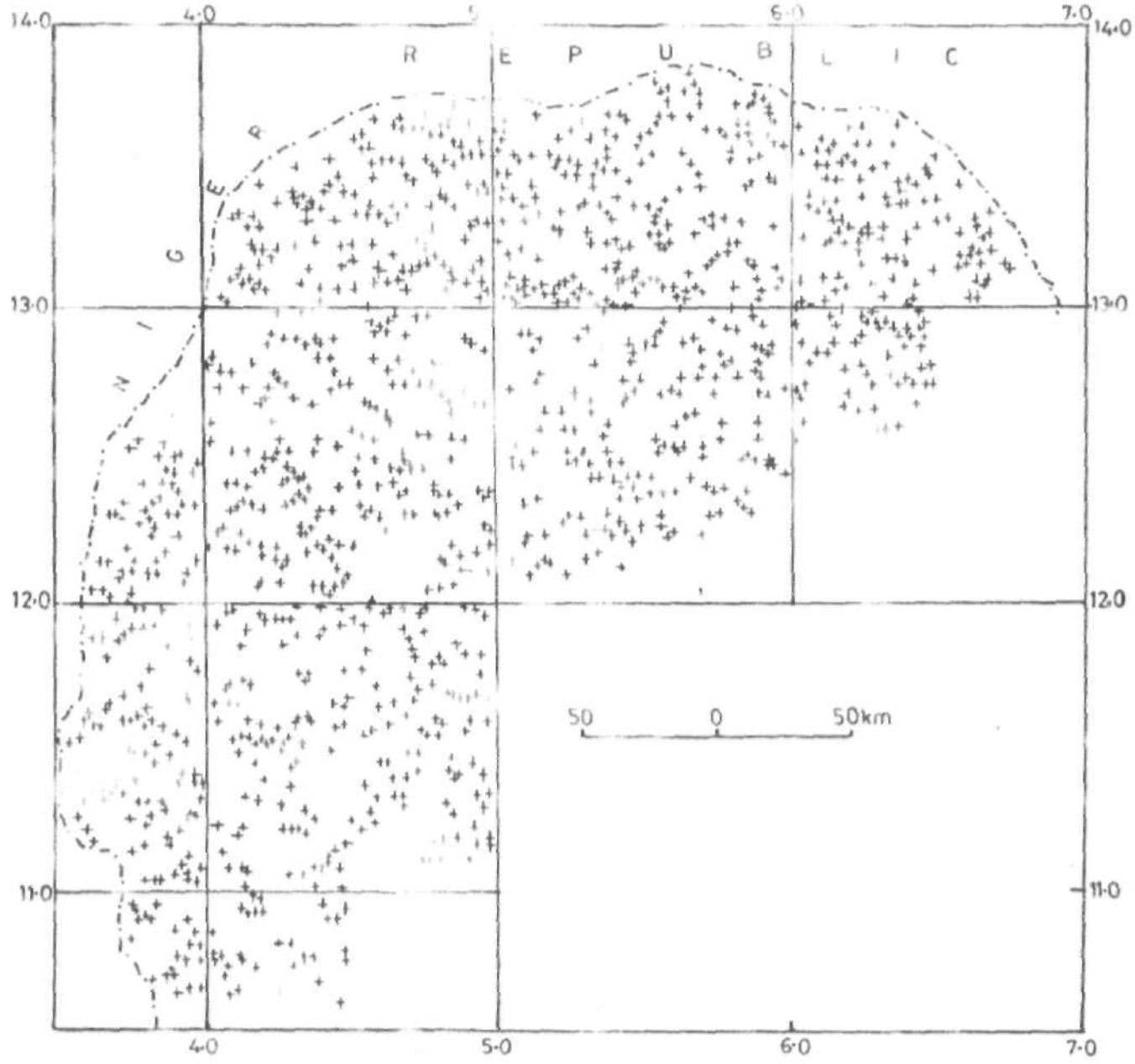


Fig. 5.8 The depth points transcribed from Werner deconvolution profile and used as the basis for the contoured depth to basemement map.

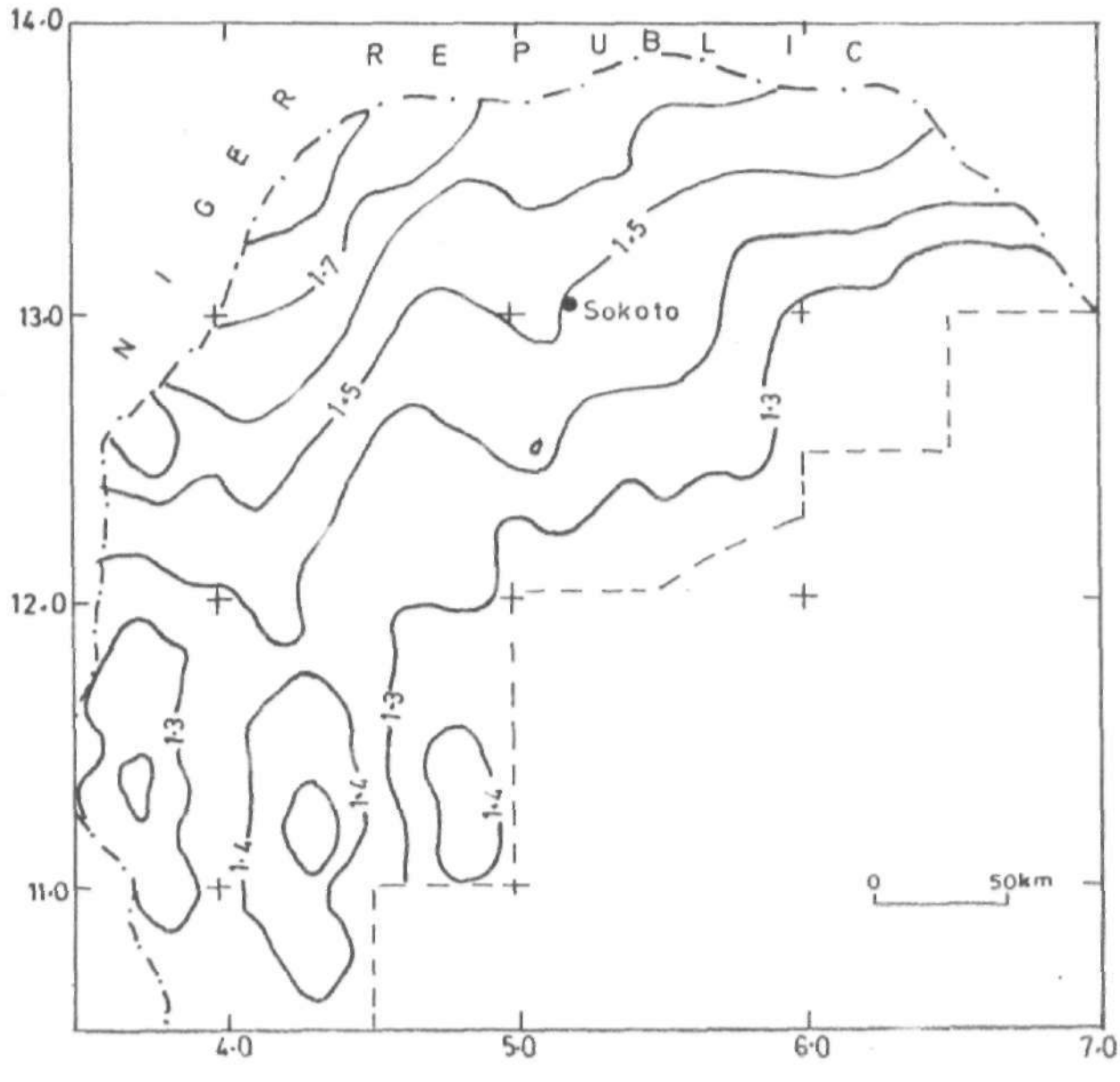


Fig. 5.9 Generalised magnetic basement depth map. (Contour interval 0.1 km)

5.3.7 Discussion of the Magnetic Basement Depth Map

The results of the quantitative interpretation shown in Figures 5.9 and 5.10 suggest that the magnetic basement surface beneath the sediments in the basin is generally shallow and of low relief. Depths to magnetic basement range from 1.2 km near the sediment-basement boundary to 1.8 km at the northwestern boarder with Niger Republic. The regional dip is very gentle, infact hardly measurable in most places, with a value of 0.4^{o} in a northwesterly direction.

The depth contours have two characteristic trends, dividing the area into two tectonic zones (Figure 5.10). South of 12^{o} N latitude, the N-S trend is deminant while to the north of the same latitude degree the NE-SW trend is superimposed on a series of alternating N-S trending troughs and ridges (Figure 5.10). This is an evidence that the basement has been subjected to at least two or more tectonic events whose imprints are expressed by these trends. The boundary between these two zones is roughly coincident with the magnetic boundary observed earlier on the composite map (Figure 5.2). On the surface it also coincides with the boundary between the continental Illo Formation to the South and the other younger formations to the north.

The depth contours (Figure 5.10) depict a number of basement depressions the most prominent of which is an elongate N-S trending depression centered on the

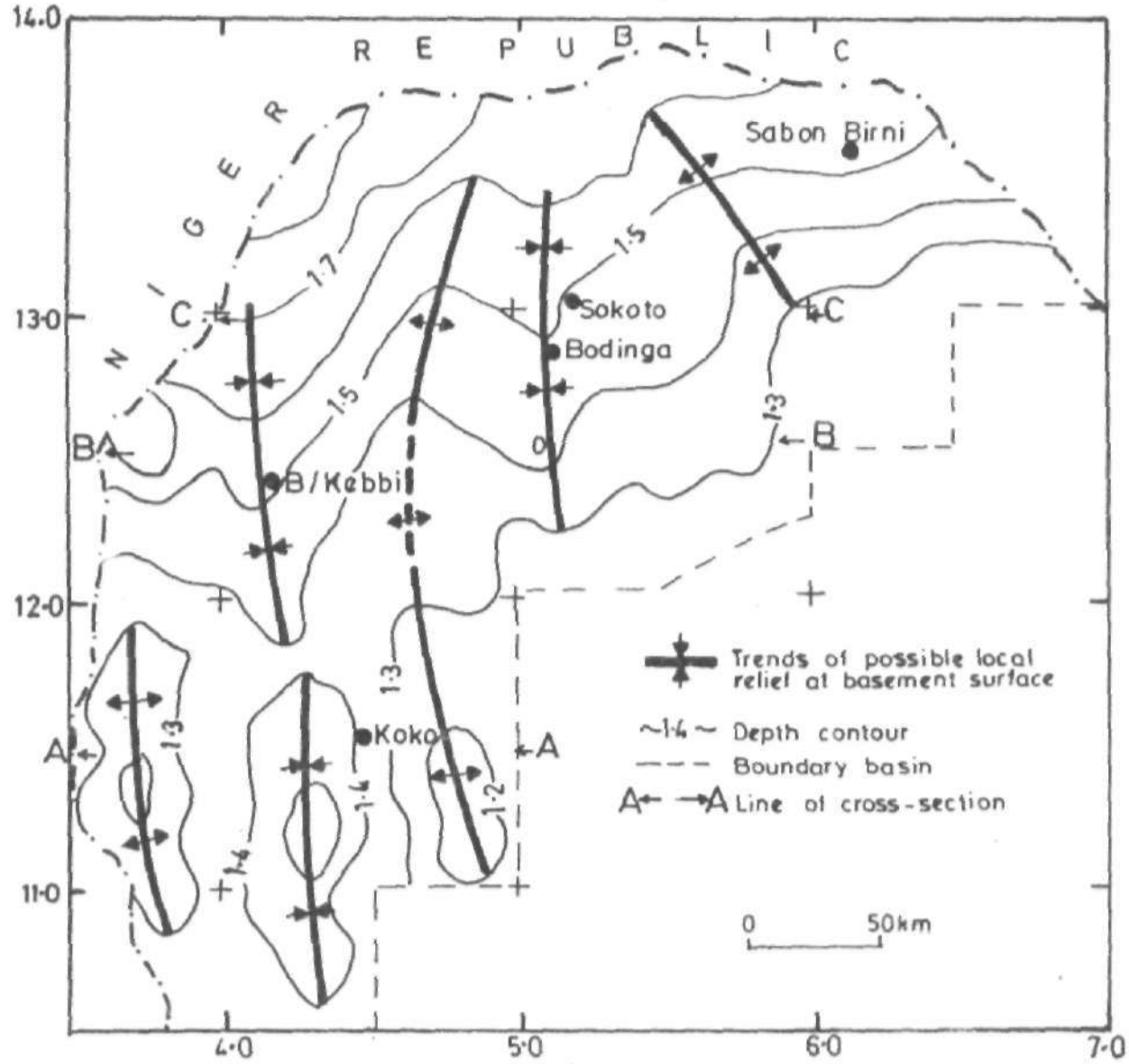


Fig. 5.10 Some inferred structural features on the basement surface superimposed on the generalised magnetic basement depth map.

Illo Formation which occupy the southern end of the basin (Figure 5.10). This depression is bounded to the east and west by ridge-like features, giving this portion of the basin a bowl-type cross section as illustrated in Figure 5.11(b). This depression in the subsurface basement topography is terminated abruptly at the tectonic boundary just south of 12° N latitude.

The other depressions are in the form of a series of N-S trending troughs and ridges (Figure 5.10), suggestive of gentle folding of the subsurface basement rocks. Two other cross-sectional views through latitudes 12.5° and 13° N which are illustrated in Figures 5.11 (a) and 5.12(a) help to buttress this claim. It is therefore suggested that the basement rocks underlying the basin have been gently deformed into a series of antiforms and synforms with axes trending roughly N -S, at wavelength scales of approximately 100 km and amplitude of only a few hundred meters (Figures 5.10, 5.11, and 5.12). Minor deviations in fold trends mainly in a northwesterly direction are also noticeable. The N - S trending folds probably belong to the two phases of isoclinal folding episodes which affected the basement and its supracrustal cover during the Pan African Orogeny (McCurry, 1976). The synforms and other depressions are filled with more than average thickness of sediments and are therefore probable targets for groundwater expleration.

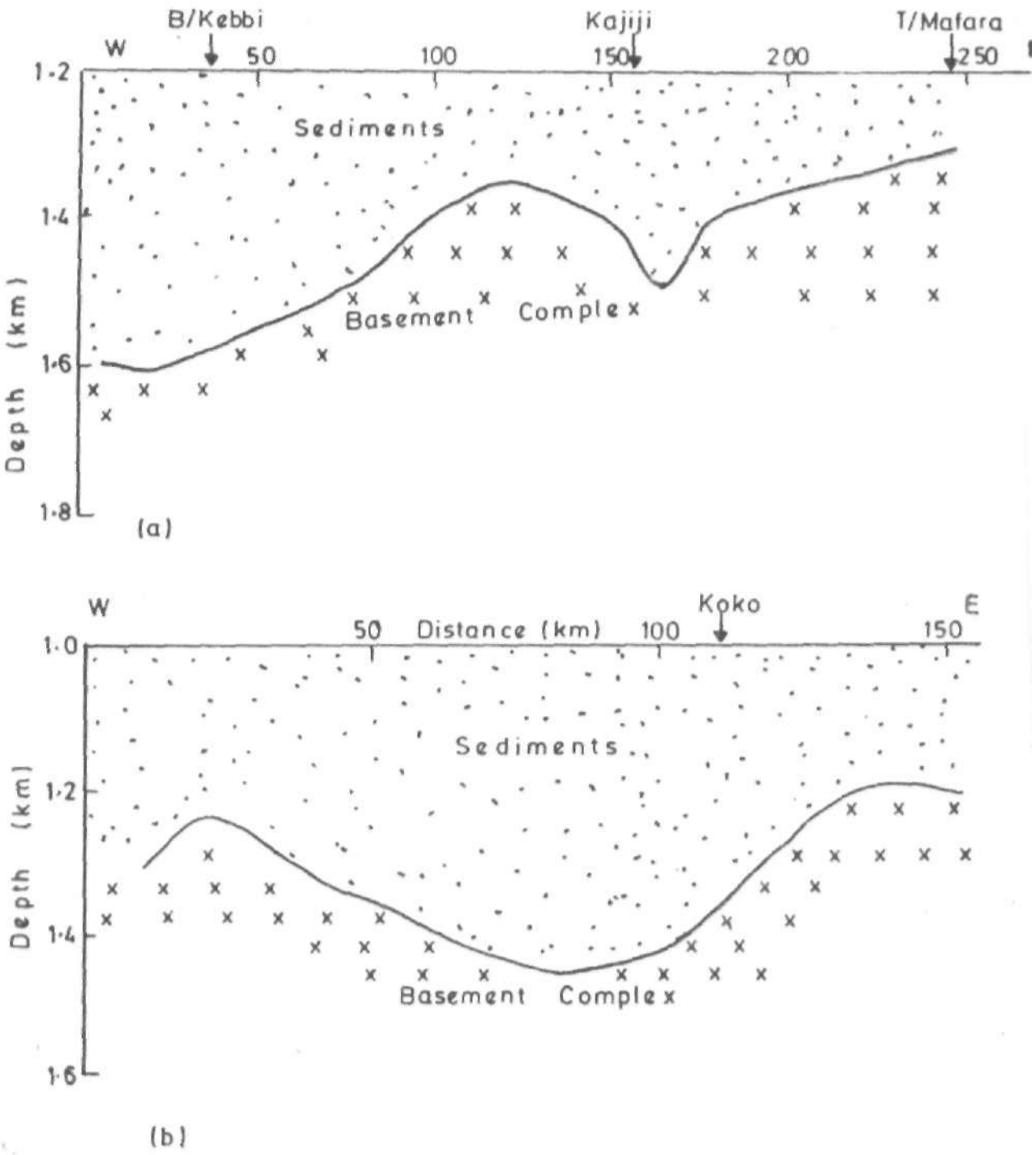


Fig. 5.11 E-W cross sectional views of the basement surface through latitude(a) 12.5° N and (b) 11.5° N.

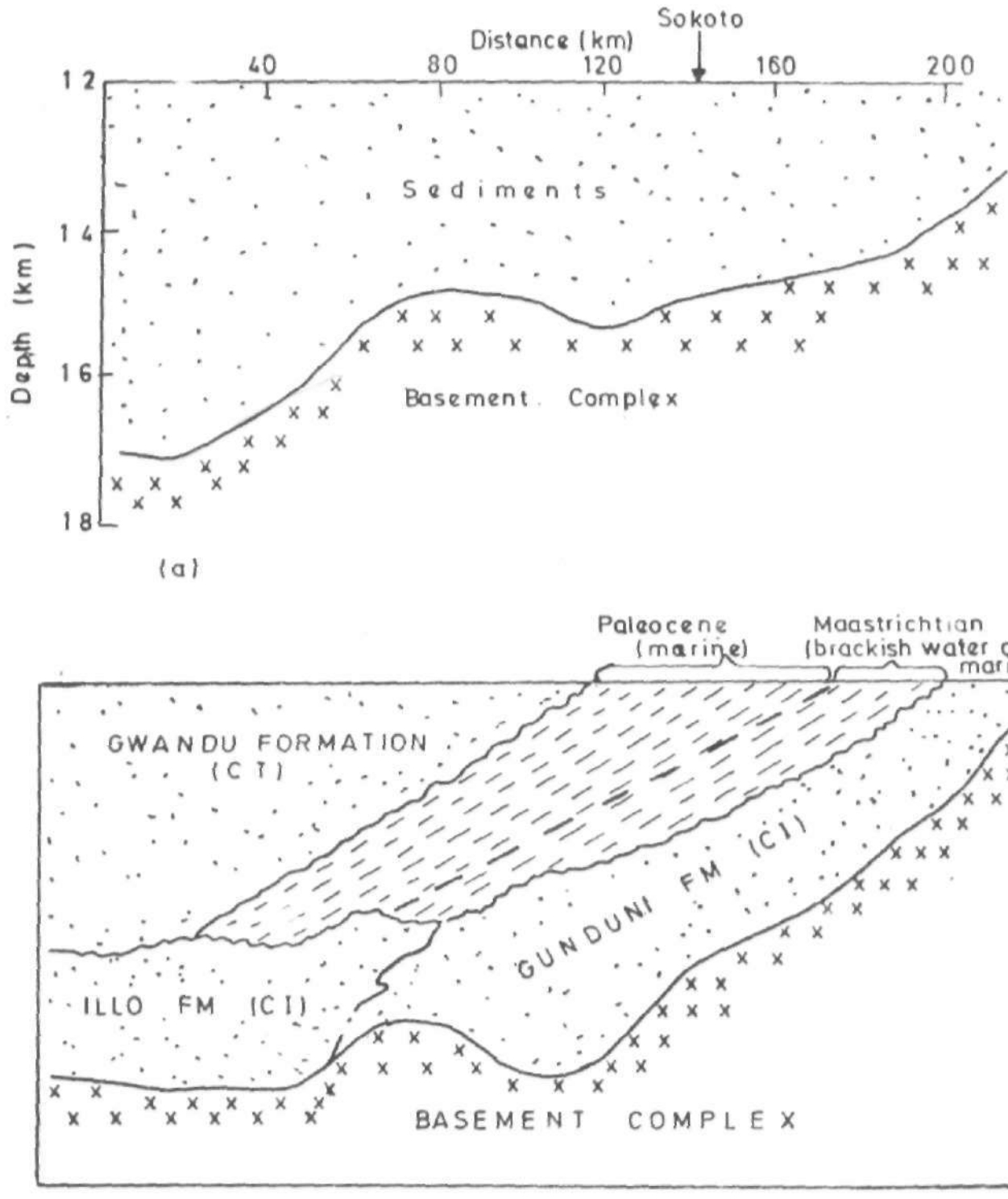


Fig. 5.12 (a) E-W cross sectional view of the basement surface through latitude 13° N (b) idealised section of the Sokoto Basin (after Kogbe, 1979).

The general low gradient of the depth contours even near the sediment - basement boundary is suggestive of a gradual decrease in the basement depth from the basin towards the boundary. This view is also evident on the cross sectional views shown in Figures 5.11(a) and 5.12(a), as well as on the idealised section of the Sokoto Basin given by Kogbe (1979), which is reproduced here for comparison as Figure 5.12(b). Thus if the contact between the Gundumi Formation and the Basement is as mapped (Figure 2.2), and this contact marks the eastern boundary of the Sokoto Basin, then the magnetic basement depth analysis presented above indicates that the contact is gentle and probably not faulted. Thus the southeastern sector of the Iullemmeden Basin, locally known as the Sokoto Basin (Sokoto Embayment) in Nigeria, probably developed from a gentle epeirogenic movement of the basement rocks in contrast to the eastern margin near the Goa Trench where there was strong tectonic movement resulting in faulted sediment basement contact (Furon, 1963; Kogbe, 1979 and 1981; and Wright et al., 1985). These results tend to support the complex basin type with irregular profile ascribed to the Iullemmeden Basin by Chatellier and Slevin (1988).

CHAPTER SIX

S U M M A R Y A N D C O N C L U S I O N S

6.1 Introduction

The Sokoto Basin in Nigeria forms the south-eastern sector of the much larger, nearly circular Mesozoic basin - the Iullemmeden Basin of West Africa, centered north of Niamey in Niger Republic (Figure 2.1). Problems relating to the origin and structure of the Iullemmeden Bas have not been adequately addressed in most published materials available in Nigeria. This may partly be due to the fact that a comprehensive geological/geophysical investigation of the entire basin had not been undertaken because of the vastness of the basin which occupies 700,000 km^2 (Kogbe, 1981) in six countries (Figure 2.1) of which five are Francophone and only one, Nigeria, is Anglophone. Thus differences in cultural background and political inclinations during colonial period had precluded necessary cooperative projects and affected free flow of published materials. In Nigeria most of the available published materials have generally been concerned with the Nigerian sector of the basin which constitutes only one tenth (Oteze, 1976) of the entire basin. In this sector the sedimentology, palaeontology, and hydrogeology of the basin have been studied in great details by Jones, (1948), Ogilbee and Anderson, (1965), Oteze, (1976), Kogbe, (1979 and 1981), and JICA, (1989) among others. From these studies,

structural information on the subsurface basement has been scanty and very generalised. For example the Iullemmeden Basin is classified as complex with an irregular profile, (Chatellier and Slevin, 1988); and that it developed as a post-Pan African pre-Hercynian depression from tectonic epeirogenic movements (Kogbe, 1981; Wright et al., 1985).

Geophysically, the little that was known about the basin in Nigeria prior to the present survey has come from ground water exploration surveys - mainly electrical resistivity and seismic refraction surveys, as well as borehole drilling (Ogilbee and Anderson, 1965; JICA, 1989). All these surveys have however been targeted at the various aquifers within the sedimentary strata with the result that very little is known about the structure of the underlying basement rocks in the Sokoto Basin. This survey is thus the first comprehensive geophysical investigation of the structure of the basin using gravity and magnetic methods. The primary aim was to contribute to the general knowledge of the regional subsurface structure of the Sokoto Basin, with the hope that this would throw more light on the structure and possible origin of the entire Iullemmeden Basin. A secondary objective was to establish regional gravity and magnetic data banks for the production of regional gravity and magnetic anomaly maps which would provide a framework for selecting areas of interest for further detailed investigations.

6.2 Summary of Results

6.2.1 Summary of the Gravity Results

The study area is characterised by negative Bouguer anomalies in the range of -64 to -42 mGals with a mean value of -51 mGals. The northeast trending regional field (Figure 4.6) decreases southeastwards with a gradient of 0.01 mGal km^{-1}, and this regional gradient has been attributed to a thickening of the crust in the southeasterly direction.

The residual anomaly map (Figure 4.7) indicates six major anomalies most of which correlate well with surface geology and whose causative bodies have been studied quantitatively. For example within the basement area, the 10 mGals negative anomaly coincides with outcrops of Older Granites around Gusau (Figure 4.8) while the only positive anomaly (no. 5) coincides with outcrop of a metasedimentary sequence at the eastern margin of the basin at Talata Mafara (Figure 4.8). Three of the four major negative closures over the basin (nos. 2 - 4) were ascribed to increased thickness of the sediments overlying basement depressions. The fourth negative closure (anomaly no.1) is interpreted as a granitic intrusive underlying a thin sedimentary cover.

Three-dimensional modeling of the negative anomaly centered on the three Older Granite outcrops around Gusau (Figure 4.8) yielded one big pluton which extended laterally at depth several kilometers beyond

the mapped contacts at the surface. Thus it appears from the gravity data these isolated outcrops originated from one magma chamber at depth. The modelled body is outward dipping (75° to the west and 64° to the east) to a depth of 1.3 km and then inward dipping to the maximum depth of 4.3 km. The sharp contact with the host rock tend to support magmatic stoping as the likely mode of emplacement, and the N-S strike suggests that the Older Granites probably belong to the end of Proterozoic Pan African Orogeny (600 ± 150 Ma) (Turner, 1983).

The 10 mGal positive anomaly at the eastern margin of the basin is centered on the phyllite outcrop (density, 2.78 x 10^3 kg m^{-3}) at Talata Mafara (Figure 4.8). The modelled body suggest that this roughly NNE striking metasedimentary sequence attains a general thickness of 2.5 km except along the axis of a probable synclinal structure where it reaches a maximum depth of 3.5 km. On account of the simple structural style of the phyllite body, the Anka Schist Belt has been tentatively grouped with the younger metasediments as proposed by Turner (1983), and Fitches et al., (1985).

Over the basin the general deduction from the modeling along the four profiles is that the sediments are very shallow, less than 1 km thick over most of the area. The regional dip is very gentle (less than 1° on all the profiles studied) and is generally away from

the Nigerian landmass towards the border with Niger Republic. Locally the sediments dip towards local depressions at varying degrees and directions. At the four marked depressions, the sediments attain maximum thicknesses ranging from 0.5 to 1.0 km. As almost all the sedimentary formations in the basin contain aquifers (Oteze, 1976), these sediment filled depressions are likely to provide more favourable targets for major groundwater exploration programs.

There is evidence of simple folding of the underlying basement rocks as some of the depressions on adjacent profiles are aligned along the same N - S axis that probably represent the fold axis. However no clear evidence of major faulting even at the sediment-basement boundary can be deduced from the gravity results.

6.2.2 Summary of the Magnetic Results

A regional set of digital total intensity magnetic data has been effectively recovered from the available contour maps, and used in the compilation of the first composite magnetic-anomaly map of the Sokoto Basin at a scale of 1 : 3,000,000. An examination of the composite map revealed three prominent linear belts A-A, B-B, and C-C trending NNE-SSW, NW-SE, and N-S respectively (Figure 5.1), marking zones of probable crustal weakness along which are concentrated a system of large-scale NE-SW and NW-SE magnetic lineations, and

intensive intrusive activities. A tectonic origin was established for the magnetic lineations as their directions are consistent with the predominant tectonic trends in the country. Also some of these magnetic lineations w-w, y-y, and z-z (Figure 5.3) coincide with prominent fractures mapped earlier in the basement rocks, which suggests that some of the other lineations identified in this study might represent faults or fractures hitherto unmapped in the basement complex. In view of the close association of mineralization with regional tectonics, these linear belts could thus be loci of economic mineralization.

A generalised depth to magnetic basement map (Figure 5.9) was produced from a preliminary quantitative interpretation of magnetic profile data. The map reveals a generally shallow basement surface which dips gently in a northwesterly direction, attaining a maximum depth of 1.8 km beneath the ground surface at the northwestern border with Niger Republic. The depth estimates are accurate to within 14 percent, and this sets an upper limit of approximately 2.0 km on the maximum depth to the magnetic basement beneath the sediments in the Sokoto Basin.

Also the depth to magnetic basement map (Figure 5.10) reveal that the basement rocks in this region carry the imprint of at least two tectonic events which has resulted in the N-S and NE-SW structural features evident on this map. Gentle folding of the basement

rocks along N-S trending axes has produced a series of synforms and antiforms at wavelength scales of roughly 100 km and amplitudes of only a few hundred meters. Superimposed on the N-S fold pattern is a NE-SW trending structural grain that affected only the part of the basin north of 12° N latitude. The N-S trending folds probably belong to the Pan African event while the NE-SW structural grain might possibly have resulted from the middle Eocene uplift movements.

The characteristic sediment-basement boundary fault at the western and northeastern parts of the Iullemmeden Basin around the Goa Trench and the Air ranges respectively (Figure 2.1) are absent in the Nigerian sector of the basin, where a very gradual decrease in basement depth from the basin to the contact with the basement is revealed. This would imply that the Sokoto sector of the Iullemmeden Basin probably developed from gentle epeirogenic warping, as opposed to the strong tectonic movements which led to faulting in the western and northeastern parts of the basin.

6.3 Correlation of Gravity and Magnetic Results

Gravity and magnetic surveys have continued to serve geophysicists in providing an insight into the geology of an area quickly and economically. Both methods exploit the fact that variations in the physical properties of rocks in-situ give rise to variations in some physical quantity which may be

measured remotely. Also both methods employ a two-stage process: (1) measurement of anomalies at or above the ground surface; and (2) interpretation of anomalies in terms of rock property variations within the subsurface in a way which adds to knowledge of the geology (Paterson and Reeves, 1985). But whereas in the case of gravity, the physical rock property of interest is density of rocks at all depths, which depends upon the porosity and gross mineralogy of rocks in bulk; for the magnetic method, the rock property is magnetic susceptibility and/or remanent magnetization within the uppermost 30-40 km of the earth's interior, which essentially is a reflection of the properties and concentrations of a single accessory mineral - magnetite.

When the same area has been surveyed with both methods, the confidence in the results of the respective interpretations is strengthened if they correlate well with each other and with known geology and weakened if otherwise. The results of the gravity and magnetic interpretations over the survey area were critically examined against this background.

Results from the application of both the gravity and magnetic methods have revealed that the basin is generally shallow, and that the underlying basement rocks are gently folded, and the basement surface dips gently in a northwesterly direction. The absence of any major sediment-basement boundary faults is also

evident from both results. These results are in agreement with the findings from earlier geological studies over the basin (Jones, 1948; Kogbe, 1979 and 1981; and Wright et al., 1985).

Also the negative gravity closures in the vicinities of Birnin Kebbi, Bodinga and Sabon Birni (Figure 4.9) are roughly located along the axes of synformal structures of the buried basement surface deduced from the magnetic data (Figure 5.10). This thus validates the assumption made in the gravity interpretation to the effect that the negative closures within the basin are due to increased sedimentary thickness at basement depressions.

If the assumption that anomaly no. 1 is due to increased sediment thickness at basement depression is valid, the gravity data yielded a maximun basement depth of 1.0 km at the centre of the depression (Figure 4.12). The depth to magnetic basement analysis on the other hand indicate that the N-S trending depression at the southern end of the basin (Figure 5.10) which coincides with the location of anomaly no. 1 yielded a basement depth of roughly 1.4 km at the same location. Similarly, profile B-B' (Figure 4.14) indicate a basement depth of approximately 0.8 km at Birnin Kebbi corresponding to anomaly no. 2, while the magnetic data gave a depth to basement of nearly 1.6 km at the same location (Figure 5.11(a)). Thus there is much difference in the depth to basement estimates from

both methods, the magnetic depth estimates being larger in the two cases. Several factors could be responsible for the observed large difference in the depth estimates. One major factor relates to the source of the digital magnetic data utilised for the quantitative interpretation. Both the initial contouring process of the recorded digital aeromagnetic data, and the subsequent recovery of the digital data from the contour maps discussed in chapter three of this report are equivalent to successive low pass filtering of the original data set. Thus both operations would remove the high frequency (shallow) anomalies, and the resulting data set would result in deeper magnetic sources. Another possible cause for the observed difference in the results is the sampling interval of the magnetic data, which if not sufficiently small would also lead to deeper magnetic sources. However this factor would not have affected the results appreciably because with the interval of 0.28 km utilised, the first operator length of 1.4 km did not yield any consistent solutions even when the weighting factor was relaxed to two. In addition when comparing these results, one must take into account the fact that the term 'magnetic basement' may not always correspond to the geologic basement, and this would also lead to differences in the depth estimates deduced from gravity and magnetic interpretations.

Finally, it is possible that wrong estimates of formation density may have also affected the depth estimates from the gravity interpretation, but this fact was recognised from the beginning, and a thorough density analysis was undertaken. Obviously depth estimates from both methods would correlate better if digitally recorded magnetic data are made available, and borehole and/or seismic information are available to constrain the models and lessen the inherent ambiguities in potential field data interpretation.

One major weakness of the magnetic method which has serious implications on the above discussions is the fact that it responds exclusively to magnetic contrasts, it can therefore miss important structures in homogeneous or weakly magnetic rocks; on the other hand it can locate differences which cannot be observed by geologists, either because they are not detectable in hand specimens, or because the rocks are not exposed (Boyd, 1969). For these reasons the magnetic interpretation and the gravity and geologic interpretations may be different; the methods are therefore intended to complement each other.

6.4 Conclusions

The first comprehensive geophysical investigation in the Sokoto Basin has thrown some light into the understanding of the geology, and helped to answer some basic questions raised regarding the subsurface

structure of the basin. Among the major contributions of the study are:

1. Estimation of the thickness of the sediments in different parts of the basin. The results of the gravity and magnetic interpretations have established an upper limit of 2 km thickness for the sediments in the Sokoto Basin. One important significance of this result is in consideration of the hydrocarbon accumulation potential of the basin. The probable source beds in the basin are the marine Maastrichtian Rima and Sokoto Groups which overlie the continental beds at an estimated maximum thickness of 900 m (Kogbe, 1979). If all other conditions for hydrocarbon accumulation are favourable, and the average temperature gradient of 1^{o} C per 30 m which obtains in the Niger Delta is applicable, then the minimum thickness of sediments to achieve the threshold temperature of 115^{o} C for the commencement of oil formation from organic remains (Wright et al., 1985) would be 2.3 km approximately. Thus on the basis of the shallow depth of the probable source beds in the Nigerian sector of the Iullemmeden Basin, the prospect for hydrocarbon accumulation is not particularly promising. Nevertheless, a number of sediment - filled troughs and depressions on the buried basement surface have been revealed which form probable targets for groundwater exploration.

2. The absence of any major sediment-basement boundary faults as deduced from this study, support the view that the Nigerian portion of the Iullemmeden Basin in particular and probably other parts have developed from gentle epeirogenic warpings within cratonic rocks. This is in contrast to the western margin of the basin which is marked by prominent NW-SE trending faults around the Goa Trench or the northeastern margin which is dissected by a series of NE-SW and NW-SE trending faults in the vicinity of the Air Ranges (Figure 2.1) (Kogbe, 1979). One other possible hypothesis which has been proposed for the origin of the Iullemmeden Basin is stretching and rifting (Kogbe, 1979). From the results of this survey, some of the phenomena of rifts such as major faulting and uplift are not apparent to validate the rifting hypothesis in this portion of the basin. However this hypothesis can not be completely ruled out because of the observed intense intrusive activity revealed along the linear belts which is evidence of volcanism, and also the area covered by the present survey is only about 10 percent (Oteze, 1976) of the entire basin which has been reported to be complex (Chatellier and Slevin, 1988), and as such data from a larger portion of the basin would be required for the hypothesis to be adequately tested.

3 Recovery of a regional set of digital data, and compilation of composite magnetic - anomaly maps. The regional set of digital data would hence permit rapid mechanical production of contour maps and other plots on a variety of scales and map projections, and is also essential for quantitative interpretation. The composite map has established a framework for the study of limited areas and for selecting areas for more detailed investigation.

4. The study has identified three zones of probable crustal weakness in the NNE-SSW, NW-SE and N-S directions respectively, along which are concentrated igneous activities and a set large scale magnetic lineations of probable tectonic origin. This result is significant both from economic point of view as well as seismicity. The established control of mineralization by regional tectonics delineates these zones for further detailed investigations; and the concentration of magnetic lineations some of which coincide with major mapped faults and fractures in the region, makes these zones prone, even though remotely, to seismic harzards.

Finally it is important to point out here that the interpretations of the data embodied in this report is a geophysical appraisal of the data based on the geologic information available to the author at the

time of writing. As additional geophysical/geological and more importantly drill-hole data become available, it may be necessary to re-evaluate the significance of some features described in this report.

6.5 Recommendations

The Bouguer anomaly maps deduced from the DMAAC data set (Figure 4.2(b)) reveal a large negative gravity anomaly (marked A) centered at latitude 11.8° N and longitude 7.5° E within the basement block of northern Nigeria. This anomaly A was also evident in the Bouguer anomaly map of Africa contained in Brown and Girdler (1980); and it appears to have influenced the 'local regional' field deduced from this survey data which decreases towards the location of anomaly A. Previous gravity studies in adjacent regions (Ojo and Ajakaiye, 1976; Gandu et al., 1985), both indicate regional fields decreasing towards the same anomaly A. It is therefore recommended that a regional gravity survey of the entire basement block of northern Nigeria be undertaken to determine the source of this anomaly and the trend of the regional gravity field in the region.

The advantages of the composite magnetic anomaly map are numerous and perhaps obvious as has been demonstrated by the compilation over the Sokoto Basin. It is therefore recommended that this compilation be utilised as the basic building block for assembling a more comprehensive magnetic data bank and in compiling a composite magnetic anomaly map of the entire country.

This study has delineated three zones of possible crustal weakness, along which are concentrated igneous activities an a set of large scale magnetic lineations. In view of the established tectonic control of mineralization in this region, detailed geophysical and geological investigations are recommended along these zones as they could be loci of economic mineralization.

The depth to basement estimates obtained from the gravity and magnetic interpretations respectively are markedly different to warrant further investigation. For such an investigation to improve on these results, some borehole and/or seismic information are required to constrain the models. It is recommended that the Federal Government agencies working presently with JICA in various parts of the Sokoto Basin should endeavour to make a few boreholes to reach the basement, and also ensure that a proper density and lithologic logging are done. Also if the original digitally recorded aeromagnetic data from the various flight operations are made available, the accuracy and reliability of results from future studies will be enhanced.

Finally, there is need for the Federal Survey Department to update the available roadmaps, and properly secure already established benchmarks as well as establish new benchmarks along recently constructed roads. These measures will no doubt increase the speed and accuracy of future gravity surveys.

R E F E R E N C E S

Adeniyi, O. O. (1987). Gravity survey of the Older Granite plutons in Zaria area of Kaduna State, Nigeria. Unpublished M. Sc. Thesis. Ahmadu Bello University, Zaria, Nigeria.

Ajakaiye, D.E. (1970). Gravity measurements over the Nigerian Younger Granite Province. Nature, 225: 50 - 52.

Ajakaiye, D.E. and Burke, K. (1973). A Bouguer gravity map of Nigeria. Tectonophysics, 16: 103 -115.

Ajakaiye, D.E. Hall, D.H. and Miller, T.W. (1985). Interpretation of aeromagnetic data across the central crystalline shield area of Nigeria. Geophys. J.R. astr. Soc., 83: 503 - 517.

Ajakaiye, D.E. Hall, D.H. Millar, T.W, Verheijen, P.J.T. Awad, M.B. and Ojo, S.B. (1986). Aeromagnetic anomalies and tectonic trends in and around the Benue Trough. Nature, 319(6054): 582 - 584.

Ajayi, C. O. and Ajakaiye, D. E. (1981). The origin and peculiarities of the Nigerian Benue Trough: another look from recent gravity data obtained from the Middle Benue. Tectonophysics, 80: 285 - 303.

Ajibade, A.C. (1976). Provisional classification and correlation of the schist belt in northwestern Nigeria. In: Kogbe, C.A. (Ed.) Geology of Nigeria - Elizabethan Pub. Co., Lagos, pp. 85 - 90.

Ajibade A.C. and Wright, J.B. (1988). Structural relationships in the schist belt of north-western Nigeria. In: Oluyide, P. O. (Ed.) Precambrian Geology of Nigeria- Geological Surv. of Nigeria, Kaduna, pp. 103 - 109.

Ananaba, S.F. (1983). Evaluation of remote sensing application to geophysical studies in Nigeria. Unpublished Ph.D. Thesis. Ahmadu Bello University, Zaria, Nigeria.

Ananaba, S.F. and Ajakaiye, D.E. (1987). Evidence of tectonic control of mineralization in Nigeria from lineament density analysis: A Landsat - study. Int. J. Remote Sensing, 8(10): 1445 - 1453.

Ball, E. (1980). An example of very consistent brittle deformation over a wide intracontinental area: The late Pan-African fracture system of the Taureg and Nigerian Shield. Tectonophysics, 61: 363 - 379.

Baranov, W. (1975). Potential Fields and their Transformations in Applied Geophysics. Gebruder Berntraeger, Stuttgart, pp. 82 - 89.

Boyd, D. (1969). The contribution of airborne magnetic surveys to geological mapping. In: Morley, L. W. (Ed.) - Mining and Groundwater Geophysics/1967. Economic Geology Report No.26, Geological Survey of Canada.

Brown, C. and Girdler, R.W. (1980). Interpretation of African gravity and its implication for the breakup of the continents. Journal of Geophysical Research, 85(B11): 6443 - 6455.

Chatellier, J. and Slevin, A. (1988). Review of African petroleum and gas deposits. Journal of African Earth Sciences, 7: 561 - 578.

Cordell, L.E. and Grauch, V.J.S. (1985). Mapping basement magnetization zones from aeromagnetic data in the San Juan basin, New Mexico. In: Hinze, W. J. (Ed.) The Utility of Regional Gravity and Magnetic Anomaly Maps - Society of Exploration Geophysicists, U.S.A. pp. 181 - 197.

Cratchley, C.R. and Jones, G.P. (1965). An interpretation of the geology and gravity anomalies of the Benue Valley, Nigeria. Geological Surv. Nigeria Rpt No. 1405.

Dehlinger, P. (1978). Marine Gravity. Elsevier Scientific Pub. Co., Amsterdam. pp. 136 - 140

Dods, S.D. Tesky, D.J. and Hood, P.J. (1985). The new series 1:1,000,000-sacle magnetic anomaly maps of the Geological Survey of Canada: compilation techniques and interpretation. In: Hinze, W.J. (Ed.), The Utility of Regional Gravity and Magnetic Anomaly Maps - Society of Exploration Geophysicists U.S.A., pp. 69 - 87.

Dyrelius, D. (1983). Aerodig: A digitizing computer program. Department of Solid Earth Physics, Uppsala University, Sweden.

---------- (1983). Regusurf: A polynomial surface fitting program. Department of Solid Earth Physics, Uppsala University, Sweden.

European Association of Exploration Geophysicists (EAEG), (1985). Tidal gravity corrections for 1986. Service Hydrographique de la Marine and Compagnie Generale de Geophysique, pp. 1 - 17.

European Association of Exploration Geophysicists (EAEG), (1986). Tidal gravity corrections for 1987. Service Hydrographique de la Marine and Compagnie Generale de Geophysique, pp. 1 - 17.

Falconer, J. D. (1911). The Geology and Geography of Northern Nigeria. Macmillan Publishers, London, pp. 45 - 145.

Fairhead, J.D. and Okereke, C.S. (1987) A regional gravity study of the West African rift system in Nigeria and Cameroon and its tectonic interpretation. Tectonophysics, 143: 141 - 159.

Fitches, W.R. Ajibade, A.C. Egbuniwe, I.G. Holt, R.W. and Wright, J.B. (1985). Late Proterozoic schist belts and plutonism in NW Nigeria. J. geol. Soc. London, 142: pp. 319 - 337.

Friedberg, J.L. (1975). Understanding and use of Werner deconvolution in aeromagnetic interpretation. Aero Services Corporation, Houston, Texas, pp. 1 - 29.

Furon, R. (1963). The Geology of Africa. Hafner Publishing Company, New York, pp. 145 - 173.

Gandu, A.H. Ojo, S.B. and Ajakaiye, D.E. (1985). A gravity study of the Precambrian rocks in the Malumfashi area of Kaduna State, Nigeria. Tectonophysics, 126: 181 - 194.

Gay, S.P. (Jr) (1967). Standard curves for interpretation of magnetic anomalies over long tabular bodies. In: Society of Exploration Geophysicist's Mining Geophysics Vol.(II). The Society of Exploration Geophysicists, Tulsa, Oklahoma, pp. 512 - 548.

Geological Survey of Nigeria (GSN), (1985). Structural Map of Nigeria. (First Edition).

Goguel, J. (1954). A universal table for the prediction of Lunar-Solar correction in gravimetry (Tidal gravity correction). Geophysical Prospecting, II: Suppl.

Grant, F. S. and West, G. F. (1965). Interpretation Theory in Applied Geophysics. McGraw-Hill Book Company, NewYork, pp.192 - 200.

Grant, F.S. (1972). Review of data processing and interpretation methods in gravity and magnetics, 1964 -1971. Geophysics, 37(4): 647 - 661.

Grant, N.K. (1978). Structural distinction between a metasedimentary cover and an underlying basement in the 600 Ma. old Pan-African domain of north-western Nigeria; West Africa. Bull. Geol. Soc. Am., 89: 50 - 58.

Hammer, S. (1939). Terrain corrections for gravimeter stations. Geophysics, 4: 184 - 194.

Hartman, R.R. Tesky, D.J. and Friedberg, J.L. (1971). A system of rapid digital aeromagnetic interpretation. Geophysics, 36(5): 891 - 918.

Heiskanen, W. A. and Vening-Meinesz, F. A. (1958). The Earth and its Gravity Field, McGraw - Hill Book Company Inc., New York, p. 54.

Holt, R.W. Egbuniwe, I.G. Fitches, W.R. and Wright, J.B. (1978). The relationships between low-grade metasedimentary belts, calc-alkaline volcanism and the Pan-African Orogeny in N.W. Nigeria. Geol. Rdsch., 67: 631 - 646.

Jacobsen, P. (Jr) (1961). An evaluation of basement depth determinations from airborne magnetometer data. Geophysics, 26(3): 309 - 319.

Jain, S. (1976). An automatic method of direct interpretation of magnetic profiles. Geophysics, 41(3): 531 - 541.

Jakosky, J.J. (1950). Exploration Geophysics. Trija Publishing Company, Los Angeles, pp. 196 - 197.

Japan International Cooperation Agency, (J.I.C.A.) (1989). The study for groundwater development in Sokoto State: Progress Report 2, pp. 20 - 175.

Jones, B. (1948). The Sedimentary rocks of Sokoto Province. Bull. Geol. Survey of Nigeria, No. 18 pp. 1 - 72.

Klingele, E. and Dyrelius, D. (1972). Interpol: an interpolation program. Department of Solid Earth Physics, Uppsala University, Sweden.

---------- (1972). Isorey: a contouring program. Department of Solid Earth Physics, Uppsala University, Sweden.

Kogbe, A.C. (1979). Geology of the South-eastern (Sokoto) sector of the Iullemmeden Basin. Bulletin, Department of Geology, Ahmadu Bello University, Zaria, Nigeria, pp. 1 - 300.

Kogbe, A.C. (1981). Cretaceous and Tertiary of the Iullemmeden Basin in Nigeria (West Africa). Cretaceous Research, 2: 129 - 186.

Koulomzine, Th. Lamontagne, Y. and Nadeau, A. (1970). New methods for the direct interpretation of magnetic anomalies caused by inclined dykes of infinite length. Geophysics, 35(5): 812 - 830.

Lacoste & Romberg Inc. (1976). Instrument manual for Lacoste & Romberg Inc. Model G Gravity meter £G - 446. Austin, Texas, pp. 5 - 6.

McCurry, P. (1976). The geology of the Precambrain to Lower Palaeozoic rocks of Northern Nigeria - a review. In: Kogbe, C.A. (Ed.) Geology of Nigeria - Elizabethan Pub. Co., Lagos, pp. 15 - 39.

McCurry, P. (1978). Geology of degree sheets 10 (Zuru), 20 (Chafe), and parts of 9 (Katsina), Nigeria. Overseas Geol. Miner. Resour., London, No. 53.

Nabighian, M.N. (1972). The analytic signal of two-dimensional magnetic bodies with polygonal cross-section: its properties and use for automated anomaly interpretation. Geophysics, 37(3): 507 - 517.

Neev, D. Hall, J.K. and Saul, J.M. (1982). The Pelusium megashear system across Africa and associated lineament swarms. Journal of Geophysical Research, 87(32): 1015 - 1030.

Nettleton, L.L. (1954). Regionals, residuals, and structures. Geophysics, 19(1): 1 - 22.

Nwegbe, P.O. (1987). Spectral analysis and interpretation of aeromagnetic anomalies over the Upper Benue Trough, Nigeria. Unpublished M.Sc. Thesis, Ahmadu Bello University, Zaria, Nigeria.

Odeyemi, I.B. (1988). Lithostratigraphy and structural relationships of the Upper Precambrian metasediments in Igarra area, southwestern Nigeria. In: Oluyide, P. O. (Ed.) Precambrian Geology of Nigeria - Geological Surv. Nigeria, Kaduna, pp. 111 - 125.

Ogezi, A.E.O. (1977). Geochemistry and geochronology of basement rock from north-western Nigeria. Unpublished Ph.D. Thesis, Leeds University.

Ogilbee, W. and Anderson, H.R. (1965). Exploratory drilling for groundwater in western Sokoto province, Nigeria: with special reference to artesian aquifers in the Gwandu Formation. United States Geological Survey and Geological Survey of Nigeria.

Ojo, S.B. and Ajakaiye, D.E. (1976). Preliminary interpretation of gravity measurements in the Middle Niger Basin, Nigeria. In: Kogbe, C. A. (Ed.) Geology of Nigeria - Elizabethan Publishing Co. Lagos, Nigeria, pp. 295 - 307.

Ojo, S. B. (1985). Magdpeth - a magnetic interpretation program. Department of Physics, Ahmadu Bello University, Zaria, Nigeria.

Oladesu, M. O. (1987). A gravity survey of the igneous intrusions in the Rano area of Kano State, Nigeria. Unpublished M. Sc. Thesis. Ahmadu Bello University, Zaria, Nigeria.

Oluyide, P.O. (1988). Structural trends in the Nigerian Basement Complex. In: Oluyide P. O. (Ed.) Precambrian Geology of Nigeria - Geological Surv. Nigeria, Kaduna.

Osazuwa, I. B. Ajakaiye, D. E. and Verheijen, P. J. T. (1981). Analysis of the structure of part of the Upper Benue Rift Valley on the basis of new geophysical data. Earth Evolution Sciences, 2: 126 - 135.

Osazuwa, I.B. (1984). Gravred: An unpublished gravity reduction program. Department of Physics, Ahmadu Bello University, Zaria, Nigeria.

Osazuwa, I.B. (1985). Primary gravity network of Nigeria. Unpublished Ph.D. Thesis, Ahmadu Bello University, Zaria, Nigeria.

Oteze, G. E. (1976). The hydrogeology of the north-western Nigeria basin. In: Kogbe, C. A. (Ed.) Geology of Nigeria - Elizabethan Pub. Co. Lagos, pp. 373 - 390.

Oyawoye, M.O. (1964). The geology of the Nigerian basement complex. J. Mining Geol. and Metalls. Soc. 1: 87 - 102.

Paterson, N.R. and Reeves, C.V. (1985). Application of gravity and magnetic surveys: The state-of-the-art in 1985. Geophysics, 50(12): 2558 -2594.

Raeburn, C. and Tattam, C.M. (1930). A preliminary note on the sedimentary rocks of Sokoto Province. Bull. Geol. Survey of Nigeria, No.13, pp. 57 - 60.

Rahaman, M.A. (1976). Review of basement geology of southwestern Nigeria. In: Kogbe, C.A. (Ed.) Geology of Nigeria - Elizabethan Pub. Co., Lagos, pp. 41 - 58.

Reford, M.S. and Sumner, J.S. (1964). Aeromagnetics: review article. Geophysics, 29(4): 482 - 516.

Skeels, D.C. (1967). What is residual gravity? Geophysics, 32(5): 872 - 876.

Talwani, M. and Ewing, M. (1960). Rapid computation of gravitational attraction of three-dimensional bodies of arbitrary shape. Geophysics, 25(1): 203 - 225.

Talwani, M. (1965). Program for computing the gravity anomaly caused by a three-dimensional body of arbitrary shape. Lamont Geological Observatory, pp. 1 - 12.

Tunyi, G.N. (1984). Geostatistical analysis and interpretation of aeromagnetic anomalies of the Southeastern part of the Jos Plateau, Nigeria. Unpublished M.Sc. Thesis. Ahmadu Bello University, Zaria, Nigeria.

Turner, D.C. (1983). Upper Proterozoic schist belts in the Nigerian sector of the pan-African Province of West Africa. Precambrian Research, 21: 55 - 79.

Udensi, E.E. Oje, S.B. and Ajakaiye, D.E. (1985). A three-dimensional interpretation of the Bouguer anomalies over the Minna batholith in Central Nigeria. Precambrian Research, 32: 1 - 15.

U.S. Defence Mapping Agency Aerospace Centre (DMAAC), (1988). 1 x 1 mean free-air gravity anomalies DMAAC\DSGB\May - 1988. Missouri, U.S.A.

Uwah, E.J. (1984). Investigation of radiometric anomalies by nuclear and other methods: A case study of the Sokoto Basin of Nigeria. Unpublished Ph.D. Thesis. Ahmadu Bello University, Zaria, Nigeria.

Verheijen, P. J. T. and Ajakaiye, D. E. (1978). A gravimeter calibration line for Nigeria. Survey Review, 24(190): 373 - 380.

Verheijen, P.J.T. and Ajakaiye, D.E. (1980). Analysis of errors in barometric elevations in northern Nigeria. Geophysics, 45(7): 1144 - 1152.

Werner, S. (1953). Interpretation of magnetic anomalies at sheet-like bodies. Sveriges Geologiska Undersokning, Ser. C. Arsbok 43, n:06, Stokholm, Sweden.

Wilcox, L.E. (1974). An analysis of gravity prediction methods for continental areas. Tech. Pap., 74 - 001, Office of Distribution Services, U.S. Defence Mapping Agency, Washington D.C.

Wright, J.B. (1968). South Atlantic continental drift and the Benue Trough. Tectonophysics, 6(4): 301 - 310.

Wright, J.B. (1976). Fracture systems in Nigeria and initiation of fracture zones in the South Atlantic. Tectonophysics, 34: T43 - T47.

Wright, J.B. Hastings, D.A. Jones, W.B. and Williams, H.R. (1985). Geology and Mineral Resources of West Africa. George Allen & Urwin, London, pp. 90 - 120.

A P P E N D I X A

LaPerte's Method of Regularization

If we consider a point where the value of the function f(x,y) must be interpolated as the origin, it is reasonable to approximate the element of surface near the point by a paraboloid whose equation is written as

$$F(x,y) = C_1 x^2 + C_2 xy + C_3 y^2 + C_4 x + C_5 y + C_6 \quad \ldots A(i)$$

It depends on six unknown coefficients C_1 to C_6, and consequently at least six points, (x_i, y_i, f_i), are needed to calculate the coefficients. In reality more than six points, which must not all lie on the same side of the origin, are usually taken from which we obtain more than six equations which will be solved by least squares. The actual number of points included depends on the search radius R, determined in advance, and whose value is constrained by local conditions such as station density and distance between profiles.

The six coefficients C_i must be calculated such that the separation of the paraboloid F(x,y) from the surface f(x,y) decreases as the point (x,y) approaches the origin. Each separation is therefore assigned a weight P which is a function of distance $\delta = \sqrt{(x^2 + y^2)}$. It is desirable that the weight be zero at the circumference of circle of radius R, and to increase as the distance decreases, theoretically becoming infinite for $\delta = 0$. A good expression for P is given as

$$P = \{ (R^2 - \delta^2)/(\delta^2 + \eta^2)\}^2 \qquad \ldots\ A(ii)$$

where η is a small accessory quantity to make numerical calculations possible when a measurement point falls on the origin.

The method consists of minimising the quantity

$$S = \sum_i P_i \{F(x_i, y_i) - f(x_i, y_i)\}^2 \qquad \ldots\ A(iii)$$

Thus the six partial derivatives of S with respect to the unknown C_i, are set equal to zero, which results in a system of six equations of the type:

$$C_1\Sigma Px^4 + C_2\Sigma Px^3y + C_3\Sigma Px^2y^2 + C_4\Sigma Px^3 + C_5\Sigma Px^2y + C_6\Sigma Px^2 = \Sigma Px^2f.$$

$$C_1\Sigma Px^3y + C_2\Sigma Px^2y^2 + C_3\Sigma Pxy^3 + C_4\Sigma Px^2y + C_5\Sigma Pxy^2 + C_6\Sigma Pxy = \Sigma Pxyf$$

$$C_1\Sigma Px^2y^2 + C_2\Sigma Pxy^3 + C_3\Sigma Py^4 + C_4\Sigma Pxy^2 + C_5\Sigma Py^3 + C_6\Sigma Py^2 = \Sigma Py^2f$$

$$C_1\Sigma Px^3 + C_2\Sigma Px^2y + C_3\Sigma Pxy^2 + C_4\Sigma Px^2 + C_5\Sigma Pxy + C_6\Sigma Px = \Sigma Pxf$$

$$C_1\Sigma Px^2y + C_2\Sigma Pxy^2 + C_3\Sigma Py^3 + C_4\Sigma Pxy + C_5\Sigma Py^2 + C_6\Sigma Py = \Sigma Pyf$$

$$C_1\Sigma Px^2 + C_2\Sigma Pxy + C_3\Sigma Py^2 + C_4\Sigma Px + C_5\Sigma Py + C_6\Sigma P = \Sigma Pf$$

The unknown that is of interest is C_6, since it is the value of f(x,y) at the origin, i.e. $f(0,0) = C_6$; that is required.

APPENDIX B

Magnetic Anomaly of a Thin Dyke

If the concept of magnetic 'charge' or pole strength is employed, then the magnetic anomaly due to a thin tabular body (dyke) can be obtained (Gay, 1967). Two left-handed coordinate systems are defined with a common origin at any point on the plane of observation, directly over the upper edge of the dyke, and a common z axis positive vertically downward as illustrated in Figure B(1). The unprimed system has its y axis along the magnetic north, and the primed system has its y'-axis perpendicular to the strike of the dyke. The strike is defined as the clockwise angle from the positive y axis to the positive x' axis. If the total earth's magnetic field T_0 is resolved into two components along the x' and y' directions, then only the component in the y' direction is effective in inducing magnetic poles on the dyke's surfaces, and is termed the effective total intensity T_0'. T_0' can further be resolved into two components (Figure B2), T_d - the dip component and T_c - the cross component. The induced pole strength per unit area on the upper edge of the dyke is given by

$$M_d = k_d T_d \qquad \ldots \quad B(i)$$

where k_d is the apparent magnetic susceptibility of the dyke to T_d. On the upper and lower planar surfaces of the dyke, the induced magnetic pole strength per unit area is

$$M_c = k_c T_c \qquad \ldots \quad B(ii)$$

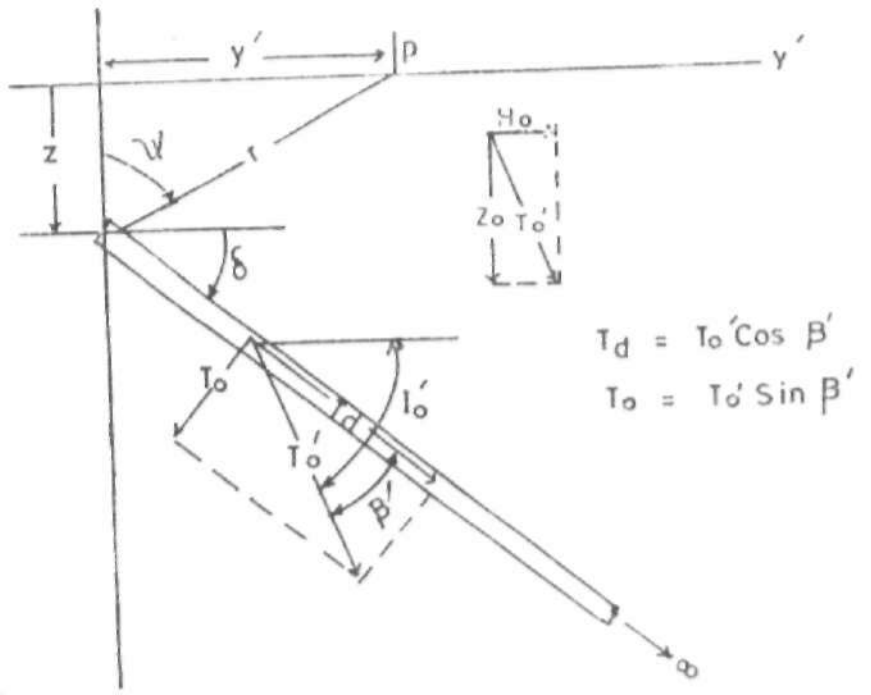


Fig. B2 Geometry of the thin dyke in the y'z-plane

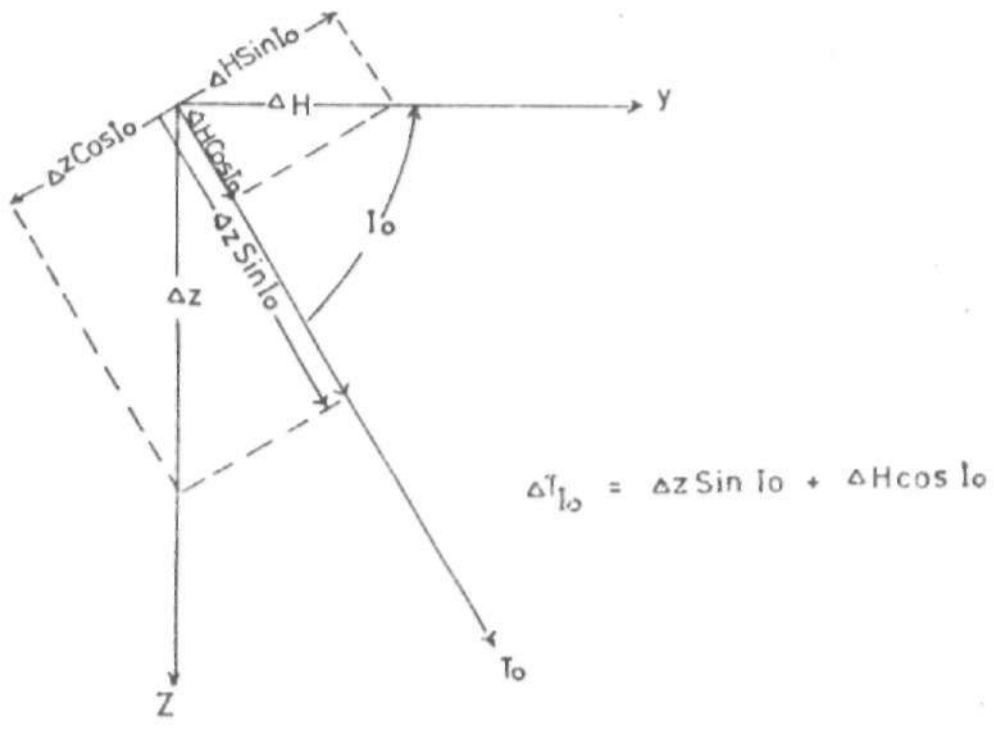


Fig. B3 The anomalies in the different components of total intensity

where k_c is the apparent susceptibility of the dyke to T_o.

At point P on the plane of observation, the long linear distribution of poles on the apical edge gives rise to the so-called logarithmic potential

$$V_d = 2k_d T_d t \log(y^2+z^2)^{\frac{1}{2}} \qquad \ldots B(iii)$$

The potential due to magnetic charges resulting from the cross component of magnetization on the planar surfaces of the dyke is given by (Jakosky, 1950)

$$V_o = 2k_c T_c t(90^o - \delta + \tan^{-1} y'/z) \qquad \ldots B(iv)$$

By adding B(iii) and B(iv) and taking the proper derivatives, the vertical and horizontal intensity anomalies can be derived:

$$\Delta z = -\frac{\partial v}{\partial z} = \frac{2k_d T_d tz}{z^2+y'^2} + \frac{2k_c T_c ty'}{z^2+y'^2} \qquad \ldots B(v)$$

$$\Delta H' = \frac{\partial v}{\partial y'} = \frac{-2k_d T_d ty'}{z^2+y'^2} + \frac{2k_c T_c tz}{z^2+y'^2} \qquad \ldots B(vi)$$

$\Delta H'$ is the anomaly in the component of the horizontal intensity in the direction of y', and is related to the commonly measured component in the direction of the magnetic north as follows:

$$\Delta H = \Delta H' \sin\alpha \qquad \ldots B(vii)$$

The anomaly in the component of T in the direction of the undisturbed field is related to the various components as follows (Figure B3):

$$\Delta T_{I_o} = \Delta z \sin I_o + \Delta H \cos I_o \qquad \ldots B(viii)$$

Substituting equations B(v), B(vi), and B(vii) into B(viii) gives

$$\Delta T_{I_o} = \frac{2t(M_d \sin I_o + M_c \sin\alpha \cos I_o)z + 2t(M_c \sin I_o + M_d \sin\alpha \cos I_o)y'}{z^2 + y'^2} \qquad \text{B (ix)}$$

Equation B(ix) can be written in the general form of the expression for the total magnetic field due to a thin dyke with infinite strike length and depth quoted by Hartman et al. (1971)

$$\Delta T_{I_o} = \frac{Ay' + Bz}{y'^2 + z^2} \qquad \ldots \text{ B(x)}$$

where $A = 2t\,(M_c \sin I_o + M_d \sin\alpha \cos I_o)$

and $B = 2t\,(M_d \sin I_o + M_c \sin\alpha \cos I_o)$